誌　謝

本論文可順利完成，首先感謝指導教授許千樹老師及陳信龍老師於博士班期間的指導，並提供了良好的研究環境及極具深度之研究題目，二位老師讓我自由地於其中發揮，無拘無束的想像空間，讓我養成了獨立思考及自動自發的研究精神。尤其是陳信龍老師的不吝指導，使我在老師身上看到做研究的精神－
”*愈難的問題，愈要有耐心來思考並解決問題，最終才會看到答案的曙光*”。
實在讓我於研究之路受用不盡，對於二位老師，深深給予最深的感謝及敬意。

感謝口試委員：曹正熙博士、余子隆教授、吳建興教授與陳建宏教授於學生的論文上提供了非常寶貴的建議，讓學生的論文得以更為完整。尤其是曹正熙博士，提供了珍貴小角度中子散射的beamtime；於處理小角度中子散射之數據上，曹博士不僅幫助我們建立許多fitting model，分析數據上亦提供了許多寶貴的意見。亦感謝陳建宏老師提供了DLS的數據，有助於以不同角度來思考溶液態之聚集行為。此外，感謝同步輻射中心的鄭有舜博士，學生於同步幅射中心擔任研究助理時，從鄭博身上學習到許多小角度散射的原理及處理方法。

於清大實驗室時，感謝學長姐及學弟妹們給予許多實驗上的建議及生活上的幫忙，當然也少不了吃喝玩樂。具創意的歐陽老師，實驗室大學長小胖及阿茂，親切的怡君，健談的維隆，一定要握一下的阿Man，認真男人最帥的蛋哥，熱心的阿亮，善良的大仁，酷酷的軍佑，生力軍昇哥，開朗的美玲，和我一起在NIST渡過吃begal日子的啟聖，貼心的學妹怡帆、睿妤，害羞的阿賢，互相漏氣求進步的維崙，相見恨晚的TYT，電腦達人昇韋，外冷內熱的建興，最佳人緣獎美足，有廣大後援會的昭麟，認真的哲毅，愛笑的阿昌，愛唱歌的紹憬，開心果瑋珊，實驗室最棒的助理逸榛，實驗室的博士後研究員Sunny、Rahman，有你們大家的一路支持，使得我在研究的路上並不寂寞。

雖然我很少回去許千樹老師實驗室，認識我的人也不多，但大家熱情的伸出援手，尤其是小燕在最後口試的關頭幫了我不少忙。

啟蒙老師吳建興老師，及交大的好友：啟賢學長、均文學姐，同窗好友濱陽、壁君、維賢，學弟妹煥錩、孟屏、懋華、文鈺、小鄭、阿草、錫煌。

另外感謝多年的好友正彥、元忠、文範、文勝，大家聚在一起的互相打氣，使我們忘記生活上的不愉快。

轉眼間，八年的研究生涯，有著許許多多酸甜苦辣的回憶，彷彿在昨日才發生。一路上，到了一些不同的地方，碰到了許許多多的朋友，因為有你們相伴，才讓我的博士班求學生涯不孤獨，你們也都成為我人生中最美好的點點滴滴，和你們的相處，除了學術上的教學相長，也給了我不同且豐富的人生經驗。

最後僅以此論文獻給最親愛的家人們以及我最敬愛的母親－

媽，您辛苦了。

於人生路上陪著我分享各種酸甜苦辣並照顧著我的金霞－

謝謝妳。

2007/02/06 于風城

半硬式共軛高分子於溶液態構形及聚集行為之研究

研究生：黎彥成　　指導教授：許千樹博士

共同指導教授：陳信龍博士

國立交通大學應用化學研究所 博士班

摘 要

共軛高分子由於具有優越的電學及光學半導體性質，因此在學界及產業界均投入廣泛地研究。然而，許多文獻利用光譜証明共軛高分子既使於稀薄溶液中亦會形成分子鏈間的聚集體，進而影響其發光性質。然而，此聚集體之形成之原因及構形則鮮少有文獻報導。在此篇研究中，我們將研究共軛高分子 poly(diphenyl phenylenevinylene) (DP-PPV) 高分子於溶液態之分子構形及其分子間聚集行為。

Poly(2,3-diphenyl-5-hexyl-1,4-phenylenevinylene) (DP6-PPV) 分子鍵於不同溶液性質中(氯仿、甲苯)，均具有聚集的情況發生，且聚集體之碎形尺度(mass fractal dimension)大約於 2.2 ~ 2.7 之間。此聚集體中於氯仿溶液中形成較為鬆散結構但在甲苯溶液中變的較為緊密的結構，乃由於 DP6-PPV 分子鍵在甲苯溶液中，高分子鏈間之作用力所致。於甲苯溶液中，此種較弱的分子鏈間作用力可藉由增加系統溫度而去除之。然而，加熱至高溫時，依然有許多的分子鏈間作用力無法被完全消除，因此，在分子鏈間存在著另一種具有高穩定性之作用力。此種高穩定性的分子鏈作用力存在於氯仿及甲苯溶液之中。此種高穩定性之作用力形成原因為 π-π complex 存在於 DP6-PPV 粉末中。高分子鏈被此作用力緊緊地綁在一起並於溶劑中形成了網狀結構，因此降低了高分子之溶解度。

另一方面 Poly(2,3-diphenyl-5-decxyl-1,4-phenylenevinylene) (DP10-PPV)為具有較長側鍵之高分子於溶液態之構形亦於本研究討論之。其實驗結果發現，於氯仿溶液中，DP10-PPV 分子鍵具有較佳之分散行為，推論為 DP10-PPV 之長側鍵可有效的抑制 π-π complex 於 DP10-PPV 粉末的產生，因此分子間之作用力較 DP6-PPV 來的弱。所以 DP10-PPV 高分子可均勻分佈於氯仿溶液中。而於低濃度時，DP10-PPV 分子鍵承呈現 worm-like chain 行為，且其抗彎長度(persistence length)與濃度成正比。另一方面於甲苯溶液中，其分子間作用力變強，因此，DP10-PPV 分子鍵形成碎形之聚集體。其聚集體之結構隨濃度增高而更緊密，此種聚集體具 disklike 之行為，而其厚度可藉由 Kratky-Porod 方程式來求得其 disklike 之厚度(T ~ 20Å)。由此結果可推論 DP10-PPV 於甲苯溶液中所形成之聚集體為其分子鍵互相交錯而成。

Conformational Structure and Aggregation Behavior of Semi-Rigid Conjugated Polymers in Solution State

Student: Yen-Cheng Li

Advisor: Dr. Chain-Shu Hsu
Co-Advisor: Dr. Hsin-Lung Chen

The Department of Applied Chemistry
National Chiao Tung University

Abstract

Conjugated polymers constitute a family of semi-rigid polymer which have found great potential in opto-electronic applications due to their unique semiconducting properties and solution processability. The solutions of light-emitting polymers are usually homogeneous in appearance; however, their conjugated segments may exhibit some extent of aggregation in the solution and such an aggregation may exert dramatic impact on the photophysical properties of the polymer in the solutions. Previous studies based primarily on absorption and photoluminescence spectroscopies have indicated that these polymers underwent inter-chain aggregation in the solution state even at large dilution; however, the origin of this event and the structure of the resultant aggregates remain the crucial issues to be resolved.

This thesis centers on the studies of the conformational structures and aggregation behavior of two poly(diphenyl phenylenevinylene)s (DP-PPVs) bearing different side chains in the solutions states. We reveal that the inter-chain aggregation

of the conjugated polymer, poly(2,3-diphenyl-5-hexyl-1,4- phenylenevinylene) (DP6-PPV) composing hexyl side chains, in the solutions with chloroform and toluene generates network aggregates with the hydrodynamic radii of several μm. Small angle neutron scattering (SANS) demonstrates that the internal structure of these aggregates can be characterized by the mass fractal dimensions of 2.2 ~ 2.7. The networks are looser in chloroform but become highly compact in the poorer toluene solvent due to severe segmental association. Increasing the temperature alleviates the segmental association in toluene while largely retaining the mass fractal dimension of the aggregates. However, the inter-chain aggregation is never completely dissipated by the heating, suggesting the existence of two types of segmental association with distinct stability. The highly stable segmental association that can neither be solvated by chloroform nor be disrupted thermally in toluene is attributed to the π-π complex already present in the DP6-PPV powder used for the solution preparation. The chains tied firmly by this complex form network aggregates in the solution and hence reduce the entropy of mixing of the polymer. In the poorer toluene solvent further segmental association takes place within the pre-existing aggregates, making the networks more compact. This type of segmental association can be disrupted by moderate heating and its occurrence is ascribed to the poor affinity of the aliphatic side chains of DP6-PPV to toluene.

The conformational structure and the aggregation behavior of another hairy-rod conjugated polymer, poly(2,3-diphenyl-5-decyl-1,4-phenylenevinylene) (DP10-PPV) bearing decyl side chains, in the solutions with chloroform and toluene have also been investigated by means of SANS and DLS. The results are systematically compared with those of DP6-PPV to reveal the effect of side chain length on the aggregation behavior. The DP10-PPV chains well dispersed in chloroform are found to exhibit the expanded wormlike chain conformation with the persistent length increasing with

overall polymer concentration. This molecular level dissolution is in contrast with the colloidal dissolution of DP6-PPV in chloroform, indicating that increasing the length of the side chain tends to suppress the segmental aggregation of DP-PPVs. DP10-PPV however aggregates significantly to form aggregates of several μm in size in toluene. The internal structure of the aggregates is characterized by a fractal dimension of 1.3 at the overall polymer concentration of 0.1 wt%, indicating that the aggregates are loose networks. Compact disklike domains develop within the aggregates as the concentration increases to 0.5 wt% and 1.0 wt%. The thickness of the disk domains determined from the Kratky-Porod approximation is ca. 20 Å, implying that the DP10-PPV chains formed a bilayer structure in the domains. The formation of the layer like structure is assisted by the longer side chains attached to DP10-PPV compared with DP6-PPV.

Contents

Acknowledgment……I
Abstract (in Chinese)……...Ⅲ
Abstract (in English)……..……...V
Contents……...……..……VIII
Table Contents……..…….……X
Figure Contents…….…..…….…XI

Chapter 1. Introduction and Literature Review

1.1 Histroical Development of Semiconducting Polymers…..……..1
1.2 The Light Emission, Conduction Mechanism and Electronic Structure of Conjugated Polymers……...6
1.2.1 Electronic Structure of Conjugated Polymers……6
1.2.2 Fluorescence and Phosphorescence……...11
1.2.3 Aggregate and Energy Transfer……14
1.3 Hairy-rod Polymer……..19
1.4 Self-Assembly……21
1.5 Small-Angle Scattering……..25
1.6 Scattering of Polymer in Solutions……27
1.7 Fractals……...30
1.8 The Motivations and Overview of the Study……33

Reference…….……37

Chapter 2. Fractal Aggregates of Poly(2,3-diphenyl-5-hexyl-1,4-phenylenevinylene) (DP6-PPV) in Solution State

2.1 Introduction……42
2.2 Experimental Section……45
2.3 Result and Discussion……47
2.3.1 Aggregate Structure in DP6-PPV/Chloroform Solutions……47
2.3.2 Aggregate Structure in DP6-PPV/Toluene Solutions……..59
2.3.3 The Nature of the Segmental Associations……..64

Reference……..67

Chapter 3. Conformational Structure and Aggregation Behavior of Poly(2,3-diphenyl-5-decyl-1,4-phenylenevinylene) (DP10-PPV) in Solution State

3.1 Introduction……69
3.2 Experimental Section……72
3.2.1 Materials……72
3.2.2 Scattering……72
3.3 Result and Discussion……75
3.3.1 Conformational Structure of DP10-PPV in Chloroform…….75
3.3.2 Aggregation Behavior of DP10-PPV in Toluene…….90

References……..101

Chapter 4. Conclusions and Suggestions for Future Works

4.1 Conclusions……..104
4.2. Suggestions for Future Works…….106

Table Contents

Table 1-1. Examples of self-assembly……...24
Table 2-1. The values of the parameters obtained from the unified equation fits for DP6-PPV/chloroform solutions…….….56

Figure Contents

Figure 1-1. Chemical structure of polyacetylene……..4

Figure 1-2. (a) The chemical structures of molecules Alq_3, TPD, and PBD that have been use in thin-film EL devices; (b) The device of Tang and Vanslyke……4

Figure 1-3. The single layer device structure of polymer light-emitting diode based on PPV……5

Figure 1-4. The chemical structure of MEH-PPV……5

Figure 1-5. Band picture for an insulator, a semiconductor and a metal (conductor)……9

Figure 1-6. Diagrammatic representation of the energy levels of π molecular obritals with increasing size of the molecule for $(CH)_x$……9

Figure 1-7. Illustration of the formation of bipolaron……10

Figure 1-8. The energy level of polaron and bipolaron……...10

Figure 1-9. A typical Jabłoński diagram……13

Figure 1-10. Diagram for energy transfer between different extents of Aggregations……18

Figure 1-11. Example of self-assembly (a) Crystal structure of ribosome. (b) self-assembly of peptide-amphiphile nanofibers. (c) Thin film of a nematic liquid crystal on an isotropic substrate. (d) A school of fish (dymanic self-assembly)……..24

Figure 1-12. Schematic representation of the part of the polymer viewed at different length scales……31

Figure 1-13. A schematic representation of the different asymptotic regions for the *q*-dependence of a s wormlike chain and their link to the different chain conformation on various length scales……...31

Figure 1-14. Computer simulated non-equilibrium growth processes produce three-dimensional structures with characteristic mass fractal dimensions……....32

Figure 1-15. Illustration of power-law scattering from fractal objects…….32

Figure 2-1. The room-temperature SANS profiles in log-log plots of DP6-PPV in the solutions with chloroform at different concentrations. Two power-law regimes were identified in the scattering profiles irrespective of the concentration. The intensity exhibited a power law of $I(q) \sim q^{-2.7}$ in the middle- to low-region characterizing the mass fractal dimension of the network aggregates. The q-dependence transformed to another power law of $I(q) \sim q^{-1}$ at high q corresponding

to the form factor of the rodlike sub-chains between the junction points in the networks. The solid curves are the fitted results using the unified equation……48

Figure 2-2. G(q)q vs. q plot of 1.0 wt% DP6-PPV/chloroform solution for the determination of the molar mass per unit length (M_L) from the asymptotic value of the plo……..50

Figure 2-3. The concentration-normalized SANS profiles of DP6-PPV/chlororofm solutions. I(q)/c in the low-q region was found to increase with increasing overall polymer concentration, indicating that DP6-PPV exhibited significant inter-chain aggregation……...53

Figure 2-4. Schematic illustration of the network aggregates formed by DP6-PPV in the solution state. The networks were looser in chloroform but became highly compact in toluene……...54

Figure 2-5. The distribution of hydrodynamic radius R_h in the 1.0 wt% chloroform and toluene solutions at 25 ^oC. The R_h profile displayed three peaks with each stemming from a characteristic relaxation mode in the system. The largest R_h was attributed to the average hydrodynamic radius of the aggregates in the solution, while the two small peaks were attributed to the internal relaxation mode of the networks and the motions of the rodlike segments…….……58

Figure 2-6. The room-temperature SANS profiles in log-log plots of DP6-PPV in the solutions with toluene at different concentrations. Only one asymptotic power law was identified at q > ~ 0.02 $Å^{-1}$. The corresponding power law exponents were attributed to the mass fractal dimensions of the highly compact networks formed by the inter-chain aggregation of DP6-PPV in the solvent……60

Figure 2-7. The temperature-dependent SANS profiles of 1.0 wt% DP6-PPV/toluene solution collected in a heating cycle. The low-q intensity depressed progressively with increasing temperature while largely retaining its slope. Accompanied with this intensity depression was the gradual emergence of the q^{-1} power law in the high-q region. The q^{-1} regime became clear at 85 ^oC. The inset displays the SANS profiles normalized by the contrast factors for 1.0 wt% DP6-PPV/toluene solution at 85 ^oC and 1.0wt% DP6-PPVchloroform solution at room temperature. It can be seen that the two scattering profiles were nearly identical……...63

Figure 2-8. The WAXS scans of the as-received DP6-PPV powder used for the solution preparations, the powder having been annealed at 330 ^oC and

the film cast from chloroform. A peak associated with π-π complex was observed at 29° for all samples……..65
Figure 3-1. The SANS profiles in log-log plots of DP10-PPV/chloroform solutions with different concentrations at room temperature. The insert shows the Kratky-Porod plot over the q region where the intensities closely follow q^{-1} dependence. The radius of the rodlike segments can be obtained from the slope of the plot……...76
Figure 3-2. The concentration-normalized SANS profiles of DP10-PPV in chloroform solutions. The divergence of the scattering curves of higher concentration (0.5 and 1.0 wt%) suggest that the stretched chain segments and leading the rod-like behavior extended to lower q region ……..78
Figure 3-3. The hydrodynamic radius distributions of DP10-PPV/chloroform solutions with different concentrations at room temperature……...81
Figure 3-4. AFM topographic images of DP10-PPV cast from 0.1 mg/ml chloroform solution on HPOG…….……84
Figure 3-5. AFM topographic images of DP10-PPV cast from 0.008 mg/ml chloroform solution on HPOG. The two images on the right provide a better view on the topological feature of the aggregates formed by the polymer chains…….84
Figure 3-6. A comparison between the contrast-normalized SANS intensities of 1 wt% DP6-PPV and DP10-PPV solutions. DP6-PPV solution is found to exhibit a much stronger low-q intensity, signaling significant degree of inter-chain aggregation…….87
Figure 3-7. The wide-angle X-ray scattering (WAXS) scans of DP6-PPV and DP10-PPV powders used for the solution preparations. DP6-PPV powder is seen to exhibit strong diffraction peaks signaling the presence of a significant degree of crystallinity. The crystal diffraction becomes nil for DP10-PPV showing that the polymer is essentially uncrystalline in the powder. A scattering peak at 2θ = 29° (corresponding to a Bragg spacing of 3.2 Å) associated with the π-π complex is also identified for DP6-PPV powder…….88
Figure 3-8. The DLS result of DP10-PPV in toluene solutions with different concentration. The bimodal relaxation mode has been observed in toluene and the profiles dominated by slow mode suggesting the chain is confined and construct a large cluster……...90
Figure 3-9. The log-log plot SANS profiles of DP10-PPV dissolved in toluene solutions with different polymer concentration at room temperature.

The chain segments aggregate into the fractal object in the toluene and the fractal dimension relative to the concentration. In higher concentration, the fractal objects display the disklike structure……...91

Figure 3-10. The contrast-normalized SANS profiles of DP10-PPV dissolved in different solvent. The scattering intensity of toluene solution is much higher than chloroform especially in high concentration. Asserting the aggregation behavior is prevalent and toluene is relative poor solvent for DP10-PPV molecules…….93

Figure 3-11. Illustration of DP10-PPV/toluene with 0.1 wt%. The chain segments construct the network in toluene solutions……...94

Figure 3-12. The chain segments aggregates into a compact desklike domain which can be model-independently determined from the slope of fitting line in $\ln[I(q)q^2]$ vs. q^2 of SANS data. The thickness of disklike domain obtain from the Eq. (5) is 20 Å…….95

Figure 3-13. The illustration of DP10-PPV chain segments aggregate in higher polymer concentration (i.e. 0.5 and 1.0 wt%). The disklike domain compose of two layers of polymer chain……..98

Figure 3-14. A series of SANS profiles of DP10-PPV 1.0 wt% toluene solution in a heating cycle. While increasing the system temperature, the aggregate components were dissipated completely and this behavior response to the scattering intensity in the low-q region……..99

Figure 3-15. The scattering profiles of DP10-PPV 1.0 wt% in toluene solutions during the cooling cycle. The slow re-aggregation behavior upon cooling cycle indicated DP10-PPV with poor thermal reversibility due to its longer alkyl side chains which prevent the chain segment reaggregation efficiency…….100

CHAPTER 1

Introduction and Literature Review

1.1 Historical Development of Semiconducting Polymers

Traditionally, polymers have been considered as a class of insulating materials. Indeed, a conventional application of polymer is the safe insulation of metallic conductors. Since the discovery of electrical conductivity of doped polyacetylene in 1977,[1, 2] remarkable progress has been made in synthesizing conducting polymers, in understanding their properties, and in developing them for use in electronic and optical devices.[3] The backbone of polyacetylene (Figure 1-1) consists of *conjugated* double bonds. Conjugated polymers derive their semiconducting properties from delocalized π-electron bonding along the polymer chain. The extended π-conjugation reduces the energy gap between the highest occupied molecular orbital (HOMO) and the lowest unoccupied molecular orbital (LUMO) of the π-system. The electrons in π orbital are easier to move but they are still highly localized. Doping of the material by removing electrons from the π-system (i.e., creating a hole) or adding electrons into it substantially increases its conductivity by allowing migration of the holes or the extra electrons along the polymer chain. Interchain hopping of charges permits bulk conductivity.

Shortly afterwards, development of organic electroluminescent (EL) thin film was spurred in the 1980s through the work of Tang and Vanslyke[4] at Eastman Kodak company. They found for the first time the efficient electroluminescence in a two-layer organic thin-film device. The EL device consisted of a hole-transporting layer of an aromatic diamine and an emissive layer of 8-hydroxyquinoline aluminum (Alq_3), as shown in Figure 1-2. They employed indium-tin oxide (ITO) as the

transparent hole-injecting anode and a magnesium-sliver alloy as the electron-injecting cathode on glass substrate to improve the extraction of light. The use of this two-layer structure, purified material, and properly chosen electrodes permitted organic light-emitting diodes (OLEDs) to operate at voltages below 10 V for the first time with high quantum efficiency (1 % photon electron) and good brightness (> 1000 cd/m^3). A large number of other molecular materials have later been developed as the charge transporting or emissive layer in light-emitting diodes (LEDs) (*cf.* Figure 1-2) and to date, LEDs based on vacuum-sublimated small molecules follow this Kodak technique. From then on, the development of organic LEDs grew rapidly and devices with high quantum efficiencies have been reported.

In 1990, the Cambridge University group of Friend announced that they had achieved green-yellow EL using the conjugated polymer poly(*p*-phenylene vinylene)(PPV) in a single-layer device structure[5, 6] shown in Figure 1-3. PPV, with its aromatic phenyl ring and conjugated vinylene linkage, was first synthesized by Wessling at Dow in 1968[7-9] and has a π-π^* electronic energy gap of about 2.5 eV. The ITO layer functions as a transparent electrode, which allows the light generated within the diode to leave the device. The top electrode is formed by thermal evaporation of aluminum. The levels of efficiency of this first, simply PPV-based LED was relatively low, of the order of 10^{-4} photons generated within the device per electron injected (an internal quantum efficiency of 0.01%.)[10]

PPV is insoluble in common solvents, and as such requires special processing steps to produce a conjugated thin film necessary for EL device application. In this case, a precursor polymer that is soluble is first prepared, then a film is applied from solution by spin casting, which then thermally converted to the conjugated form. Cambridge Display Technology (CDT) was founded in 1992 to exploit a key patent of Cambridge University in light emission from conjugated polymers.[11] In 1991 Heeger

and co-workers at the University of California at Santa Barbara announced the EL application of a soluble derivative of PPV, namely poly(2-methoxy-5-2'-ethyl-hexyloxy)-1,4-phenylene vinylene) or MEH-PPV[12] (*cf.* Figure 1-4), in which the dialkoxy side chains are attached to the main chain of PPV. Owing to its side-group substituents the polymer not only renders solubility in common organic solvents such as chloroform and toluene, but also changes the electrical and optical characteristics. The emission of MEH-PPV is shifted to the orange-red region with the wavelength of 605 nm, which is a red-shift from that of PPV.[12, 13] This synthesis of the soluble conjugated polymer urges a great deal of basic scientific and applied researches with the goal of commercialization of PLEDs.

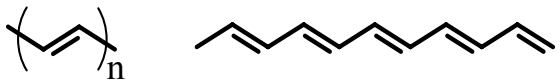

Figure 1-1 Chemical structure of polyacetylene.

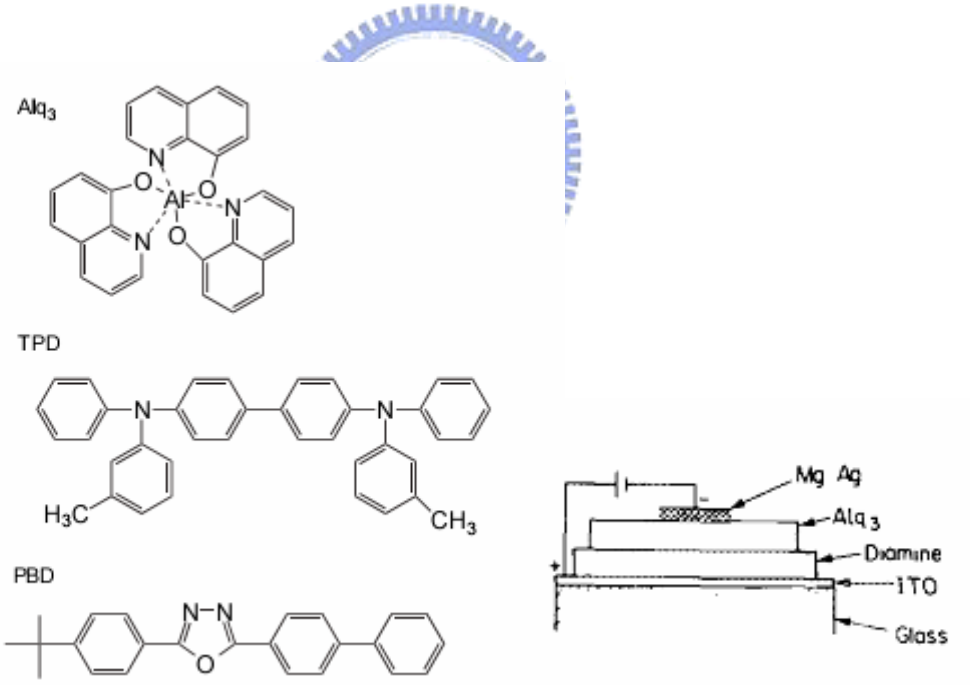

(a) (b)

Figure 1-2. (a) The chemical structures of molecules Alq_3, TPD, and PBD that have been use in thin-film EL devices; (b) The device of Tang and Vanslyke.

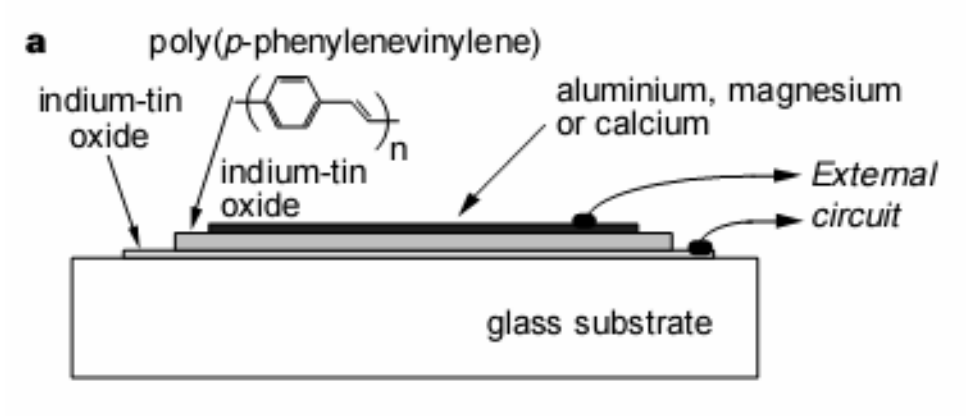

Figure 1-3. The single layer device structure of polymer light-emitting diode based on PPV.

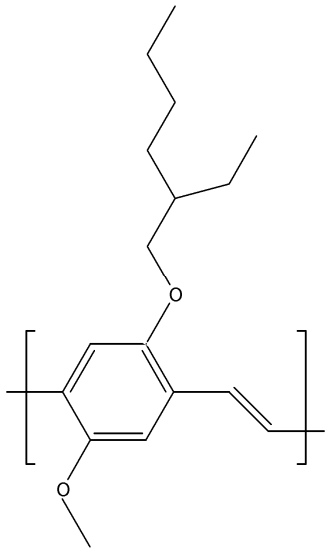

Figure 1-4 The chemical structure of MEH-PPV

1.2 The Light Emission, Conduction Mechanism and Electronic Structure of Conjugated Polymers

1.2.1 Electronic Structure of Conjugated Polymers

As two atoms approach each other and become bonded, the two atomic orbitals overlap each other with the formation of two molecular orbitals of different energy. The split energy levels will form a “band-like” shape (called energy bands) when many atoms are involved in the bond formation. We call the difference between two energy bands the “band-gap”. Briefly, the energy spacing between the highest occupied and the lowest unoccupied band is called the band gap. The highest occupied band is called the “valence band” and the lowest unoccupied one the “conduction band”. The electrical properties of a material is determined by its electronic structure that can be simply described by the Band Theory.[14, 15] Basically, we can classify the materials into three types, namely, an insulator, a semiconductor, and a conductor. In a conductor, the atomic orbitals overlap with equivalent orbitals of their neighbouring atoms in all directions to form molecular orbitals. With so many molecular orbitals spaced together in a given range of energies, they form an apparently continuous band of energies with effectively no gap between valance and conduction bands (illustrated in Figure 1-5). The conductivity of a metal is due to a zero band gap, so that weak applied energies can redistribute the electrons: electrons at higher energy and holes at lower energy. This situation is suitable for rapid charge transport.

For inorganic semiconductors, the mechanism of charge generation from incident photons is well established. Because these materials are typically crystalline solids with an exceedingly large number of atoms in the periodic lattice, their electronic structure can be appropriately described in terms of energy bands. For an idealized

semiconductor, the electronic structure consists of a conduction band (LUMO band) and a valence band (HOMO band) separated by an energy gap, the size of which depends upon the material. Conjugated conducting polymers may also act as semiconductors, and their electronic properties appear to be somewhat analogous to those of inorganic semiconductors. Most semiconducting polymer appear to have a band gap that lies in the range of 1.5 to 3.0 eV, in contrast to that of 0.66 to 1.42 eV for inorganic semiconductor devices working in the visible light range.

Doping of semiconducting polymers may enormously enhance the conductivity. The role of the dopant is either to remove or to add electrons to the polymer. For example, an iodine (I_2) molecule will abstract an electron from polyacetylene to form an I_3^- ion.[16] The electron is removed from the top of the valence band of the semiconducting polymer, such as polyacetylene, therefore a vacancy (hole) is created. Those electron-hole pair is called a "radical cation" (or positive polaron) and it can migrate along the polyacetylene chain upon the application of an electric field (Figure 1-6). On the other hand, one can use sodium to dope the polymer to form radical anion (a negative polaron). With continuing doping, a second electron is removed from an already-oxidized section of the polymer, either a second independent polaron may be created or the unpaired electron of the first polaron is removed to from a bication (also called a bipolaron). Figure 1-7 illustrates the bipolaron.[16]

Figure 1-8 illustrates the variation of band picture of conjugated polymer with the extent of doping (using I_2 for oxidization process).[16] After doping, two new energy level are formed between the original valance band (HOMO) and the conduction band (LUMO). Polaron is formed in the conjugated polymer upon slightly doping. Further doping can generate bipolaron and many bipolarons formed can narrow down the bipolaron bands. Polaron and bipolaron are movable because of the rearrangement of

the single-double bonds in the conjugated system. The mechanisms of transport of the charge combined with the band theory is very useful for explaining the conductivity and optical properties after doping.

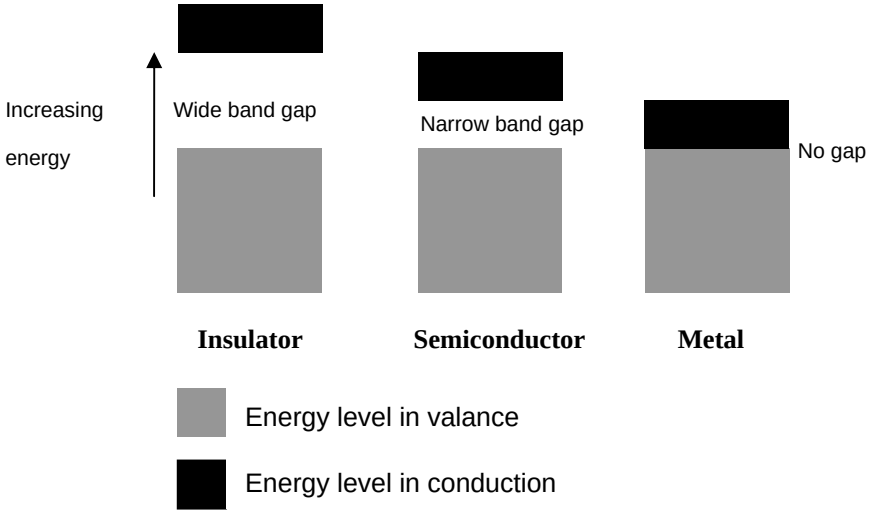

Figure 1-5 Band picture for an insulator, a semiconductor and a metal (conductor).

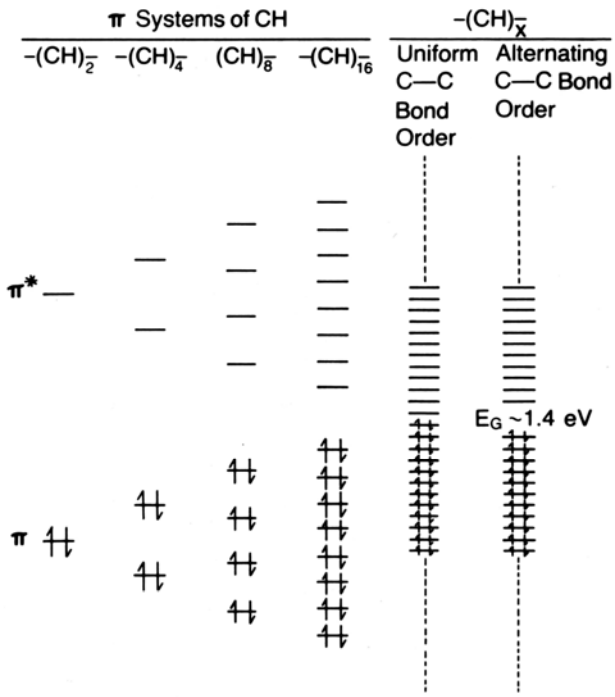

Figure 1-6 Diagrammatic representation of the energy levels of π molecular obritals with increasing size of the molecule for $(CH)_x$.

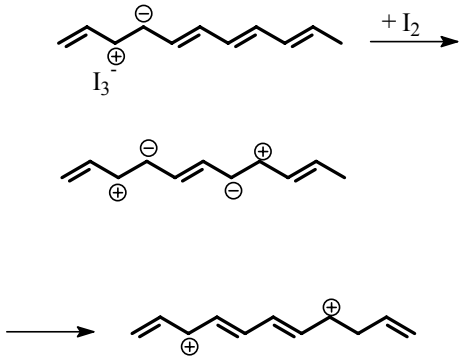

Figure 1-7. Illustration of the formation of bipolaron.

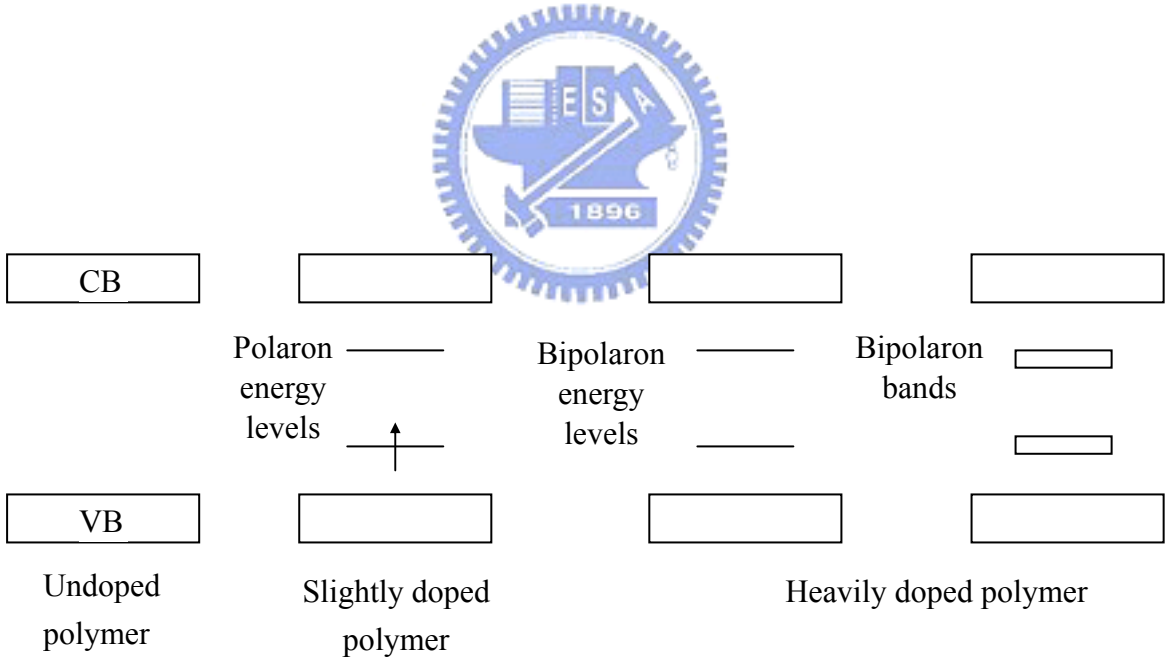

Figure 1-8. The energy level of polaron and bipolaron.

1.2.2 Fluorescence and Phosphorescence

In most cases, conjugated polymers present broad, inhomogeneous optical absorption bands. This broadness is originated from distribution of chain lengths, chain conformation, or defects. In other words, the broad absorption spectrum reflects the distribution of conjugation lengths. By definition, the absorption edge at the high wavelength end corresponds to the absorption by entities of the longest conjugation lengths, and therefore approximates the band gap of the system. Basically, we can use Jabłoński diagram (Figure 1-9) to explain the mechanism of fluorescence and phosphorescence.[17] The diagram presents the molecular electronic and vibrational energy levels; the singlet ground, first and second electronic states are denoted by S_0, S_1, and S_2 respectively, and in any electronic state there exists a number of vibrational energy levels. These are denoted by 0, 1, 2, etc. The singlet ground state (S_0) means that even number of electrons occupying two by two and spin-paired (↑↓) at the lowest molecular orbitals for most stable molecules. When the fluorescent molecules absorb ultraviolet or visible light, the electron in the ground state will be excited to the higher vibrational energy level of either S_1 or S_2. The spin state of electron in the excited state is still anti-parallel to its paired electron in the ground state. The molecules in the excited electronic state (S_1 or S_2) usually relax to the lowest vibrational energy level ($\nu = 0$) due to molecular collisions. The vibrational energy can be transformed into thermal energy or transferred to other molecules because of molecular collisions. This process is called "internal conversion" and generally occurs in 10^{-12} second or less. The electron in the lowest-energy vibrational state of S_1 or S_2 returns to the ground state S_0, leading to the radiation emission called fluorescence with lifetimes typically near 10^{-8} second.

In addition to the singlet state, a triplet state (T_1) is defined as the spin state of the excited electron being parallel to its paired electron (↑↑). The mechanism of

phosphorescence is similar to fluorescence except for the process of emission. The electrons in the phosphorescent molecules are also excited to the singlet excited state when they absorb light. But as the energy of an excited triplet state overlaps the excited singlet state, the electron in the excited singlet state may convert its spin state to the triplet state. This spin conversion process is called “intersystem crossing”. Emission from T_1 is generally shifted to longer wavelengths (lower energy) relative to the fluorescence.

Occasionally, energy of the excited state could be lost because the excited molecules may interact with the unexcited molecules and solvents by collision. Energy will be released in the form of heat and this phenomenon is called “external conversion”.

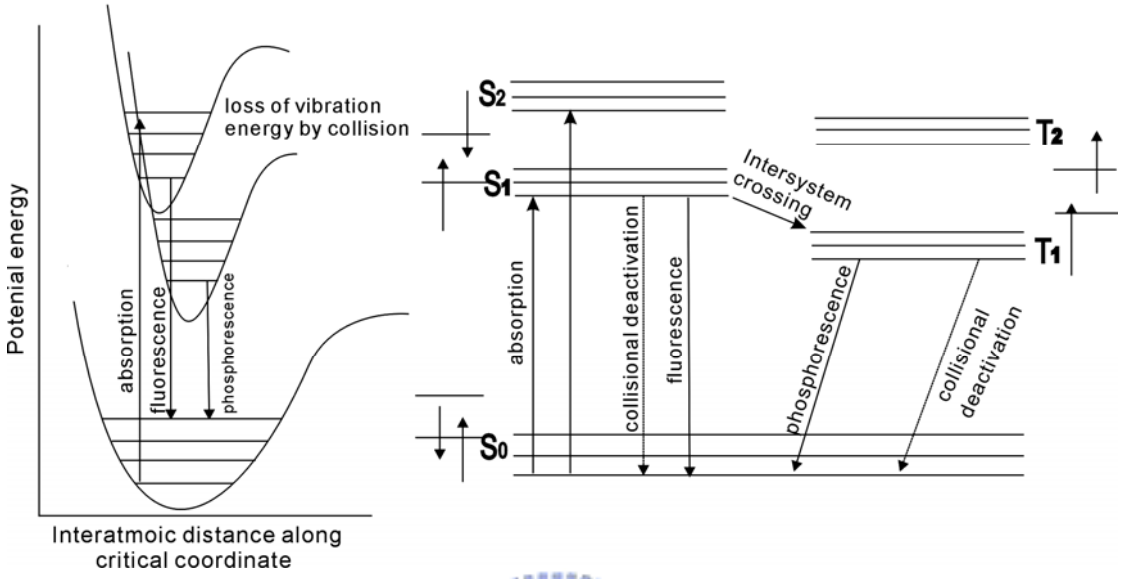

Figure 1-9. A typical Jabłoński diagram.

1.2.3 Aggregate and Energy Transfer

The definition of aggregate in conjugated polymers is not very clear and is still controversial. It is generally accepted that the ground state and excited state wave functions are delocalized over one or more chromophores in the same chain or different chains of polymer.[18] In other words, aggregate means the conjugated system is extended from several single chromophores to re-hybridize to form new species having their own ground state and/or excited state. Therefore aggregate can be excited directly and emit light at the longer wavelength because of the extension of conjugated system.[19, 20]

In 1995, Köhler et al. have found that ladder-type poly-(paraphenylene) (LPPP) may form aggregates in the film for photovoltaic devices.[21] Besides the photocurrent in the blue spectral range (higher energy) associated with intra-chain absorption, the yellow part of the spectrum (lower energy) was also observed. The weak absorption of this part was also observed by UV. They have proposed that the aggregates formed over several aggregated polymer chains exist in the polymer film, and energy transfer from intra-chain chromophore into aggregates would happen and affect the dynamics of excitations in the solid film.[22]

In 1996, Blatchford et al. used poly(p-pyridyl vinylene) (PPyV) as the model conjugated polymer to investigate its photophysics and find the relation between photophysics and film morphology.[23, 24] They have found that PPyV could form aggregates in the bulk state. The PL spectra for PPyV film is red-shifted by about 100nm versus the solution state and is featureless. The emission efficiency is also reduced in the film relative to that in solution. Some species formed through interchain interactions, such as aggregates, excimers, and exciplexes was adopted to explain these observations. Excimers and exciplexes are only stable in the excited state, so they can not be excited directly from the ground state. From the absorption

and PLE spectra, the new species possessing lower-energy state has been found to exist in the polymer films. Consequently, the formation of excimers has been ruled out. The absorption spectrum shows the evidence of extra lower-energy absorption in the film. However, the PLE spectrum of the film is dramatically different from that of the solution. The peak position where the solution absorbs is essentially zero. If only one chromophore exists, the UV and PLE spectra should be similar. Since the new species may be excited directly and recorded by PLE, PLE spectrum will differ from the UV spectrum. By comparing the analysis of spectra, they suggested that aggregates form in the polymer film.

So far formation of aggregates has been established for the polymer films only. In the case of the dilute solution used for film casting, where the polymer concentration may be too low for inter-chain interactions, it is usually believed that the polymer can be dissolved down to the molecular level in the solvent. However, some recent studies have revealed that interchain interaction depends not only upon the polymer concentration but also upon the solvent quality. Hsu et al. used poor solvent to induce the aggregation of poly(2,5-dioctyloxy p-phenylene vinylene) (DOO-PPV) in dilute solution.[25] The solubility of DOO-PPV in toluene could be varied at temperatures between 10 and 80℃. Lowering the temperature reduce the solubility and hence induce the interchain interactions. These interchain interactions are likely to led to the formation of dimer-like aggregates as suggested from the UV spectra.

Energy transfer is indeed observed in nature, such as photosynthesis is plants, where the excitation energy is released from one species at higher energy state to another at the lower energy state.[26] Polymers with a high density of lumophores also have this feature where energy is transferred intramolecularly or intermolecularly between different lumophores.

Schwartz et al. prepared a polymer composite to control the energy transfer by

changing the conformational of MEH-PPV.[27] MEH-PPV was placed in the hexagonally arrayed channels of mesoporous silica glass. They have found that energy could be transferred from aggregates outside the pores to isolated, aligned single polymer chains within the pores which are at lower energy due to extension of the conjugation length.

In conjugated polymers such as PPVs, randomly distributed tetrahedral defects are unavoidably introduced during the Gilch-type polymerization[28] or from incomplete elimination of the Wesslin-type precursor polymer.[29] These synthetic methods inevitably affect the distribution of tetrahedral defects and interrupt conjugations along the polymer chains. In this case energy is found to be transferred from shorter to longer conjugated segments.[29] Therefore it is difficult to identify energy transfer mechanism in fully conjugated polymers.

Peng et al. used poly(distyrylbenzene) poly(DSB) as a model compound with fixed conjugation length[30] to investigate energy transfer mechanism. They have found that lumophore interactions exist at both dilute and concentrated solutions. In dilute solutions, lumophore interactions are owing to intramolecular aggregates while intermolecular aggregates were formed in concentrated solutions and films. The intermolecular aggregates can be further classified into loose, compact, and the most aligned aggregates. Energy has been found to be transferred from individual lumophores to the most aligned aggregates via loose and compact aggregates (Figure 1-10). Using this proposed energy transfer model, one may explain the relation between polymer morphology and photophysics of electroluminescent polymers.

Recently, Schwartz et al. and Yang et al. have investigated the effects of a series of variables, such as concentration and solvent, on the photophysics of MEH-PPV in solution state and in the solvent-cast films.[31-34] The processing conditions of spin casting and thermal annealing have also been considered. By adjusting these variables,

they could control the degree of aggregation in solution state and revealed a memory effect where the solution structure was transferred to the film during spin or drop casting processes. Schwartz et al. have shown that the conformation of MEH-PPV varies greatly in different solvents. MEH-PPV chains dissolved in chlorobenzene (CB) are found to be more extended than those in tetrahydrofuran (THF), therefore, the concentration of aggregates formed in CB is larger than that in THF due to easier chain packing. Yang et al. proposed that the aggregation of MEH-PPV molecules in aromatic solvents, such as CB and toluene, resulted in aromatic polymer backbone facing the solvent, while the side chains pointing inwards toward each other because this type of solvent was poor for the side chains. In nonaromatic solvents, such as chloroform and THF, the aromatic polymer backbone exhibited a twisted conformation which decreased the conjugation length. In the solvent-cast process, the structure in the solution may be transferred into the film; therefore, different solvents used may result in different polymer film morphology and hence different photophysical and electroluminescent properties. In addition to the solvent quality, the solution concentrations may also affect the solution structure. The extent of aggregation increased with increasing concentrations and the concentration for loose aggregate formation (CLA) in MEH-PPV solution where the polymer chains started to penetrate into each other and entangled to form intermolecular aggregates has been identified.

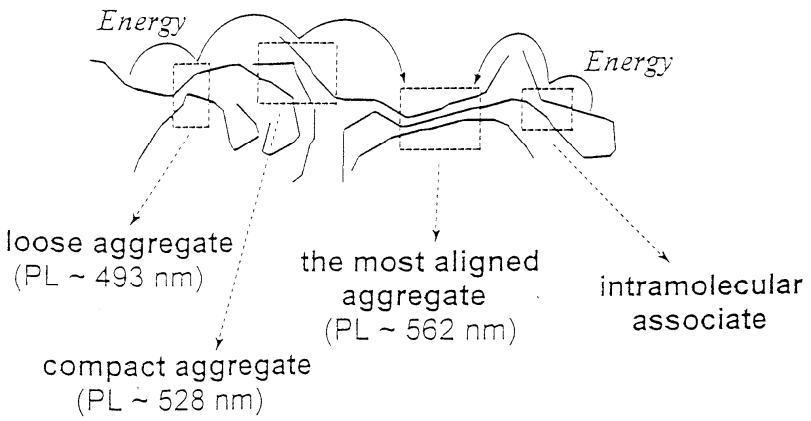

Figure 1-10. Diagram for energy transfer between different extents of aggregations.

1.3 Hairy-rod Polymer

As has been pointed out, the semi-rigid backbones of conjugated polymers are usually grafted with short flexible side chains to enhance the solubilities of the polymers in common organic solvents for device fabrication. In a coarse-grained picture, the segments of these polymers may be represented by the “hairy rods” and the polymers may be called the “hairy-rod polymers”.

A hairy-rod polymer is indeed one of the representatives of the comb polymer famil.[35-38] In general rigid-rod polymers do not melt and dissolve only poorly, if at all, in common solvents due to a strong aggregation tendency and a small gain of conformational entropy upon dissolution or melting. By covalent connection of substituent groups (notably flexible alkyl chains) to the backbone, a system is achieved where the semi-rigid polymer can be regarded to dissolve in the background of the side chains due to the attractive interaction between the solvent molecules and the backbone. This causes melting point depression without loss of rigidity of the backbone.[39]

The concepts of self-organization and improved solubility for these polymers of semi-rigid backbone and covalently bonded flexible side chains have gained firm footing. Supramolecular hairy-rod polymers self-organize through the side groups connected to the backbone by physical bonds.[40, 41] As with other block copolymers, they also tend to self-organize to form nanoscale structure in bulk and in solutions. The electrical conductivity of such architectures has received a lot of attention, since the backbones consist of conjugated polymers. Besides block copolymeric self-organization, there is an even more important reason why semi-rigid polymers have attracted so much interest, which is the ability of these polymers to form liquid crystalline phases.

Rigid rodlike and semi-rigid polymers can form lyotropic (in concentrated solution within a specific concentration range) or thermotropic (in the bulk state at certain temperatures) liquid-crystalline mesophases. In the liquid-crystalline state, cooperative interactions will enhance the influence of even weaker forces. A high degree of order can thus be induced in them by some interaction with an external agent, for example, the interaction between an external electric field and molecular dipole moments, diamagnetic anisotropy and strong magnetic fields, interactions with a planar surface or inhomogeneous flow pattern. Therefore, understanding the phase behavior of rigid-rod polymers[42] is important to design liquid crystallinity,[43, 44] which allows facile alignment of the otherwise crystalline infusible and intractable polymers. With conjugated polymers,[45] the alignment results in anisotropy of their optical and electronic properties. The alignment of conjugated polymers in thin films can also result in completely new structural features[46] compared to the bulk. Introduction of specific side chains, such as enantiomerically pure side chains, that result in rich photonic phenomena, such as circularly polarized luminescence,[47] provide another domain for their structural investigation. Such studies have elucidated the formation of a highly ordered phase in solution where the excited state splits into two exciton levels.

1.4 Self-Assembly

The phase behavior of conjugated polymers in bulk and solution state is closely related to the "self-assembly" process. Self-assembly is the fundamental principle which generates structural organization on all scales from molecules to galaxies. (*cf.* Figure 1-11) It is defined as a reversible processes in which pre-existing parts or disordered components of a system form structures of patterns. Self-assembly can be classified as either static or dynamic.[48] In static self-assembly the ordered state occurs when the system is in equilibrium and does not dissipate energy. Dynamic self-assembly, on the other hand requires dissipation of energy of the ordered state. Examples of self-assembling systems include weather patterns, solar system, histogenesis and self-assembled monolayers (table 1-1). The most well-studied subfield of self-assembly is molecular self-assembly. Molecular self-assembly is the assembly of molecules without guidance or management from an outside source. There are two types of such self-assembly, intramolecular self-assembly and intermolecular self-assembly. Intramolecular self-assembling molecules are often complex polymers with the ability to assemble from the random coil conformation into a well-defined stable structure. An example of intramolecular self-assembly is protein folding.[49] Intermolecular self-assembly is the ability of molecules to form supramolecular structures. A simple example is the formation of micelles by surfactant molecules in solution. [50] Self-assembly can occur spontaneously in nature, for example in cells (such as the self-assembly of the lipid bilayer membrane[51]) and other biological systems, as well as in human engineered systems such as a Langmuir monolayer. It usually results in the increase in internal organization of the system. Biological self-assembling systems, including synthetically engineered self-assembling peptides and other biomaterials, have been shown to have superior

handling, biocompatibility and functionality. These advantages are due to direct self-assembly from biocompatible precursors creating biomaterials engineered at the nano-scale.

Also, self-assembly is a manufacturing method used to construct things at the microscale, which is comprised of structures with at least one dimension that is less than 100 microns. Many systems use self-assembly to assemble various molecules and structures.[52-54] Imitating these strategies and creating novel molecules with the ability to self-assemble into supramolecular assemblies is an important technique in nanotechnology. In self-assembly the final structure is ”encoded” in the shape and properties of the molecules that are used, as compared to traditional techniques, such as lithography, where the desired final structure must be carved out from a larger block of matter. Self-assembly is thus referred to as a 'bottom-up' manufacturing technique, as compared to lithography being a 'top-down' technique. An example of self-assembly in nature is the way that hydrophilic and hydrophobic interaction cause molecules to self assemble. Molecular self-assembly is a strategy for nanofabrication that involves designing molecules and supramolecular entities so that shape-complementarity causes them to aggregate into desired structures. Self-assembly hence has became a rapidly growing part of organic field for two reason: first, it is a concept that is crucial to understand many structures important in biology and second, it is one solution to the problem of synthesizing structures larger than molecules. Self-assembly also poses a number of substantial intellectual challenges. The brief summary of these challenges is that we do not yet know how to do it, and cannot even mimic those processes known to occur in biological systems at other than quite elementary levels. Although there are countless examples of self-assembly all around us – from molecular crystals to mammals - the basic rules that govern these assemblies are not understood in useful detail, and self-assembling

processes cannot, in general, be designed and carried out "to order". Many of the ideas that are crucial to the development of this area – “molecular shape”, the interplay between enthalpy and entropy, nature of non-covalent forces that connect the particles in self-assembled molecular aggregates – are simply not yet under the control of investigators. The design of components that organize themselves into desired final patterns and functions is the key to applications of self-assembly. The components must be able to move with respect to one another. Their steady-state positions balance attractions and repulsions. Although self-assembly originated in the study of molecules, it is a strategy that applicable at all scales. Molecular self-assembly involves non-covalent force or weak covalent interactions (i.e. van der Waals, electrostatic, and hydrophobic interactions, hydrogen and coordination bonds). In the self-assembly of larger components – meso- or macroscopic objects – interactions can often be selected and tailored, and can include interactions such as gravitational attraction, external electromagnetic fields, and magnetic, capillary, and entropic interactions, which are not important in the case of molecules. Larger molecules, molecular aggregates, and forms of organized matter more extensive than molecules cannot be synthesized bond-by-bond. Self-assembly is one strategy for organizing matter on these larger scales. By utilizing interactions as diverse as aromatic $\pi - \pi$ stacking and metal-ligand coordination for the information source for assembly processes, chemists in the last decade have begun to construct nanoscale structures and superstructures with a variety of forms and functions. Therefore, self-assembly necessarily play the important role of nanoscale science in future.

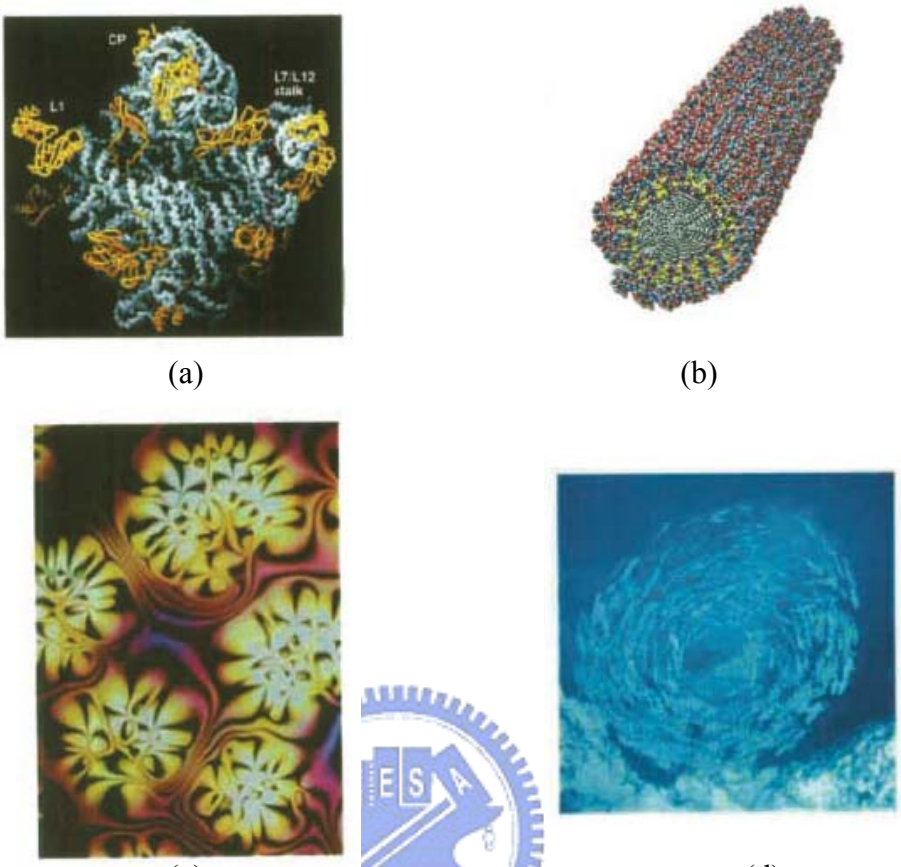

(a) (b)

(c) (d)

Figure 1-11. Example of self-assembly (a) Crystal structure of ribosome. (b) self-assembly of peptide-amphiphile nanofibers. (c) Thin film of a nematic liquid crystal on an isotropic substrate. (d) A school of fish (dymanic self-assembly).

Table 1-1. Examples of self-assembly

System	Type	Applications/importance	References
Atomic, ionic, and molecular crystals	S	Materials, optoelectronics	(*1, 4, 5*)
Phase-separated and ionic layered polymers	S		(*19*)
Self-assembled monolayers (SAMs)	S, T	Microfabrication, sensors, nanoelectronics	(*8*)
Lipid bilayers and black lipid films	S	Biomembranes, emulsions	(*20*)
Liquid crystals	S	Displays	(*21*)
Colloidal crystals	S	Band gap materials, molecular sieves	(*9, 18*)
Bubble rafts	S	Models of crack propagation	(*22*)
Macro- and mesoscopic structures (MESA)	S or D, T	Electronic circuits	(*14–16*)
Fluidic self-assembly	S, T	Microfabrication	(*23*)
"Light matter"	D, T		(*10*)
Oscillating and reaction-diffusion reactions	D	Biological oscillations	(*6, 7*)
Bacterial colonies	D, B		(*11*)
Swarms (ants) and schools (fish)	D, B	New models for computation/optimization	(*12, 13*)
Weather patterns	D		(*1*)
Solar systems	D		
Galaxies	D		

(S: static, D: dynamic, T: templated, B: biological)

1.5 Small-Angle Scattering[55-57]

The small-angle scattering (SAS) technique is a method for determining structure on a length scale from 10 Å or larger. SAS experiments give an intensity distribution in reciprocal space and usually considerable effort has to be invested in the data analysis in order to obtain the corresponding real-space structure. Information on such relatively large-scale structure is contained in the intensity of the scattered x-ray or neutrons at small angels, typically at 2θ less than 2°. However, all the methods developed for the analysis of wide-angle data are applicable to the analysis of small-angle data as well. In addition, there are theoretical results that have been developed specifically for the analysis of small-angle data. These incorporate some additional assumptions about the nature of the sample or some additional approximations applicable only to small-angle scattering. For example, in small-angle scattering, $\sin\theta$ can always be approximated by θ. Similarly, in discussing the structure of a sample, any details of size scale less than about 10 Å are usually assumed not to exist. Such a practice corresponds to ignoring any scattering intensity observable at 2θ larger than a few degrees and performing the analysis on data observed in the small-angle region only. The scattering intensity $I(q)$ can always be calculated from a knowledge of structure or the scattering length distribution $\rho(r)$ in the sample, but the reverse is not in the true space. In other words, the inverse Fourier transform operation applied to the observed $I(q)$ merely leads to the autocorrelation function $\Gamma_\rho(r)$, from which there is no efficient way to recover $\rho(r)$. Scientists usually seek direct interpretation of either $I(q)$ or $\Gamma_\rho(r)$ in terms of a reasonable model, chosen on the basis of some additional information, as may be available from other physical measurements. Most of the models that are adopted in practice for analysis of

small-angle data belong to one of the following:

1. *The dilute particulate system*: When the concentration of the particles is sufficiently dilute, the positions of individual particles are uncorrelated to each other. For particles of well-defined geometry, the size of the particle may be determined from the scattering intensity profiles. For the particles with irregular or unknown shapes, the average R_g may be determined conveniently using the low-q intensity via the "Guinier's law".

2. *The nonparticulate two-phase system:* The two "phases" could be the different phases of a single material in a true thermodynamic sense, such as the crystalline and amorphous phases in a semicrystalline polymer. The analysis of the scattering from such a system leads to determination of parameters characterizing the state of dispersion of the materials in the samples. And,

3. *The periodic system:* For example, semicrystalline polymers consisting of stacks of lamellar crystals and block copolymers having ordered, segregated microdomains. The methods developed for the analysis of wide-angle diffraction from crystalline solids are directly applicable to such periodic systems.

1.6 Scattering of polymers in solutions

In amorphous media, the interference of the incident wave with the heterogeneities in the material provides structural information. These heterogeneities may be several to hundreds of radiation wavelengths long. In the amorphous polymers and polymer solutions, structural information such as the concentration fluctuation, shape and size, number of objects, and long-range correlation is expressed in the scattering patterns at small angles. The scattering of polymers shows different dimensions, depending on the q range of the measurement and its relation to the dimension of the polymer. q is the scattering vector, which is defined as[55, 56, 58]:

$$q = \frac{4\pi}{\lambda}\sin(\frac{\theta}{2}) \qquad (1)$$

where θ is the scattering angel with respect to the incident beam path. Figure 1-12 presents a schematic representation of different length scales in a solvated polymer as a function of the relation between q, the persistence length (l_p), and the radius of gyration (R_g) of the polymers. The scattering data reveal a series of different regimes with a behavior characteristic of the various length scales of the polymer chains. The exact dimensions depend on the molecular weight of the polymer and its interactions with the environment. If the polymers are fully solvated, at small q at which qR_g approaches 0, each polymer molecule forms a random coil that is viewed as a center of mass. With increasing q, at which q^{-1} is greater than R_g, the entire dimension of the coil is observed, and R_g is measured. The scattered intensity I(q) becomes insensitive to structural details and is dominated by the finite overall length of the particles, and we can determine the radius of gyration R_g of the particles. This region is the so-called Guinier regime and the corresponding size of the coil is well

described by Guinier approximation.[59, 60] Further increase of q to $l_p < q^{-1} < R_g$ (i.e l_p: persistence length) results in an insight into the segmental distribution within the coil. I(q) becomes much sensitive to the local aggregate structure, and polymer theory for flexible polymer coils predicts that I(q) should decay with a power-law of the form I(q) ~ $q^{-\alpha}$, where α = 1.66 for a wormlike chain behavior and 2.0 for an ideal random walk chain (Gaussian coil). Finally, for $q^{-1} << l_p$, I(q) is controlled by distances over which polymers are rod-like rather than flexible, and we expect a crossover an asymptotic q^{-1}-dependence for I(q) which is typical for locally cylindrical structures. However, a real polymer is not an infinitely thin chain. Therefore, at large values of q, the local cross sectional structure of the chains give rise to a cross section Guinier behavior and a strong decrease in the scattering intensity at still large q value (*cf.* Figure 1-13). Therefore, tuning the q range of the measurement allows us to focus on different length scales.

Study the structures of these complex fluids requires probing dimensions from several angstroms to the nanometer length scale, at which individual polymer molecules can be detected, to the 100 nm range, at which the aggregates and correlations within networks can be observed. The technique must also be sensitive to small changes in the amorphous media. With the natural difference in the scattering length densities of hydrogen and deuterium and in the scattering length densities of hydrogen and fluorine, small-angle neutron scattering (SANS) has been at the core of the investigation of structure and association in polymer solutions. In general, the scattering intensity in solution state as a function of q can be expressed by: [55-57]

$$I(q) = AI_0 N_p V_p^{\,2} (\Delta\rho)^2 P(q) S(q) + B_{incoh} \qquad (.2)$$

where I_0 is the intensity of the incident beam and A is a constant that encapsulates instrumental factors. N_p is the number concentration of scattering objects, V_p is the

volume of one scattering particle, $(\Delta\rho)^2$ is the scattering length density (SLD) between particles and solvents. *P(q)* is the form factor which describes the scattering interference of a single particle. *S(q)* is the scattering factor, describing the interference between scattering from different objects. B_{incoh} is the incoherent background of scattering.

In extremely dilute polymer solutions, different macromolecules do not overlap and their physical properties may be considered as single chain properties. As the concentration is increased, the volume fraction occupied by the chains in the solution becomes larger and interchain interactions are more and more relevant. As log as the volume fraction occupied by the chains is much smaller than one, the solutions may be considered as a gas of chains interacting essentially as hard spheres (in good solvent). When the volume fraction occupied by the chains is of the order of one, the chains start to overlap and one cannot consider them individually; their behavior becomes cooperative. The chains are in the semi-dilute regime where they start to overlap with each other and make a dilute network in the solvent. For many purposes, an equivalent semi-dilute polymer solution can thus serve as a guide and a reference in the understanding of the physical properties of polymeric gels.

1.7 Fractals

The concept of fractal geometry[61] has emerged as an essential concept for characterizing disordered materials. Further, kinetic-growth models have aided in the elucidation of the chemical and physical processes occurring in many complex system such as silicates. (*cf.* Figure 1-14) [62-64] Fractals are objects, usually disordered, of non-integral or fractional dimension,[61] and scattering data[63, 64] are now routinely interpreted using concepts of fractal geometry.

Fractals can be characterized by scattering techniques. Figure 1-15 display a collection of model structures and the result of small-angle scattering from them. The mass fractal dimension of an object can be directly determined in a scattering pattern through the application of mass fractal power-law. Using this laws, an object of mass fractal dimension d_m display a power-law described by[64]

$$I(q) \sim q^{-d_m} \quad (1 \leq d_m < 3) \tag{3}$$

A power-law of -2 is expected for the Gaussian regime. In general, the smaller the value of d_m the more open in the structure of the fractal object. As the value is reduces to 1.0, the object becomes a rod. At the length scale of the primary particle size, the power law becomes dominated by surface fractal.[62-64] Therefore, the scattering intensity can be summarized by the surface fractal power-law:

$$I(q) \sim q^{-(6-d_s)} \quad (2 \leq d_s \leq 3) \tag{4}$$

The value $d_S = 2$ corresponds to a smooth surface, while $d_S = 3$ corresponds to extreme roughness.

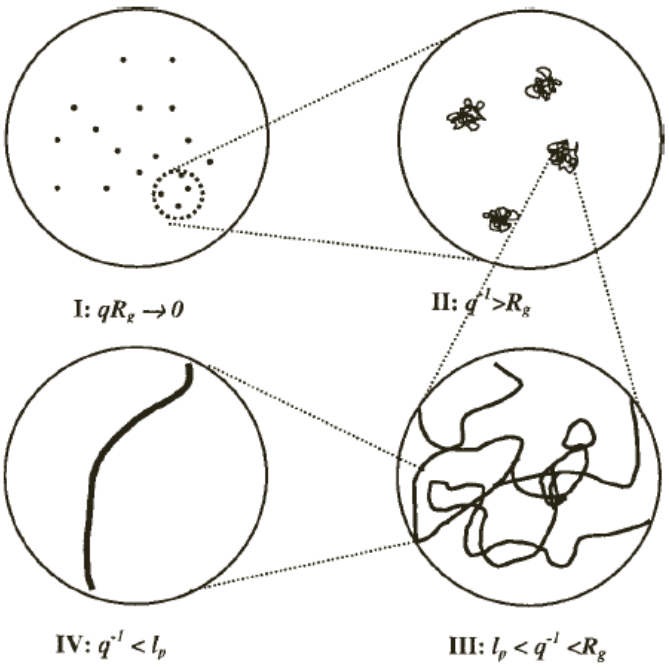

Figure 1-12 Schematic representation of the part of the polymer viewed at different length scales.

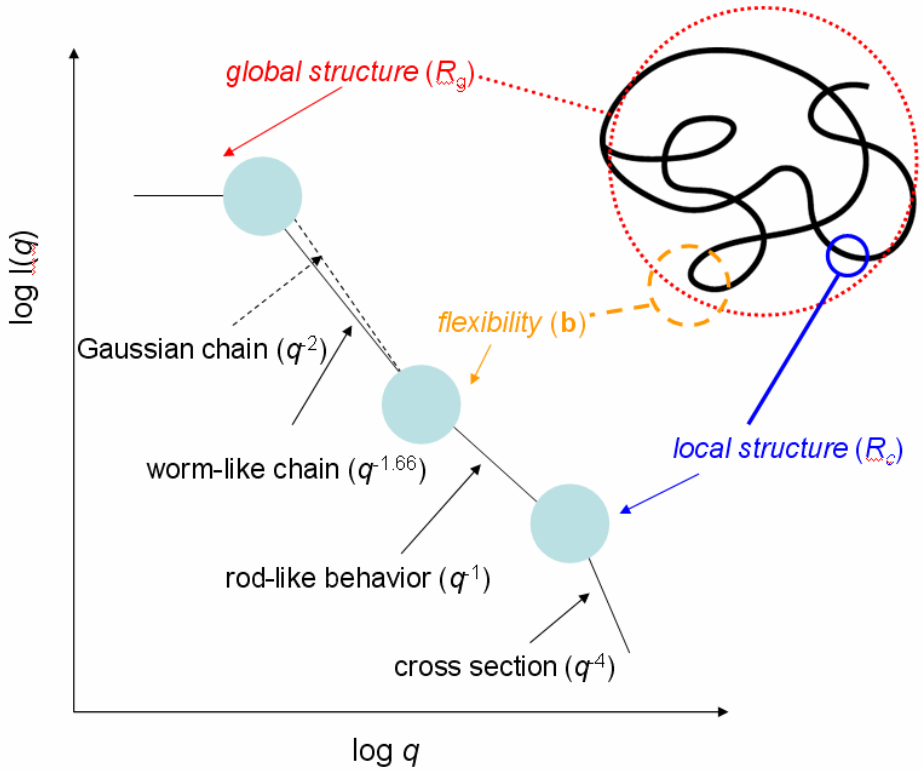

Figure 1-13 A schematic representation of the different asymptotic regions for the q-dependence of a s wormlike chain and their link to the different chain

conformation on various length scales.

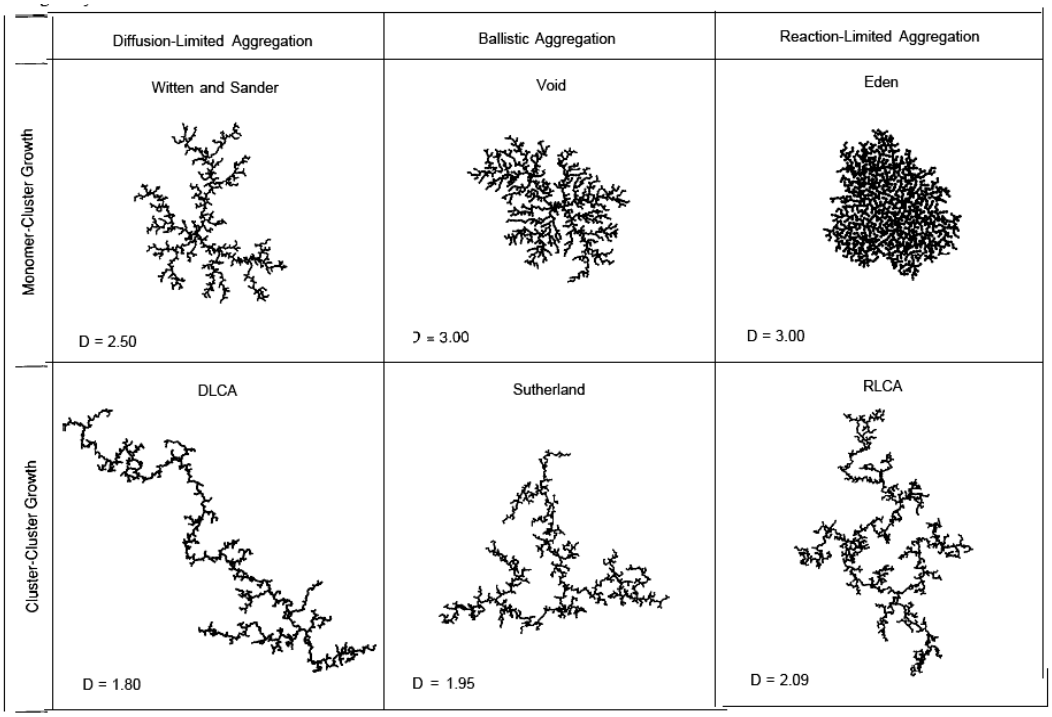

Figure 1-14 Computer simulated non-equilibrium growth processes produce three-dimensional structures with characteristic mass fractal dimensions.

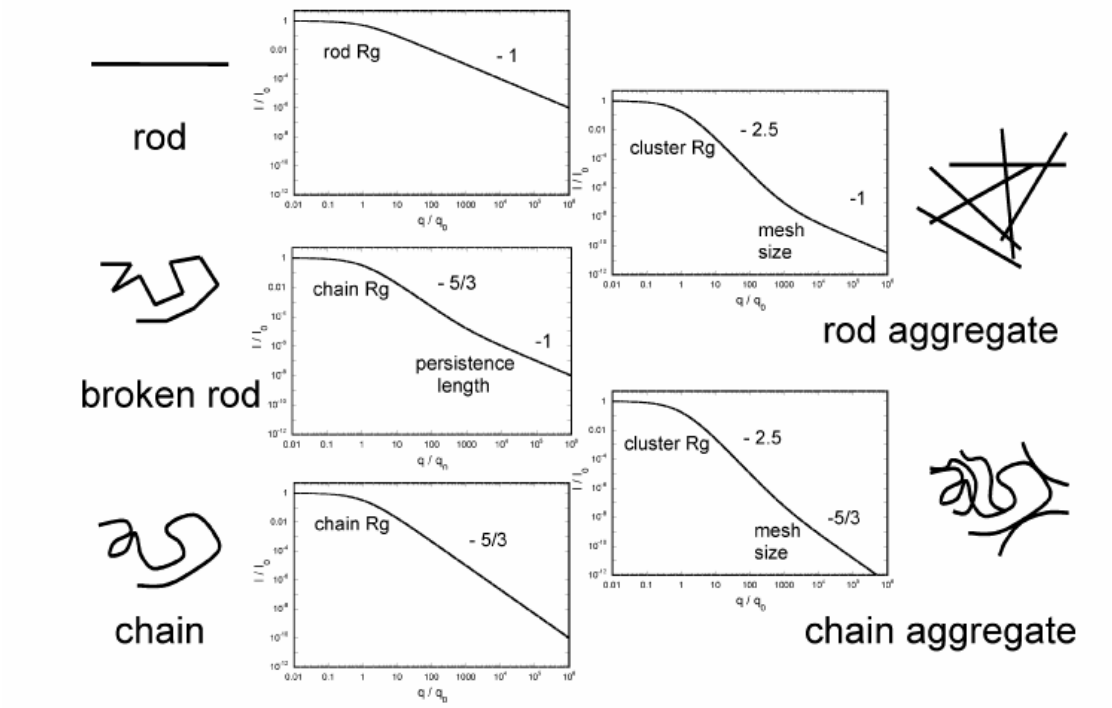

Figure 1-15 Illustration of power-law scattering from fractal objects.

1.8 The Motivations and Overview of the Study

Rigid and semi-rigid polymers may exhibit rich phase behavior compared with fexible polymers due to their intrinsically anisotropic molecular shape that leads to the formation of mesophases. [65-69] For a flexible polymer, the conformation of the chain is governed by its degree of polymerization and its interaction with the immediate surrounding.[70, 71] With the increase of the persistent length, the chain rigidity becomes a significant factor in the collective behavior. The stiffness may affect the viscosity of the solution and may induce phase separation, gelation and liquid crystallinity.[72-74] Another unique property of stiff polymers lies in the tendency of the polymer to aggregate in solvents even under large dilution.[31, 75, 76] Such an aggregation behavior still remains relatively unexplored.

Conjugated polymers constitute a family of semi-rigid polymer which have found great potential in opto-electronic applications due to their unique semiconducting properties and solution processability. Poly(phenylenevinylene) (PPV) and its derivates are one of the most important classes of conjugated polymers for light-emitting diode application. To facilitate the device processing using spin or drop casting techniques, the conjugated backbone of PPV is usually attached with short flexible side chains to endow them the nominal solubility in common organic solvents.

The solutions of light-emitting polymers are usually homogeneous in appearance; however, their conjugated segments may exhibit some extent of aggregation in the solution and such an aggregation may exert a dramatic impact on the photophysical properties of the polymer in the solution. The dispersion state of the polymer in the solution, governed by the solvent quality, concentration and temperature, further

influences the morphology and hence the photophysical properties of the light-emitting film formed after solvent removal. Yang et al.[33] reported that the threshold for gain narrowing of films prepared with tetrahydrofuran (THF) was lower than that of films prepared using chlorobenzene and p-xylene. Baltchford et al. [31] revealed different photoluminescent (PL) spectra for films prepared from different solvents. Recently, Chen et al. have found that the mesomorphic structure and the associated PL at 640 nm of MEH-PPV film were suppressed by prolonged aging of the solution used for the film preparation.[77] These instances indicate a solution-phase controlled morphology and photo-physics as the structure of the as-cast film is metastable presumably due to the fast solvent removal and the sluggish mobility of the stiff conjugated chains that prevent the polymer from attaining its equilibrium morphology during solvent casting. As a consequence, resolving the solution structure of light-emitting polymers is important not only for understanding the basic dissolution behavior of semirigid or rigid polymers but also for effectively tailoring the photophysical performance of their cast films.

This thesis centers on the studies of the conformational structures and aggregation behavior of two poly(diphenyl phenylenevinylene)s (DP-PPV) bearing different side chains in the solution states. DP-PPVs are attractive green-emitting materials for PLED application due to their high glass transition temperatures, high fluorescence efficiencies and ease of monomer and polymer syntheses[26-29] Here we intend to reveal the effects of side chain length, solvent quality, concentration and temperature on the aggregation behavior of DP-PPVs in the solutions. We employ small angle neutron scattering (SANS) as the major tool for resolving the solution structures. SANS is known as a powerful tool for characterizing the conformational structure and aggregation behavior of macromolecules in solutions[55, 56]. This technique makes use of the distinct contrast in neutron scattering length between

deuterated (d-) solvent and hydrogenous polymer (or vice versa), which offers decent scattering intensity and effectively reduces the incoherent background for probing the solution structure at relatively low polymer concentration. SANS can effectively complement the conventional spectroscopic techniques such as photoluminescence spectroscopy where the attribution of the lower-energy emission to the presence of aggregates is sometimes complicated by other emission species such as excimers and chemical defects.

In Chapter 2, we revealed that the inter-chain aggregation of poly(2,3-diphenyl-5-hexyl-1,4- phenylenevinylene) (DP6-PPV) bearing a hexyl side chain per monomer unit in the solutions with chloroform and toluene generated network aggregates with the hydrodynamic radii of several μm. SANS demonstrated that the internal structure of these aggregates could be characterized by the mass fractal dimensions of 2.2 ~ 2.7. The networks were looser in chloroform but became highly compact in the poorer toluene solvent due to severe segmental association. Increasing the temperature alleviated the segmental association in toluene while largely retaining the mass fractal dimension of the aggregates. However, the inter-chain aggregation was never completely dissipated by the heating, suggesting the existence of two types of segmental association with distinct stability. The highly stable segmental association that could neither be solvated by chloroform nor be disrupted thermally in toluene was attributed to the π-π complex already present in the DP6-PPV powder used for the solution preparation. The chains tied firmly by this complex formed network aggregates in the solution and hence reduced the entropy of mixing of the polymer. In the poorer toluene solvent further segmental association took place within the pre-existing aggregates, making the networks more compact. This type of segmental association could be disrupted by moderate heating and its occurrence was ascribed to the poor affinity of the aliphatic

side chains of DP6-PPV to toluene.

In Chapter 3, we proceeded to to reveal the conformational structure and the aggregation behavior of another DP-PPV, poly(2,3-diphenyl-5-decyl-1,4-phenylenevinylene) (DP10-PPV), which bears a longer decyl side chain per monomer unit. The results obtained here, in conjunction with those in Chapter 2 for DP6-PPV, were useful for revealing the effect of side chain length on the dissolution behavior of DP-PPVs. We showed that DP10-PPV displayed a weaker tendency toward aggregation than DP6-PPV. In chloroform DP10-PPV chains were well dispersed and exhibited the expanded wormlike chain conformation with the persistent length increasing with overall polymer concentration. Like DP6-PPV, DP10-PPV chains aggregated significantly in toluene to form aggregates of several μm in size. The internal structure of the aggregates was characterized by a mass fractal dimension of 1.3 at the overall polymer concentration of 0.1 wt%, indicating that the aggregates had a rather opened structure. Compact disklike domains developed within the aggregates as the concentration was increased to 0.5 wt% and 1.0 wt%. The thickness of the disk domains determined from the Kratky-Porod approximation was ca. 20 Å, implying that the domains consisted of two layers of DP10-PPV chains lying parallel to the domain surface.

References

1. Chiang, C. K.; Fincher, Jr. C. R.; Park, Y. W.; Heeger, A. J.; Shirakawa, H.; Louis E. J.; Gau, S. C.; and MacDiarmid, A. G.. *Phys. Rev. Lett.* **1977**, 39, 1098.

2. Shiakawa, H.; Louis, E. J.; MacDiarmid, A. G.; Chiang, C. K.; Heeger, A. J. *J. Chem. Soc. Chem. Commun.* **1977**, 578.

3. Nalwa, H. S. *Handbllk of Organic Conductive Molecules and Polymers*. Wiley: New York, **1997.**

4. Tang, C. W.; Van Slyke, S. A. *Appl. Phys. Lett.* 1987, 51, 913.

5. Burroughes, J. H.; Bradly, D. D. C.; Brown, A. R.; Marks, R. N.; Mackay, K. Friend, R. H.; Burns, P. L.; Holmes, A. B. *Nature* **1990**, *347*, 539.

6. Gruner, J.; Cacialli, F.; Friend, R. H. *J. Appl. Phys.* **1996**, 80, 207.

7. Wessling R.; Zimmerman R. U.S. Patent 3,401,152 **1968.**

8. Wessling R.; Zimmerman R. U.S. Patent 3,706,677 **1972**.

9. Wessling, R. *J. Polym. Sci. Polym. Symp.* **1985**, 72, 55.

10. Friend, R. H.; Gymer, R. W.; Holmes, A. B.; Burroughes, J. H.; Marks, R. N.; Taliani, C.; Bradley, D. D. C.; dos Santos, D. A.; Bredas, J. L.; Loglund, M.; Salaneck, W. R. *Nature* **1999**, 121, 379.

11. Friend, R. H.; Burroughes, J. H.; Bradley, D. D. C. U.S. Patent 5,247,190 **1993**.

12. Braun, D.; Heeger, A. J. *Appl. Phys. Lett.* **1991**, 58, 1982.

13. Braun, D.; Heeger, A. J. *Thin Solid Films* **1992**, 216, 96.

14. Eisberg, R.; Resnick, R. *Quantum Physics*. John Wiley & Sons: New York, **1985**.

15. Atkins, P. W., *The Elements of Physical Chemistry*. Oxford University: New York **1993**.

16. Krivoshei, I. V.; Skorobogatov, V. M. *Polyacetylene and Polyarylenes: Synthesis and Conductive properties*. Gordon and Breach Science: **1991**.

17. Lakowicz, J. R., *Principles of Fluorescence Spectroscopy*. Kluwer Academic/

Plenum: New York, **1999**.

18. Pope, M.; Swenberg, C. E. *Electronic Processes in Organic Cyrystals*. Oxford University: New York, **1982**.

19. Chien, J. C. W., *Polyacetylene : Chemistry, Physics, and Material Science*. Academic Press: Orlando, **1984**.

20. Pavia, D. L.; Lampman, G. M.; Kriz, G. S. *Introduction to Spectroscopy: a Guide for Students of Organic Chemistry*. Harcourt College: **2001**.

21. Kohler, A.; Gruner, J.; Friend, R. H.; Müllen, K.; Scherf, U. *Chem. Phys. Lett.* **1995**, 243, 456.

22. Lemmer, U.; Heun, S.; Mahrt, R. F.; Scherf, U.; Hopmeier, M.; Siegner, U.; Gobel, E. O.; Mullen, K.; Bassler, H. *Chem. Phys. Lett.* **1995**, 240, 373.

23. Blatchford, J. W.; Gustafson, T. L.; Epstein, A. J.; Vanden Bout, D. A.; Kerimo, J.; Higgins, D. A.; Barbara, P. F.; Fu, D. K.; Swager, T. M.; MacDiarmid, A. G. *Phys. Rev. B* **1996**, 54, R3683.

24. Blatchford, J. W.; Jessen, S. W.; Lin, L.-B.; Gustafson, T. L.; Fu, D.-K.; Wang, H.-L.; Swager, T. M.; MacDiarmid, A. G.; Epstein, A. J. *Phys. Rev. B* **1996**, 54, 9180.

25. Hsu, J.-H.; Fann Wunshain; Tsao, P.-H.; Chuang, K.-R.; Chen, S.-A. *J. Phys. Chem. A.* **1999**, 103, 2375.

26. Truuo, N. J., *Modern Molecular Photochemistry*. University Science Books: California, **1991.**

27. Nguyen, T. Q. W.; J., Doan, V.; Schwartz, B. J.; Tolbert, S. H. *Science* **2000**, 288, 652.

28. Becker, H.; Spreitzer, H.; Ibrom, K.; Kreuder. *Macromolecules* **1999**, 32, 925.

29. Padmanaban, G.; Ramakrishnan, S. *J. Am. Chem. Soc.* **2000,** 122, 2244.

30. Peng, K. Y.; Chen, S. A.; Fann, W. S. *J. Am. Chem. Soc.* **2001**, 123, 11388.

31. Nguyen, T. Q. D.; V.; Schwartz, B. J. *J. Chem. Phys.* **1999**, 110, 4068.

32. Nguyen, T. Q.; Martini, I. B.; Liu, J.; Schwartz, B. J. *J. Phys. Chem. B.* **2000**, 104, 237.

33. Shi Y.; Liu, J.; Yang, Y. *J. Appl. Phys.* **2000**, 81, 4254.

34. Liu, J.; Guo, T. F.; Yang, Y. *J. Appl. Phys.* **2002**, 91, 1595.

35. Duran, R. B.; M.; Wenzel, M.; Wegner, G. *Macromolecules* **1988**, 21, 2897.

36. Watanabe, J.; Harkness, B. R.; Sone, M.; Ichimura, H. *Macromolecules* **1994**, 27, 507.

37. Lauter, U. M.; W. H.; Wegner, G. *Macromolecules* **1997**, 30, 2092.

38. Wegner, G. *Macromol. Chem. Phys.* **2003**, 204, 347.

39. Ballauff, M. *Angew. Chem. Int. Ed. Engl.* **1989**, 28, 253.

40. Ikkala, O. K.; M.; Ruokolainen, J.; Torkkeli, M.; Serimaa, R.; Jokela, K.; Horsburgh, L.; Monkman, A.; ten Brinke, G. *Adv Mater* **1999**, 11, 1206.

41. Knaapila, M. R.; J.; Torkkeli, M.; Serimaa, R.; Horsburgh, L.; Monkman, A. P.; Bras, W.; ten Brinke, G.; Ikkala, O. *Synth. Met.* **2001**, 121, 1257.

42. Stepanyan, R.; Subbotin, A.; Knaapila, M.; Ikkala, O.; ten Brinke, G. M*acromolecules* **2003**, 36, 3758.

43. Tashiro, K. O.; K.; Minagawa, Y.; Kobayashi, M.; Kawai, T.;Yoshino, K. *J. Polym. Sci., Part B: Polym. Phys.* **1999**, 29, 1223.

44. Prosa, T. J.; Moulton, J.; Heeger, A. J.; Winokur, M. J. *Macromolecules* **1999**, 32, 4000.

45. Winokur,M.J.;Chunwachirasiri,W. *J.Polym.Sci.,PartB: Polym. Phys.* **2003**, 41, 2630.

46. Knaapila, M.; Lyons, B. P.; Kisko, K.; Foreman, J. P.; Vainio, U.; Mihaylova, M.; Seeck, O. H.; Pålsson, L.-O.; Serimaa, R.; Torkkeli, M.; Monkman, A. P. *J. Phys. Chem. B* **2003**, 107, 12425.

47. Langeveld-Voss, B. M. W.; Janssen, R. A. J.; Christiaans, M. P. T.; Meskers, S.

C. J.; Dekkers, H. P. J. M.; Meijer, E. W. *J. Am. Chem. Soc.* **1996**, 118, 4908.

48. Whitesides G. M.; Grzybowski, B. *Science* **2002**, 295, 2418.

49. Dobson, C. M. *Nature* **2003**, 426, 884.

50. Palmer B. J.; Liu, J. *Langmuir* **1996**, 12, 746.

51. Rädler, J. O.; Koltover, I.; Salditt, T.; Safinya, C. R. *Science* **1997**, 275, 810.

52. Jenekhe, S. A.; Chen, X. L. L. *Science* **1998**, 279, 1903.

53. Jenekhe, S. A.; Chen, X. L. L. *Science* **1999**, 283, 372.

54. Ikkala,O.; Brinke, G. *Science* **2002**, 295, 2407.

55. Roe, R. J. *Methods of X-ray and Neutron Scattering in Polymer Science*. Oxford: New York, **2000**.

56. Higgins, J. S.; Benoit, H. C. *Polymers and Neutron Scattering*, Oxford: New York **1994**.

57. Lindner, P.; Zemb, Th. *Neutron, X-Rays and Light Scattering Methods Applied to Soft Condensed Matter*. Elsevier: New York, **2002**.

58. Glatter, O.; Kratky O. *Small Angle X-ray Scattering*. Academic press inc: London, **1982.**

59. Guinier, A., *Small-Angle Scattering of X-rays*. Wiley: New York, **1955**.

60. Guinier, A. *Anal. Phys.* **1939**, 12, 161.

61. Mandelbrot, B. B., *The fractal Geometry of Nature*. Freeman Press: San Francisco, **1982**.

62. Martin, J. E.; Hurd, A. J. *J. Appl. Cryst.* **1987**, 20, 61.

63. Martin, J. E. *J. Appl. Cryst.* **1986**, 19, 25.

64. Schaefer, D. W.; Martin, J. E. *Phys. Rev. Lett.* **1984**, 52, 2371.

65. Tracy, M. A.; Garcia, J. L.; Pecora, R. *Macromolecules* **1993**, 26, 1862.

66. Sato, T.; Ohshima, A.; Teramoto, A. *Macromolecules* **1994**, 27, 1477.

67. Takada, Y.; Sato, T.; Teramoto A. *Macromolecules* **1991**, 24, 6215.

68. Petekidis, G.; Vlassopoulos, D.; Fytas, G.; Rulkens, R.; Wegner, G. *Macromolecules* **1998**, 31, 6129.

69. Petekidis, G.; Vlassopoulos, D.; Fytas, G.; Rulkens, R.; Wegner, G.; Fleischer, G. *Macromolecules* **1998**, 31, 6139.

70. Rubinstein, M.; Colby, R. H. *Polymer Physics*. Oxford: New York, **2003**.

71. de Gennes, P. G. *Scaling Concepts in Polymer Physics*. Cornell University Press: New York, **1979.**

72. Liu, A. J.; Nagel, S. R. *Nature* **1998**, 396, 21.

73. Flory P. J. *Principals of Polymer Chemistry*. Cornell University Press: New York, **1953**.

74. Lopez, D.; Guenet, J.-M. *J. Phys. Chem. B.* **2002**, 106, 2160.

75. Grell, M; Bradley, D. D. C.; Ungar, G..; Hill, J.; Whitehead, K. S. *Macromolecules* **1999**, 32, 5810.

76. Collison, C. J.; Rotherberg, L. J.; Treemaneekarn, V.; Li, Y. *Macromolecules* **2001**, 34, 2346.

77. Chen, S. H.; Su, A. C.; Chang, C. S.; Chen, H. L.; Ho, D. L.; Tsao, C. S.; Peng, K. Y.; Chen, S. A. *Langmuir* **2004**, 20, 8909.

CHAPTER 2

Fractal Aggregates of Poly(2,3-diphenyl-5-hexyl-1,4-phenylenevinylene) (DP6-PPV) in Solution State

2.1 Introduction

Conjugated polymers have gained much interest due to their unique electrical and photonic semiconducting properties for the opto-electronic applications such as polymer light emitting diodes (PLED)[1-3]. This class of polymer usually composes of a semirigid conjugated backbone attached with flexible short side chains to render the polymer the nominal solubility in common organic solvents and hence facilitates the device processing using spin or drop casting techniques. Spectroscopic studies have indicated that conjugated polymers undergo inter-chain aggregation in the solution state even at large dilution[4-7]. However, the origin of this event and the structure of the resultant aggregates still remain the crucial issues to be resolved as the presence of aggregates even in trace amount can have profound impact on the photophysics of these materials[4, 8-11]. Considering that the aggregation is not accompanied with apparent macrophase separation and it may take place at very low polymer concentration, it becomes difficult to make a straightforward connection of this process to the phase transformations having been encountered in solutions of rigid macromolecules, such as crystallization and lyotropic nematic phase formation[12]. Micellization driven by the possible amphiphicility of the polymer due to the disparity in solvent affinity of the conjugated backbone and the aliphatic side chains may be a plausible mechanism for the aggregation[13]. Nevertheless, more in-depth studies are necessary to test this postulate, in particular as to whether the micelles are “segmental micelles” (formed by the local association of segments) or “molecular micelles” (formed by the aggregation of the whole polymer molecules as encountered in block copolymer solutions).

In this article, we investigate the inter-chain aggregation behavior of a conjugated polymer dissolved in two solvents of different qualities. Here we use small angle neutron scattering (SANS) as the major tool for resolving the aggregation behavior. SANS is known as a powerful tool for characterizing the conformational structure and aggregation behavior of macromolecules in solutions[14, 15]. This technique makes use of the distinct contrast in neutron scattering length between deuterated (d-) solvent and hydrogenous polymer (or vice versa), which offers decent scattering intensity and effectively reduces the incoherent background for probing the solution structure at relatively low polymer concentration. SANS can effectively complement the spectroscopic techniques such as photoluminescence spectroscopy where the attribution of the lower-energy emission to the presence of aggregates is sometimes complicated by other emission species such as excimers[4,16-19] and chemical defects[20-23].

In a recent study Perahia et al. have utilized SANS to probe the aggregate structure of a conjugated polymer, poly(2,5-dinonylparaphenylene ethynylene) (PPE), in the solution with toluene.[24,25] The triple bonds along the backbone imparted conformational rigidity to the molecule; therefore, PPE chains were essentially rodlike. The rodlike molecules were found to aggregate into large flat clusters driven by the π–π interaction below ca. 40 ^{o}C. When the aggregates were too large to freely move in the solution, a transition into a constrained or jammed phase took place transforming the viscous solution into gel.

The conjugated polymer studied here is poly(2,3-diphenyl-5-hexyl-1,4-phenylenevinylene) (DP6-PPV) with the chemical structure shown below

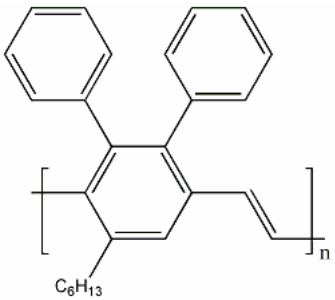

DP6-PPV is an attractive green-emitting material for PLED application due to its high glass transition temperature, high fluorescence efficiency and ease of monomer and polymer syntheses[26-29]. In contrast to PPE, the conjugated double bonds in the backbone of DP6-PPV render the chain a certain degree of flexibility, such that its conformation is more properly described by the semirigid "worm-like chain" instead of rigid rod.[13, 30] The entropic gain from the conformational flexibility may enhance the solubility of the polymer in the solution and thus reduces the aggregation power of DP6-PPV compared with that of PPE Consequently, the structure of the aggregates may be largely different from the compact plate structure formed by PPE. In the present study, we investigated the aggregation behavior of DP6-PPV in chloroform and toluene. Chloroform was considered as a relatively good solvent for the polymer whereas toluene was a relatively poor one. With the aid of dynamic light scattering (DLS), we will demonstrate that DP6-PPV underwent inter-chain aggregation in both solvents, generating aggregates with the hydrodynamic radii of several μm. The corresponding SANS profiles reveal the network internal structure for these aggregates with the mass fractal dimension of 2.2 ~ 2.7. The origin of the interchain aggregation will also be discussed in connection with the highly persistent π-π complex present in the DP6-PPV powder before dissolution.

2.2 Experimental Section

DP6-PPV was synthesized according to the procedure described elsewhere[26-29]. The weight-average molecular weight (M_w) and polydispersity index of the polymer was 448,000 and 1.3, respectively. The polymer solutions with concentrations of 0.1, 0.5 and 1.0 wt% were prepared by dissolving appropriate amount of the polymer in chloroform and toluene. d-Solvents were used for enhancing the contrast in neutron scattering length densities (SLD). The mixtures of polymer and solvent were stirred at ca. 40 ^{o}C for 12 hrs, where macroscopically homogeneous solutions were observed by naked eyes after the stirring. The solutions were allowed to equilibrate at room temperature (ca. 25 ^{o}C) for 12 hrs prior to the SANS and DLS measurements.

The SANS measurements were performed on the 8 m SANS instrument (NG1) at the National Institute of Standard and Technology (NIST)[31]. The incident neutron wavelength was λ = 8 Å with a wavelength dispersion of $\Delta\lambda/\lambda$ = 0.14. The configuration of the SANS instrument, including the collimated pinhole size and the sample-to-detector distance, was optimized to give an effectively measured q-range of 0.008 Å^{-1} to 0.12 Å^{-1}. The scattering intensity I(q) was corrected for transmission, background and parasitic scattering and normalized to an absolute intensity (scattering cross section per unit sample volume) as a function of the scattering vector q where $q = (4\pi/\lambda)\sin(\theta/2)$ (θ is the scattering length angle)[32]. The incoherent backgrounds from the pure solvents were also measured, corrected by the volume fraction displaced by the dissolved DP6-PPV, and subtracted from the reduced SANS data. Temperature (calibrated and controlled within ±0.1 ^{o}C) of the solution during SANS measurement was achieved by use of a 10-piston heating/cooling block connected to a circulating bath (50/50 mixture of water and ethylene glycol). For the measurement at each temperature, the sample was first held at the prescribed temperature for 30 min followed by data acquisition for another 30 min. This acquisition time was sufficient to give reasonable counting statistics of the scattered intensity (~ 1E+6 counts).

DLS experiments were performed using a Malvern CGS-3 equipment with an

ALV/LSE-5003 Multiple-tau digital correlator. A 22 mW laser beam (632.8 nm in wavelength) was passed through a quartz cell holding the solutions and the scattering intensity was detected at 90 ^{o} with respect to the incident beam. The scattered light was analyzed with an autocorrelator to generate the normalized electric field-time correlation function, $g^{(1)}(\tau)$.[33, 34]. For a system exhibiting a distribution of collective motions, $g^{(1)}(\tau)$ can be represented by the superposition of exponential decay functions. Laplace inversion routine of $g^{(1)}(\tau)$ was performed to yield the distribution of relaxation times $A(\tau)$, viz.

$$g^{(1)}(\tau) = \int_0^{\infty} A(\tau)\exp(-t/\tau)d\tau \qquad (1)$$

The translational diffusion coefficient distribution was obtained from $A(\tau)$ and the hydrodynamic radius distribution was eventually obtained using the Stokes-Einstein equation, $R_h = k_B T/(6\pi\eta D)$, where k_B is the Boltzman constant, T is absolute temperature, D is the diffusion coefficient and η is solvent viscosity.

2.3 Result and Discussion

2.3.1 Aggregate Structure in DP6-PPV/Chloroform Solutions.

Figure 2-1 shows the room-temperature SANS profiles of DP6-PPV in the solutions with chloroform at different concentrations. The SANS intensities followed $I(q) \sim q^{-1}$ dependence in the high-q region ($q > \sim 0.03$ Å^{-1}) irrespective of the polymer concentration, indicating the presence of rod entity under large spatial resolution[14,15]. The scattering intensity in this q region was dominated by the form factor of the rod entity, viz.[15]

$$I(q) = N\Delta\rho^2 V_{rod}^2 P_{rod}(q) \qquad (2)$$

where I(q) is the absolute intensity in the unit of cm^{-1}, N is the number density of rod particles, $\Delta\rho$ is the SLD contrast between the solvent and the particle, V_{rod} is the volume of the rod, and $P_{rod}(q)$ is the form factor function of rod particle. Let $V_{rod} = zv_u$ with z and v_u being the number of monomer units in a rod and volume of a monomer unit, respectively, and $N = cN_{av}/(zM_u)$ with c, M_u and N_{av} being the concentration in g/ml, molar mass of the monomer unit and the Avogardro's number, respectively, then Eq. (1) can be reorganized to give

$$P_{rod}(q) = \frac{I(q)M_u}{cN_{av}z\Delta\rho^2 v_u^{\,2}} = \frac{G(q)}{z} \qquad (3)$$

In the high-q limit, $P_{rod}(q) \rightarrow \pi/(qL)$[15] , Eq. (2) thus translates to

$$\lim_{q\to\infty} G(q) = \frac{I(q)M_u}{cN_{av}\Delta\rho^2 v_u^{\,2}} = zP_{rod}(q) = \frac{\pi M_u z}{qLM_u} = \frac{\pi M_L}{M_u q} \qquad (4)$$

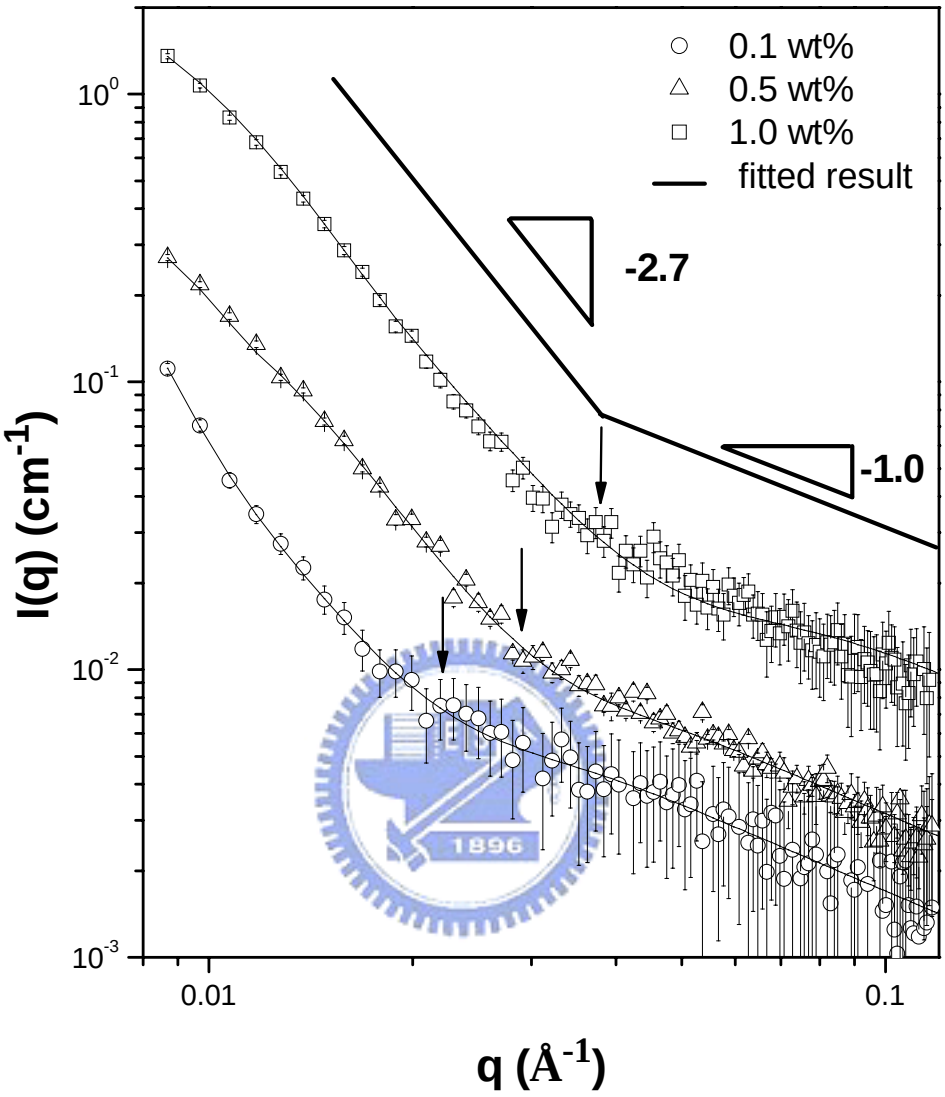

Figure2-1. The room-temperature SANS profiles in log-log plots of DP6-PPV in the solutions with chloroform at different concentrations. Two power-law regimes were identified in the scattering profiles irrespective of the concentration. The intensity exhibited a power law of $I(q) \sim q^{-2.7}$ in the middle- to low-region characterizing the mass fractal dimension of the network aggregates. The q-dependence transformed to another power law of $I(q) \sim q^{-1}$ at high q corresponding to the form factor of the rodlike sub-chains between the junction points in the networks. The solid curves are the fitted results using the unified equation.

where M_L is the molar mass per unit length of the rod. Eq. (3) prescribes that the product of G(q) and q reaches an asymptotic value given by $\pi M_L/M_u$. Figure 2-2 displays the G(q)q vs. q plot for the 1.0 wt% DP6-PPV/chloroform solution. The plot was generated using the following parameter values: $\rho_{DP6\text{-}PPV} = 1.321 \times 10^{10}$ cm^{-1}, $\rho_{d\text{-}chloroform} = 3.16 \times 10^{10}$ cm^{-2} and $v_{u,DP6\text{-}PPV} = 5.73 \times 10^{-22}$ cm^3. M_L determined from the plateau was 4.3 gmol^{-1}nm^{-1}. This value closely agreed with the molar mass per unit length of the monomer unit of DP6-PPV (= 5.0 gmol^{-1}nm^{-1}) calculated by dividing the molecular weight of the monomer unit (M_u = 338 g mol^{-1}) by the length of a monomer unit (= 6.7 Å)[35]. This attested that the rod entity probed in the high-q region corresponded to the rodlike segments constituting DP6-PPV chains.

The conformation of semirigid polymers is usually described by the "worm-like chain" possessing relatively large persistent length, l_{ps} (l_{ps} < contour length)[36-39]. In the low-q region ($q < l_{ps}^{-1}$) where the global conformation is probed, the worm-like chain approaches the coil behavior and the corresponding form factor exhibits an asymptotic power law of $I(q) \sim q^{-\nu}$ with ν = 2.0 and 1.7 in θ and good solvent, respectively[40]. Rodlike behavior corresponding to the rigid nature of the polymer chain on local scale emerges in the high-q region ($q > l_{ps}^{-1}$). In principle, the persistent length of the worm-like chain may be determined from the crossover (q_c) from the rodlike behavior to the coil behavior *via* $l_{ps} = 3.5/q_c$,[37-39] provided that the scattering profile over the q range of interest represents the form factor of the single chain or the sub-chain that is long enough to manifest the worm-like behavior. Exact determination of l_{ps} was however implausible here because, as will be shown later, the scattering profiles at q < ~ 0.03 Å^{-1} in Figure 1 were not dominated by the form factor of molecularly dissolved DP6-PPV chains. Nevertheless, the fact that the q^{-1} power law extended to ca. 0.03 Å^{-1} indicated that l_{ps} of the chain was larger than 3.5/0.03 Å^{-1} =117 Å.

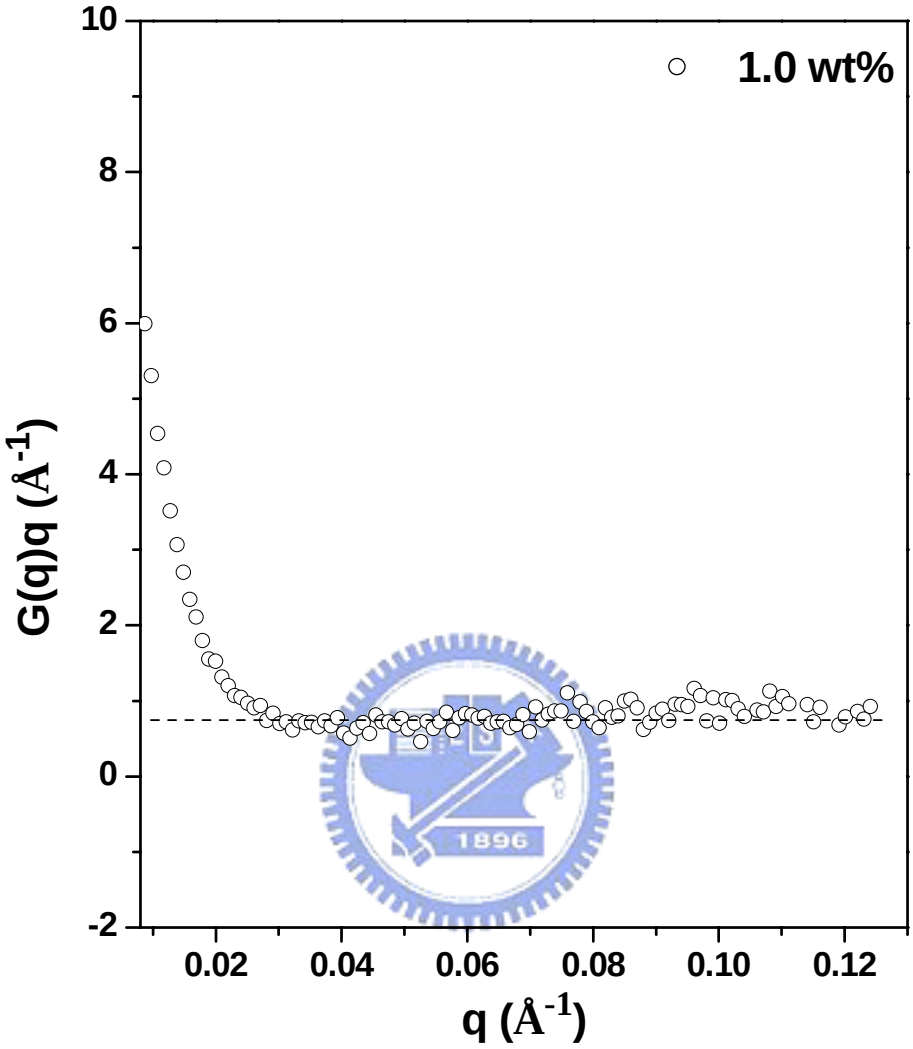

Figure 2-2. G(q)q vs. q plot of 1.0 wt% DP6-PPV/chloroform solution for the determination of the molar mass per unit length (M_L) from the asymptotic value of the plot.

The scattering intensities of DP6-PPV/chloroform solutions exhibited obvious upturns at $q < \sim 0.03$ Å^{-1}, where the corresponding slope in the log-log plot became ca. –2.7 and was virtually independent of concentration. Therefore, the scattering profiles of the three concentrations shared essentially the same feature, namely, the intensities exhibited a power law of $I(q) \sim q^{-2.7}$ in the middle- to low-q region but this q-dependence transformed to $I(q) \sim q^{-1}$ at high q corresponding to the rodlike behavior of the chain segment. Since polymer chain conformation usually depends weakly on concentration, the observed SANS profiles may be ascribed intuitively to the form factor of the molecularly dissolved polymer chains in the solution. However, the power law exponent of 2.7 at low-q was not prescribed by the asymptotic scattering behavior of worm-like chain or other form factor models of linear polymer chains. The attribution of the observed scattering pattern to single-chain form factor was further ruled out by the strong concentration dependence of the *concentration-normalized* intensity (I(q)/c), as shown in Figure 2-3. It can be seen that, instead of collapsing onto a single master curve, the concentration-normalized intensity in the low-q region increased with increasing overall polymer concentration.

The concentration dependence of I(q)/c was not prescribed by the dynamic network structure formed by the inter-chain overlap in the semidilute solution either, because in this case I(q)/c should *decrease* with increasing concentration in the low-q region ($q < \xi_d^{-1}$ with ξ_d being the dynamic mesh size) as I(q)/c is proportional to the mesh size which decreases with the increase of concentration[40].

The larger I(q)/c at higher concentration was attributable to the significant aggregation of DP6-PPV chains in chloroform. We asserted that the observed SANS profiles were overwhelmed by the structure of the inter-chain aggregates. In this case, the power law of $I(q) \sim q^{-2.7}$ signaled that over the length scale covered by the low-q region the structure of the aggregates was characterized by a mass fractal dimension of ca. 2.7 irrespective of polymer concentration. The proximity of the

observed fractal dimension to that (= 2.5) displayed by the percolation clusters suggested that the aggregates of DP6-PPV were networks generated by the segmental association of the polymer chains, as schematically illustrated in Figure 4. The sites of the segmental association acted as the (physical) junction points for the chains (with the average distance between the junction points denoted by ξ_s). Two structural levels of the aggregates were hence probed by the SANS profiles. At $q > \xi_s^{-1}$ the scattering behavior was dominated by the form factor of the sub-chains between the junction points in the networks. If ξ_s was smaller than the Kuhn length of the chain, these sub-chains were essentially rodlike and hence gave rise to the q^{-1} power law in the high-q region in Figure 1. At $R_g^{-1} << q < \xi_s^{-1}$(with R_g being the radius of gyration of the aggregates) where the structure at a more global length scale dominated the scattering behavior, the intensity displayed another power law of $I(q) \sim q^{-2.7}$ characterizing the fractal dimension of the networks. Consequently, the overall scattering profile exhibited a crossover from q^{-1} to $q^{-2.7}$ with decreasing q. Similar crossover between the power law of q^{-1} and $q^{-\alpha}$ with α lying between 2.0 and 3.0 has also been noted recently for the scattering patterns of the aggregates of carbon nanotubes in solution state.[41]

The fractal aggregates revealed here for DP6-PPV was in clear distinction with the compact plate aggregates formed by the rodlike PPE chains.[24,25] The latter was consider to posses a uniform density [24,25] whereas the fractal aggregates of DP6-PPV had an opened structure as a significant fraction of the unassociated segments remained mixed with the solvent molecules contained within the aggregates (*cf.* Figure 2-4).

It can be seen from Figure 2-1 that the crossover between the two power-law regimes (marked by the arrow) shifted to higher q with increasing polymer concentration (e.g. from 0.022 $Å^{-1}$ at 0.1 % to 0.037 $Å^{-1}$at 1.0 %), implying a smaller ξ_s at higher polymer concentration due to higher degree of segmental association. We

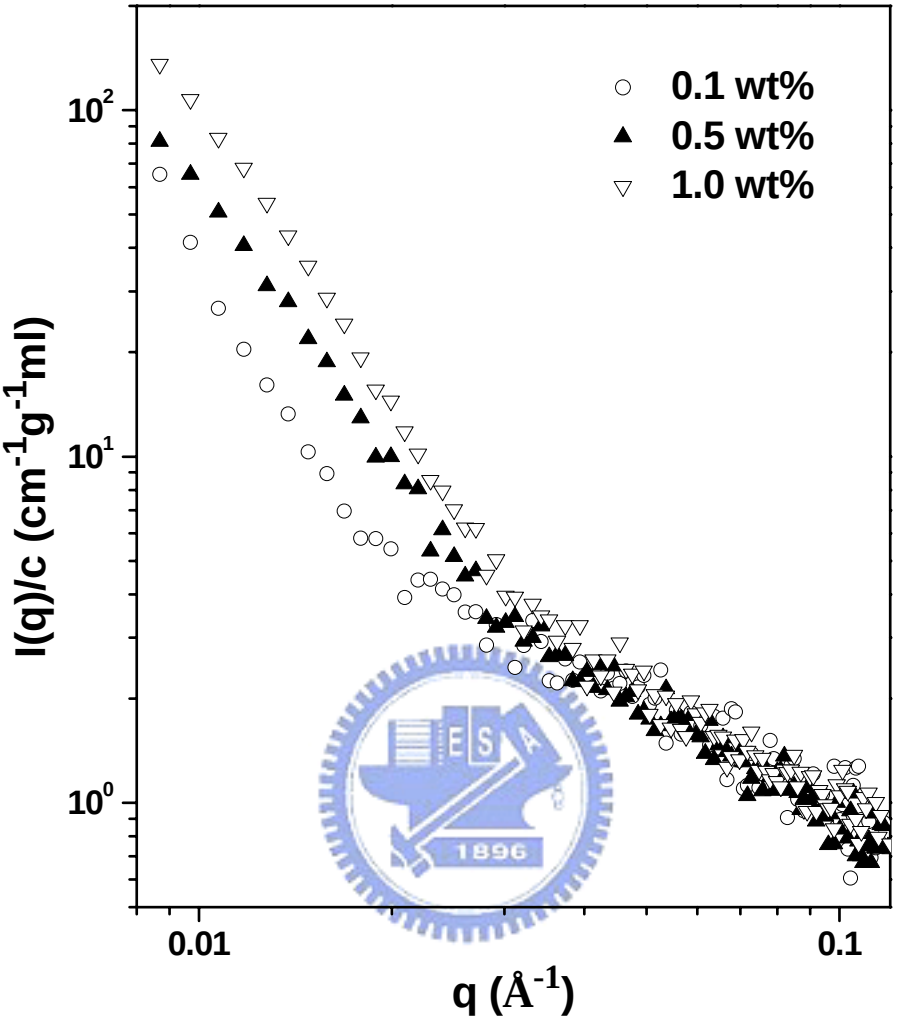

Figure 2-3 The concentration-normalized SANS profiles of DP6-PPV/chlororofm solutions. I(q)/c in the low-q region was found to increase with increasing overall polymer concentration, indicating that DP6-PPV exhibited significant inter-chain aggregation.

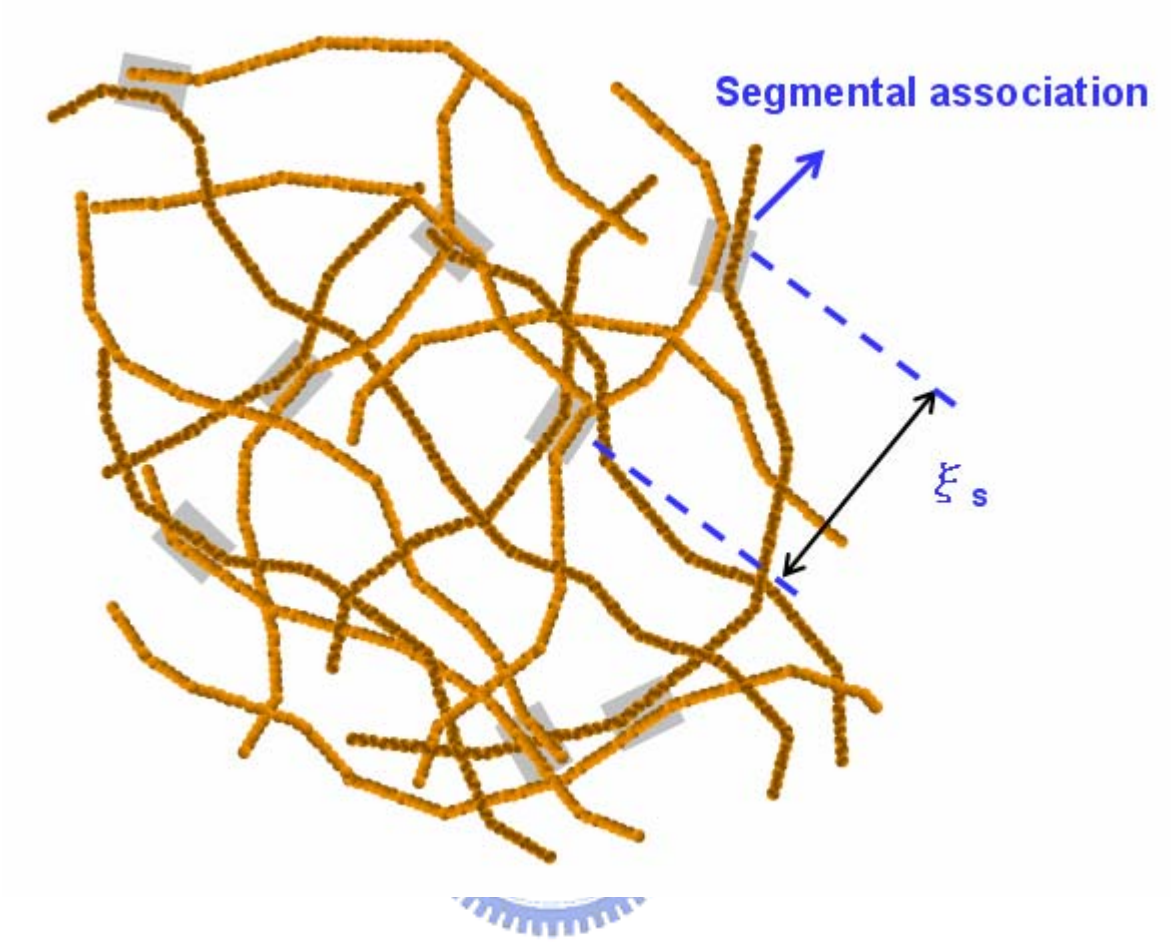

Figure 2-4 Schematic illustration of the network aggregates formed by DP6-PPV in the solution state. The networks were looser in chloroform but became highly compact in toluene.

attempted to deduce the quantitative value of ξ_s through fitting the SANS profile by the "unified equation" developed by Beaucage.[42, 43] The unified equation describes the scattering profiles of fractal objects in terms of hierarchical levels of structure in the system. Each structural level is described by a Guinier's law and a structurally-limited power law. The unified scattering function in terms of two structural levels is given by [42, 43]

$$I(q) \cong \left\{ G\exp(-\frac{q^2 R_g^{\ 2}}{3}) + B\exp(-\frac{q^2 R_s^{\ 2}}{3})(\frac{1}{q^*})^P \right\} + \left\{ G_s \exp(-\frac{q^2 R_s^{\ 2}}{3}) + B_s(\frac{1}{q_s^{\ *}})^{P_s} \right\} \quad (5)$$

where $q^* = q/[\mathrm{erf}(qkR_g/6^{1/2})]^3$ and $q_s^* = q/[\mathrm{erf}(qkR_s/6^{1/2})]^3$ with $k \approx 1.05$; G = $N_p\Delta\rho^2 V_p^2$ with N_p and V_p being the number of particles in the scattering volume and the volume of the particle, respectively. B and B_s are the prefactors specific to the types of power-law scattering characterized by the exponents P *and* P_s, respectively, they are given by

$$B = (\frac{GP}{R_g^{\ P}})\,\Gamma(\frac{P}{2}) \quad (6)$$

$$B_s = (\frac{G_s P_s}{R_s^{\ P_s}})\,\Gamma(\frac{P_s}{2}) \quad (7)$$

where Γ is the gamma function. For the present system, the first two terms in Eq. (5), which revealed the fractal feature of the aggregates, dominated the intensity at $q < \xi_s^{-1}$. The last two terms, which dominated the intensity at $q > \xi_s^{-1}$, captured the building block (i.e., the rodlike sub-chains between the junction points) with the characteristic radius of gyration of R_s of the networks.

Because the Guinier region prescribed by the R_g of the aggregates was not accessible over the q range of the present SANS experiment due to relatively large

aggregate size, the first term in Eq. (4) was omitted for the fitting. For the curve fitting we have fixed $P_s = 1.0$ (corresponding to the power-law exponent of the rodlike sub-chains), thereby leaving B, G_s, B_s, R_s and P as the fitting parameters. The fitted results were displayed by the solid curves in Figure 2-1 and the numerical values of the parameters and the error bar obtained from the fits were listed in Table 2-1. The fractal dimensions, P, obtained from the fits were close to those estimated directly from the slopes of the intensity profiles in log-log plots.

R_s corresponded to the radius of gyration of the rodlike sub-chains between the junction points, ξ_s was hence given by $\xi_s \approx (12R_s^2)^{1/2}$. The values of ξ_s thus calculated were 29.4, 22.1 and 15.2 nm for the concentration of 0.1%, 0.5% and 1.0%, respectively. The smaller ξ_s at higher polymer concentration signaled a higher degree of segmental association, as having also been manifested by the shift of the crossover between the two power-law regimes to higher q.

Table 2-1. The values of the parameters obtained from the unified equation fits for DP6-PPV/chloroform solutions.

	0.1 wt%	0.5 wt%	1.0 wt%
G_s	0.014 ± 0.008	0.026 ± 0.09	0.02 ± 0.012
B_s ($\times 10^3$)	7.7 ± 0.45	5.9 ± 0.05	11.6 ± 1.3
P	2.71 ± 0.43	2.65 ± 0.05	2.62 ± 0. 6
R_g (nm)	30.9 ± 4.2	25.3 ± 3.5	20.3 ± 0.4
R_s (nm)	8.5 ± 2.9	6.4 ± 1.1	4.4 ± 0.9
ξ_s $(=12R_s^2)^{1/2}$ (nm)	29.4	22.1	15.2

Since the accessible q range in the present SANS experiment did not allow the R_gs of the aggregates to be determined, DLS experiment was conducted to reveal the hydrodynamic radii, R_h, of the aggregates. Figure 2-5 shows the distribution of R_h in the 1.0 wt% DP6-PPV/chloroform solution at 25 ^oC. The R_h profile displayed three peaks with each stemming from a characteristic relaxation mode in the system. The dynamics of DP6-PPV in the solution was hence characterized by three modes, namely, the fast, medium and slow modes. The largest R_h of 3.8 μm associated with the slow mode may be attributed to the average hydrodynamic radius of the aggregates in the solution. Consequently, the inter-chain aggregation of DP6-PPV in chloroform generated relatively large aggregates with μm in size; down to the nanometer length scale the internal structure of the aggregates could be described by a rather well-defined fractal dimension of ca.2.7. The physical range of mass fractal dimension d_m is between 1.0 and 3.0.[14,15] In general, a small value of d_m would imply that the structure of the fractal object is more opened or has a lower dimensionality. The rather large fractal dimension of DP6-PPV aggregates in chloroform indicated that these aggregates were quite dense in structure. It is noted that the value of the fractal dimension may also be useful for resolving the mechanism of the cluster growth from the aggregation of small subunits.[44] However, such an analysis becomes even more complex for the aggregation of long polymer chains, because the building block by itself is a fractal object.

The small peak at 72 nm (corresponding the medium mode) in the R_h profile was attributed to the internal relaxation mode of the networks, while the other peak with R_h ~ 8 nm was ascribed to the motions of the rodlike segments. It is noted that the R_h of a rod entity is usually smaller than its corresponding R_g.[15, 45] However, as can be seen from Table 2-1, the radius of gyration of the rodlike subchains between the junction points (R_s = 4.4 nm) in the 1.0 wt% solution was smaller than the value of R_h (~ 8 nm) deduced from DLS. This discrepancy may be reconciled by the considering that R_h is related not only to the size of the object but also to its dynamics of motion. In the aggregates, the motions of the rodlike subchains were indeed constrained by the

junction points; therefore, the corresponding R_h became larger than that of the freed rods.

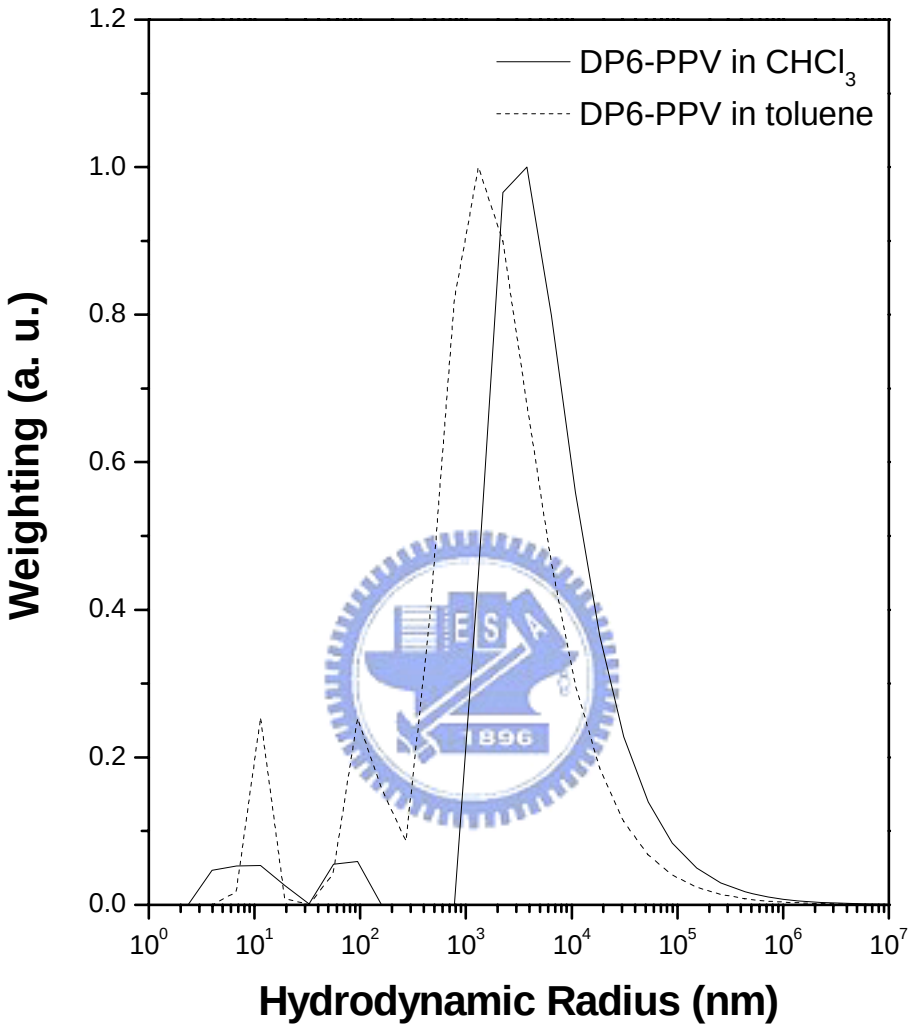

Figure 2-5 The distribution of hydrodynamic radius R_h in the 1.0 wt% chloroform and toluene solutions at 25 ^{o}C. The R_h profile displayed three peaks with each stemming from a characteristic relaxation mode in the system. The largest R_h was attributed to the average hydrodynamic radius of the aggregates in the solution, while the two small peaks were attributed to the internal relaxation mode of the networks and the motions of the rodlike segments.

2.3.2 Aggregate Structure in DP6-PPV/Toluene Solutions.

We now turn to the structure of DP6-PPV in the poorer solvent, toluene. Figure 2-6 displays the room-temperature SANS profiles of DP6-PPV in the solutions with toluene. In contrast to the two distinct power-law regimes observed for the chloroform solutions, only one asymptotic power law was identified here at $q > \sim 0.02$ $Å^{-1}$. The corresponding slopes in the log-log plots were –2.2, -2.4 and -2.7 for the concentration of 0.1, 0.5 and 1.0 wt%, respectively. These power law exponents were again attributed to the mass fractal dimensions of the networks formed by the inter-chain aggregation of DP6-PPV in toluene. The absence of the q^{-1} power-law regime in the scattering profiles implied that the networks were highly compact with very small ξ_s due to severe segmental association. In this case, the q^{-1} regime was located at the region beyond the measurable q range of the SANS experiment. The smaller fractal dimensions (compared with that observed for the chloroform solutions) coupled with highly compact internal structure indicated that the aggregates in toluene tended to collapse into objects (such as disks) with lower dimensionality due to severe segmental association.

The distribution of R_h of 1.0 wt% DP6-PPV/toluene solution at 25 ^oC is also shown in Figure 2-5. The R_h profile also exhibited three peaks centering at 1.3 μm, 95 nm and 10 nm. The largest R_h of 1.3 μm was again attributable to the average hydrodynamic radius of the aggregates. Therefore, the aggregates in toluene were smaller than those in chloroform due to more compact internal structure. The other two peaks corresponded to the network internal relaxation mode and the motion of the rodlike segments. The R_h associated with the former was larger than that found for the chloroform solution, as the corresponding motion became more restricted due to higher degree of segmental association in the aggregates.

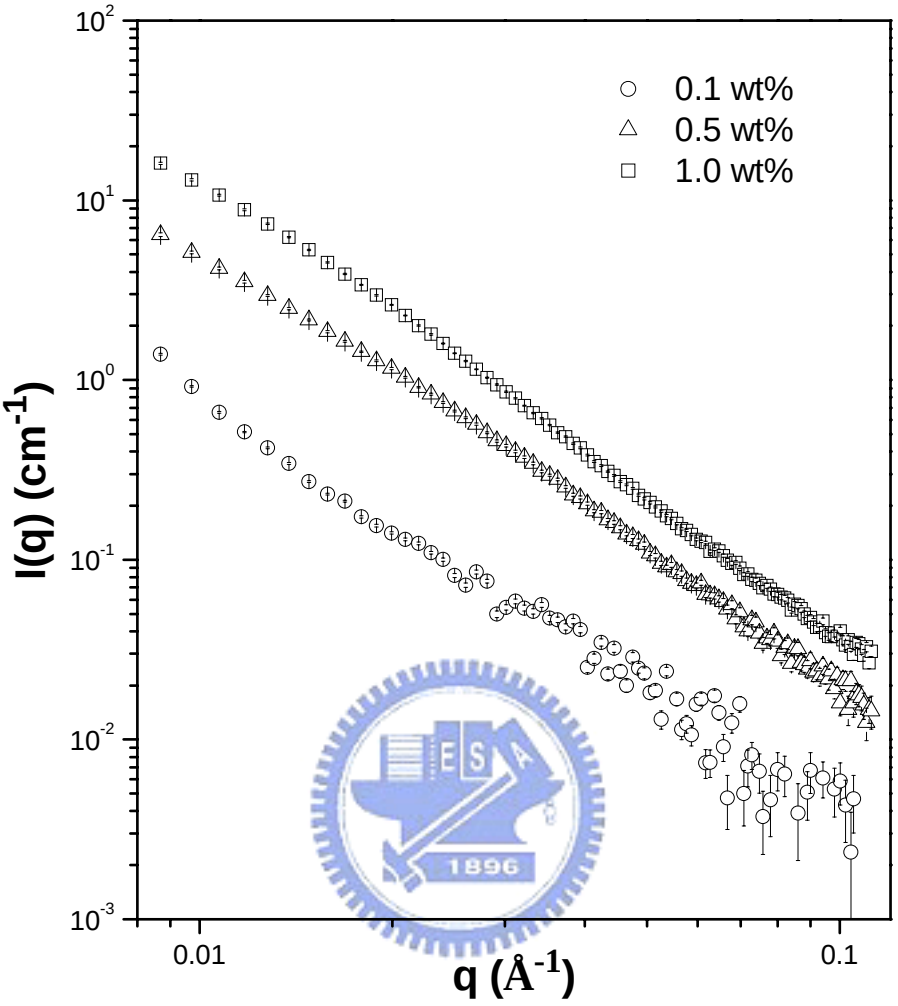

Figure 2-6 The room-temperature SANS profiles in log-log plots of DP6-PPV in the solutions with toluene at different concentrations. Only one asymptotic power law was identified at q > ~ 0.02 $Å^{-1}$. The corresponding power law exponents were attributed to the mass fractal dimensions of the highly compact networks formed by the inter-chain aggregation of DP6-PPV in the solvent.

Owing to the higher boiling point of toluene, temperature-dependent SANS experiment was conducted to examine the effect of elevating temperature on the aggregation behavior of DP6-PPV in this solvent. Figure 2-7 displays the SANS profiles of 1.0 wt% toluene solution collected *in-situ* at different temperatures in the heating cycle. The low-q intensity depressed progressively with increasing temperature, signaling the occurrence of de-aggregation upon heating. Interestingly, the fractal dimension of the aggregates remaining in the solution was found to retain at ca. 2.7, as the low-q slope in the log-log plot was essentially unaffected by increasing temperature. Accompanied with the depression of the low-q intensity was the gradual emergence of the q^{-1} power law in the high-q region ($q > 0.04$ Å^{-1}). The q^{-1} power-law regime became clear at 85 ^{o}C, which was about the highest achievable temperature before the intervention of solvent boiling. In this case, the scattering pattern was characterized by two distinct power-law regimes and became nearly identical with the room-temperature SANS profile of the corresponding chloroform solution after normalized by the respective neutron contrast factors (*cf.* the inset in Figure 2-7).

The temperature-dependent SANS experiment hence revealed that heating the toluene solution tended to reduce the degree of segmental association in the network aggregates. The segmental dissociation loosened the networks and the increase of ξ_s shifted the q^{-1} power-law regime to the accessible q range. Although the aggregates became less compact at higher temperature, their fractal dimension remained essentially unperturbed. It is further noted that the inter-chain aggregation was never completely dissipated even by heating to 85 ^{o}C, at which the aggregate structure was analogous to that in chloroform at room temperature. The results suggested that two types of segmental association with distinct stability existed in the aggregates of

DP6-PPV. The first type was prevalent in the poorer toluene solvent and could be disrupted by moderate heating. The other type of segmental association was highly stable in the sense that they could neither be solvated by the good solvent such as choroform nor be dissipated thermally at 85 ^{o}C in toluene.

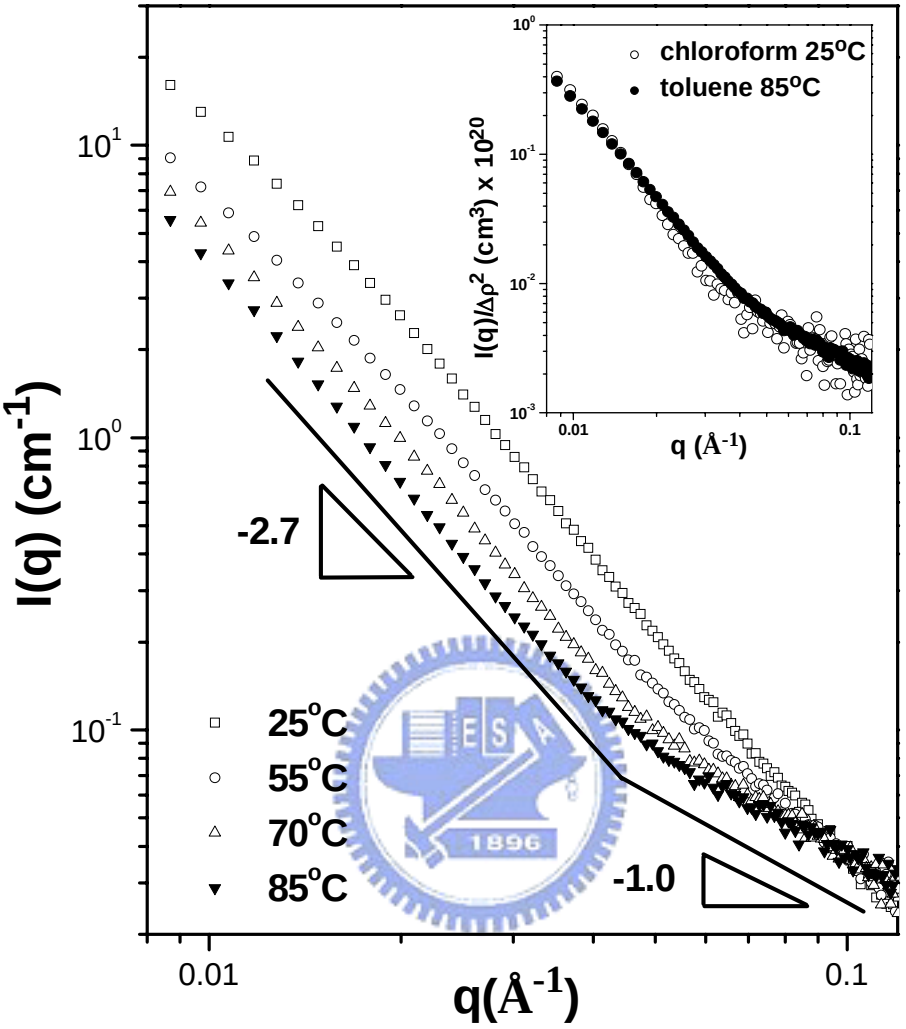

Figure 2-7 The temperature-dependent SANS profiles of 1.0 wt% DP6-PPV/toluene solution collected in a heating cycle. The low-q intensity depressed progressively with increasing temperature while largely retaining its slope. Accompanied with this intensity depression was the gradual emergence of the q^{-1} power law in the high-q region. The q^{-1} regime became clear at 85 ^{o}C. The inset displays the SANS profiles normalized by the contrast factors for 1.0 wt% DP6-PPV/toluene solution at 85 ^{o}C and 1.0wt% DP6-PPVchloroform solution at room temperature. It can be seen that the two scattering profiles were nearly identical.

2.3.3 The Nature of the Segmental Associations.

Here we attributed the highly stable segmental association to the π-π complex already present in the DP6-PPV powder used for the solution preparation. This kind of complex was formed by the in-plane stacking of the phenylene or phenyl moiety in DP6-PPV and the characteristic distance of ca. 3.0 Å between the aromatic groups forming the complex would lead to a peak at $2\theta \approx 29^{o}$ in the wide-angle X-ray scattering (WAXS) profile [45]. Figure 2-8 shows the WAXS scan of the DP6-PPV powder used for the solution preparations. The two peaks located at 18 and 22° corresponding to the interplanar spacing of 4.9 and 4.0 Å , respectively, were associated with the packings of the aliphatic side chains of DP6-PPV.[35] A π-π complex peak was clearly discernible at $2\theta = 29^{o}$. This scattering peak was found to persist even after annealing the powder at 330 ^{o}C (*cf.* Figure 2-8), showing that the π-π complex was highly stable. The WAXS profile of a DP6-PPV film cast from chloroform solution with a very rapid solvent removal is also displayed in Figure 2-8. It can be seen that the π-π complex peak still existed, which implied that the complex present in the powder remained unsolvated in chloroform, such that it was transferred into the film after solvent removal. Consequently, the WAXS results suggested the presence of a highly stable π-π complex in DP6-PPV powder. This species could neither be solvated by chloroform nor be disrupted by heating; as a result, the chains tied firmly by the π-π complex formed network aggregates in the solution. This inter-chain clustering reduced the entropy of mixing of the polymer compared with the case where all the chains were uniformly dispersed. In the poorer toluene solvent further segmental association might then take place within the pre-existing aggregates to reduce the free energy of the system. This segmental association might be driven by the amphiphicility of the DP6-PPV segments since toluene was a relatively poor and good solvent for the aliphatic side chains and the aromatic backbone, respectively.

In contrast to the π-π complex, the "micelle-like" segmental association thus generated had a poorer thermal stability and could be disrupted by moderate heating.

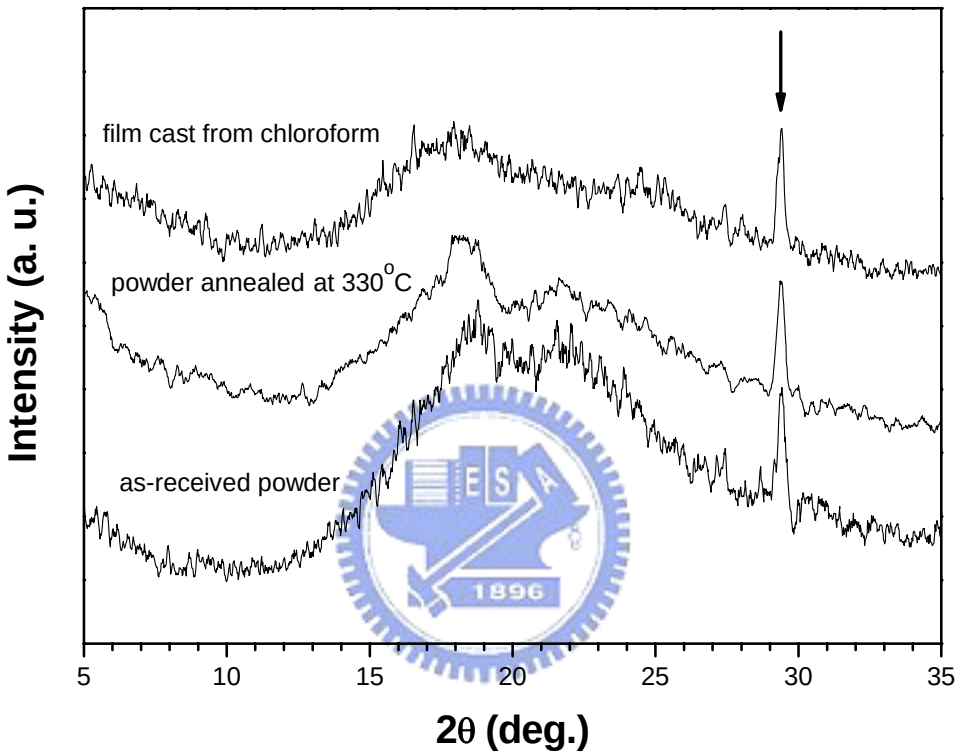

Figure 2-8. The WAXS scans of the as-received DP6-PPV powder used for the solution preparations, the powder having been annealed at 330 °C and the film cast from chloroform. A peak associated with π-π complex was observed at 29° for all samples.

References

1. Burroughes, J. H.; Bradly, D. D. C.; Brown, A. R.; Marks, R. N.; Mackay, K. Friend, R. H.; Burns, P. L.; Holmes, A. B. *Nature* **1990**, *347*, 539.
2. Friend, R. H.; Gymer, R. W.; Holmes, A. B.; Burroughes, J. H.; Marks, R. N.; Taliani, C.; Bradley, D. D. C.; dos Santos, D. A.; Brédas, J. L.; Löglund, M.; Salaneck, W. R. *Nature* **1999**, *397*, 121.
3. Spreitzer, H.; Becker, H.; Kluge, E.; Kreuder, W.; Schenk, H.; Demandt, R. and Schoo, H. *Adv. Mater.* **1998**, *10*, 1340.
4. Nguyen, T. Q.; Doan, V.; Schwartz, B. L. *J. Chem. Phys.* **1999**, *110*, 4068.
5. Grell, M; Bradley, D. D. C.; Ungar, G.; Hill, J.; Whitehead, K. S. *Macromolecules* **1999**, *32*, 5810.
6. Collison, C. J.; Rotherberg, L. J.; Treemaneekarn, V.; Li, Y. *Macromolecules* **2001**, *34*, 2346.
7. Hsu, J. H.; Fann, W. S.; Tsao, P. H.; Chuang, K. R.; Chen, S. A. *J. Phys. Chem. A* **1999**, *103*, 2375.
8. Blatchford, J. W.; Jessen, S. W.; Lin, L. B.; Gustafson, T. L.; Fu, D. K.; Wang, H. L.; Swager, T. M.; MacDiarmid, A. G.; Epstein, A. J. *Phys. Rev. B* **1996**, *54*, 9180.
9. Shi, Y.; Liu, J.; Yang, Y. *J. Appl. Phys.* **2000**, *87*, 4254.
10. Peng, K. Y.; Chen, S. A.; Fann, W. S. *J. Am. Chem. Soc.* **2001**, *123*, 11388.
11. Chen, S. H.; Su, A. C.; Huang, Y. F.; Su, C. H.; Peng, G. Y.; Chen, S. A. *Macromolecules* **2002,** *35*, 4229.
12. Jones, R. A. L. *Soft Condensed Matter*, Oxford: New York **2002**.
13. Ou-Yang, W. C.; Chang, C. S.; Chen, H. L.; Tsao, C. S.; Peng, K. Y.; Chen. S. A.; Han, C. C. *Phys. Rev. E*, **2005**, 72, 031802.
14. Roe, R. J. *Methods of X-ray and Neutron Scattering in Polymer Science*, Oxford: New York **2000**.

15. Higgins, J. S.; Benoit, H. C. *Polymers and Neutron Scattering*, Oxford: New York **1994**.

16. Samuel, I. D. W.; Rumbles, G.; Collison, C. J. *Phys. Rev. B* **1995**, R11573.

17. Nguyen, T. Q.; Matrini, I. B.; Liu, J.; Schwartz, B. J. *Phys. Chem. B* **2000**, *104*, 237.

18. Grell, M.; Bradley, D. D. C.; Long, X.; Inbasekaran, M.; Woo, E. P.; Soliman, M.; *Acta. Polym.* **1998**, *49*, 439.

19. Grell, M.; Bradley, D. D. C.; Ungar, G.; Hill, J.; Whitehead, K. S.; *Macromolecules* **1999**, *32*, 5810.

20. Gong, X.; Iyer, P. K.; Moses, D.; Bazan, G. C.; Heeger, A. J.; Xiao, S. S.; *Adv. Funct. Mater.* **2003**, *13*, 325.

21. Romaner, L.; Pogantsch, A.; de Freitas, P. S.; Scherf, U.; Gaal, M.; Zojer, E.; List, E. J. W. *Adv. Funct. Mater.* **2003**, *13*, 597.

22. Gaal, M.; List, E. J. W.; Scherf, U. *Macromolecules*, **2003**, *36*, 4236-4237.

23. Kulkarni, A. P.; Kong, X.; Jenekhe, S. A. *J. Phys. Chem. B*, **2004**, 108, 8689.

24. Perahia, D.; Traiphol, R.; Bunz, U. H. F. *J. Chem. Phys.*, **2002**, 117, 1827.

25. Perahia, D.; Jiao, X.; Traiphol, R. *J. Polym. Sci.: Part: B*, **2004**, 42, 3165.

26. Hsieh, B. R.; Antoniadis, H. *Adv. Mater.* **1995**, *7*, 36

27. Hsieh, B. R.; Yu, Y.; Forsythe, E. W.; Schaff, G. M.; Feld, W. A. *J. Am. Chem. Soc.* **1998**, *120*, 231.

28. Wan, W. C.; Antoniadis, H.; Choong, V. E.; Razafitrimo, H.; Gao, Y.; Feld, W. A.; Hsieh. B. R. *Macromolecules* **1997**, *30*, 6567.

29. Hsieh, B. R.; Yu, Y. U.S. Patent 5,945,502 **1999.**

30. Gettinger, C. L.; Heeger, A. J.; Drake, J. M.; Pine, D. J. *J. Chem. Phys.* **1994**, 101, 1673

31. Glinka, C. J.; Barker, J. G.; Hammouda, B.; Krueger, S.; Moyer, J. J.; Orts, W. J. *J.*

App. *Cryst*. **1998**, *31*, 430.

32. Cold Neutron Research Facility at the National Institute of Standard and Technology, *NG3 and NG7 30-Meter SANS Instruments Date Acquisition Manual* **1999**.
33. Schmitz, K. S. *An Introduction to Dynamic Light Scattering by Macromolecules*, Academic Press, Boston San Diego New York **1990**.
34. Brown. W. *Dynamic Light Scattering,* Clarendon Press, Oxford **1993**.
35. Huang, Y. F., Ph. D. Thesis, Institute of Material Science and Engineering, National Sun Yat-Sen University, Taiwan **2002**.
36. Aime, J. P.; Bargain. F.; Fave. J. L.; Rawiso, M.; Schott, M. *J*. *Chem*. *Phys*. **1988**, *89*, 6477.
37. Aime, J. P.; Bargain. F.; Schott, M.; Eckhardt, H.; Miller, G. G.; Elsenbaumer, R. L. *Phys*. *Rev*. *Lett*. **1989**, *62*, 55.
38. Des Cloizeaux, J. *Macromolecules*, **1973**, 6, 403.
39. Yoshizaki, T.; Yamakawa, H. *Macromolecules*, **1980**, 13, 1518.
40. Rubinstein, M.; Colby, R. H. *Polymer Physics*, Oxford: New York **2003**.
41. Bauer, B. J.; Hobbie, E. K.; Becker, M. L. *Macromolecules,* **2006**, 39, 2637.
42. Beaucage, G. *J*. *Appl*. *Crystallogr*. **1995**, 28, 717.
43. Beaucage, G. *J*. *Appl*. *Crystallogr*. **1996**, 29, 134.
44. Schaefer, D. W.; Martin, J. E. *Phys. Rev. Lett.* **1984**, 52, 2371.
45. Huang, Y. F.; Yang, S. H.; Hsu, C. S.; Chen, S. A.; Su, A. C. *ICMAT International Conference on Materials for Advanced Technologies,* Singapore **2001**.

CHAPTER 3

Conformational Structure and Aggregation Behavior of Poly(2,3-diphenyl-5-decyl-1,4-phenylenevinylene) (DP10-PPV) in Solution State

3.1 Introduction

Rigid and semi-rigid polymers may exhibit rich phase behavior compared with fexible polymers due to their highly anisotropic molecular shape that leads to the formation of mesophases. [1-5] For a flexible polymer, the conformation of the chain is governed by the degree of polymerization and interaction with the immediate surrounding.[6, 7] With the increase of the persistent length, the chain rigidity becomes a significant factor in the collective behavior. The stiffness may affect the viscosity of the solution and may induce phase separation, gelation and liquid crystallinity.[8-10] Another unique property of stiff polymer lies in the tendency of the polymer to aggregate in solvents even under large dilution. Such an aggregation behavior still remains relatively unexplored.

Conjugated polymers constitute a family of semi-rigid polymer which have found great potential in opto-electronic applications due to their unique semiconducting properties coupled with the solution processability. Poly(phenylenevinylene) (PPV) and its derivates are one of the most important classes of conjugated polymers for light-emitting diode application.[11, 12] To facilitate the device processing using spin or drop casting techniques, the conjugated backbone of PPV is usually attached with short flexible side chains to endow them the nominal solubility in common organic solvents. In a coarse-grained picture, the segments of

the polymers may be represented by the “hairy rods”.

The solutions of light-emitting polymers are usually homogeneous in appearance; however, their conjugated segments may exhibit some extent of aggregation in the solution and such an aggregation may exert a dramatic impact on the photophysical properties of the polymer in the solution. The dispersion state of the polymer in the solution, governed by the solvent quality, concentration and temperature, further influences the morphology and hence the photophysical properties of the light-emitting film formed after solvent removal. Yang et al.[13] reported that the threshold for gain narrowing of films prepared with tetrahydrofuran (THF) was lower than that of films prepared using chlorobenzene and *p*-xylene. Schwartz et al.[14] revealed different photoluminescent (PL) spectra for films prepared from different solvents. Recently we have found that the mesomorphic structure and the associated PL at 640 nm of MEH-PPV film were suppressed by prolonged aging of the solution used for the film preparation.[15] These instances indicate a solution-phase controlled morphology and photo-physics as the structure of the as-cast film is metastable presumably due to the fast solvent removal and the sluggish mobility of the stiff conjugated chains that prevent the polymer from attaining its equilibrium morphology during solvent casting. As a consequence, resolving the solution structure of light-emitting polymers is important not only for understanding the dissolution behavior of semirigid or rigid polymers but also for effectively tailoring the photophysical performance of their cast films.

In chapter 2, we have investigated the aggregation behavior of poly(2,3-diphenyl-5-hexyl-1,4- phenylenevinylene) (DP6-PPV) in chloroform and toluene.[16] With the aid of DLS, this polymer was shown to undergo inter-chain aggregation in both solvents, generating aggregates with the hydrodynamic radii of

several μm. The corresponding SANS profiles revealed the network internal structure for these aggregates with the mass fractal dimension of 2.2 ~ 2.7. The origin of the inter-chain aggregation was connected with the highly persistent π-π complex present in the DP6-PPV powder before dissolution. Here we extend the previous study to reveal the conformational structure and the aggregation behavior of another DP-PPV, poly(2,3-diphenyl-5-decyl-1,4-phenylenevinylene) (DP10-PPV), which bears a longer decyl side chain per monomer unit. The chemical structure of DP10-PPV is shown below

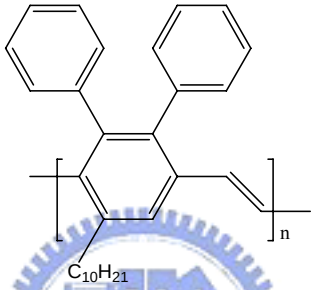

The results obtained here, in conjunction with those in chapter 2 for DP6-PPV, will be useful for revealing the effect of side chain length on the dissolution behavior of DP-PPVs. It will be shown that DP10-PPV displays a weaker tendency toward aggregation than DP6-PPV. In chloroform DP10-PPV chains are well dispersed and exhibit the expanded wormlike chain conformation with the persistent length increasing with overall polymer concentration. Like DP6-PPV, DP10-PPV chains aggregate significantly in toluene to form aggregates of several μm in size. The aggregates are found to compose of compact disklike domains at the overall polymer concentrations of 0.5 wt% and 1.0 wt%.

3.2 Experimental Section

3.2.1 Materials

The synthesis of hairy-rod polymer poly(2,3-diphenyl-5-decyl-1,4-phenylenevinylene), abbreviated as DP10-PPV here, with flexible side chain (the hairs) which the monomers were synthesized via the Diels-Alder reaction, while the polymerization was done via a modified Gilch route which involves the use of an acidic additive, such as 4-*tert*-butylbenzyl chloride.[17-20] In the present study, DP10-PPV with an weight-average molecular weight M_w = 524,800g/mol and the polydispersity index of the polymer was estimated about 1.28 was used, which determined by gel permeation chromatography in THF solvent and polystyrene as the standard. DP10-PPV molecules have been dissolved in deuterium (d-) solvent in order to enhance the contrast between the polymer and solvent. The overlap concentration of semidilute regime, c^*, ($c^* \sim 1/L_n^3$ where L_n is the end-to-end distance of DP10-PPV is 142.1 nm for 0.1wt%) of DP10-PPV in chloroform and toluene solutions is

$$0.265 \qquad \frac{410000g/mole}{(142.1nm)^3} \times \frac{mole/6.023\times10^{23}}{10^{-21}cm^3/nm^3} \times 1000mg/g \times \frac{cm^3}{1.489g} \times \frac{g}{1000mg} \times 100\%$$

and 0.458 wt%, respectively. In this work, the polymer solutions with concentrations of 0.1(dilute solution regime), and 0.5, 1.0 wt% (semidilute solution regime) were prepared by weighing appropriate amount of the polymer and dissolving it in the solvent by continuously stirring and slight heating (not higher than 50°C) for 12 hours when a macroscopically homogeneous solution was visible by naked eyes.

3.2.2 Scattering

Small angle neutron scattering (SANS) experiments were performed on the 8m-SANS instrument (NG1) at the National Institute of Standard and Technology

(NIST) Center for Neutron Research (NCNR).[21] The sample-to-detector of 8-m was chosen with the incident neutron wavelength of λ = 8Å and the wavelength dispersion of $\Delta\lambda/\lambda$ approximation 14%;[22] this resulted in an effectively q-range of 0.008 $Å^{-1} < q < 0.13$ $Å^{-1}$. The polymer solutions were encapsulated into the quartz banjo cells which the path length is 2 mm and were replaced by the Titanium demountable cells. The measurements of temperature-dependence were calibrated and controlled within ± 0.5°C of the solution during SANS measurement and was achieved by use of a 10-piston heating/cooling block connected to a circulating bath (50/50 mixture of water and ethylene glycol). For the measurement at each temperature, the sample was first held at the prescribed temperature for 30 min followed by data collection for another 30 min which is considering the reasonable counting statistic of the scattered intensity (~ 1E+6 counts) under the sample self-absorption factor.

The scattering intensity $I(q)$ was corrected for transmission, background and parasitic scattering and normalized to an absolute intensity (scattering cross section per unit sample volume) as a function of the scattering vector, q, where $q = (4\pi/\lambda)\sin(\theta/2)$ (θ is the scattering angle).[23, 24] The incoherent backgrounds from the pure solvents were also measured, corrected by the volume fraction displaced by the dissolved DP10-PPV, and subtracted from the reduced scattering data.

The dynamic light scattering (DLS) experiments were performed using ALV/CGS-3 equipment with an ALV/LSE-5003 Multiple-tau digital correlator. The 22mW laser beam (632.8nm in wavelength) was passed through a quartz cell holding the polymer solutions within the temperature controlled toluene bath and the scattering intensity was detected at 90 ° with respect to the incident beam.

The dynamic scattered light was analyzed with an autocorrelator to generate the normalized intensity correlation function, $g^{(2)}(\tau)$, which is related to the normalized electric correlation function, $g^{(1)}(\tau)$, through the Siegert relation.[25, 26] For a system

exhibiting a distribution of collective motions, $g^{(1)}(\tau)$ can be represented by the superposition of exponential decay functions. Laplace inversion routine of $g^{(1)}(\tau)$ was performed to yield the distribution of relaxation times $A(\tau)$, viz.

$$g^{(1)}(\tau) = \int_0^{\infty} A(\tau)\exp(-t/\tau)d\tau \qquad (1)$$

The diffusion coefficient, D, is obtained from $A(\tau)$, where $A(\tau)=Dq^2$, where q is the scattering vector, and the hydrodynamic radius, R_H, is eventually obtained using the Stokes-Einstein equation, $R_H = k_BT/(6\pi\eta D)$, where k_B is the Boltzman's constant, T is absolute temperature, and η is solvent viscosity.

3.3 Result and discussion

3.3.1 Conformational Structure of DP10-PPV in Chloroform

Figure 3-1 shows the SANS profiles in log-log plots of DP10-PPV in chloroform solutions. Like other conjugated polymers, the scattering intensities closely follow q^{-1} dependence in the relatively high-q region ($q > 0.02$ Å^{-1}), signaling the presence of rodlike entity in the solutions. The form factor scattering of rodlike particles in the effective q region can be approximated by the Kratky-Porod equation

$$I(q) = \frac{K}{q}\exp(-\frac{q^2R^2}{4}) \qquad (2)$$

where K is a constant and R is the rod radius. According to Eq. (1), R can be determined from the slope of ln[I(q)q] vs q^2 plot over the effective q region (*cf.* the inset of Figure 3-1). The radius of the rod entity formed by DP10-PPV in chloroform solutions thus determined is 5.0 ± 0.5 Å. This value is comparable to that deduced from the mass per unit length (M_L) of the monomer unit *via*

$$R = \left(\frac{M_L}{\pi\rho_m}\right)^{1/2} = \left(\frac{M_u}{N_{av}L_m\pi\rho_m}\right)^{1/2} = 5.7\text{Å} \qquad (3)$$

where M_u (= 394 g /mol) and L_m (= 5.7 Å) is the molecular weight and length of the monomer unkit, respectively, and ρ_m is the mass density. Consequently, the rod entity probed in the high-q region of the SANS profiles corresponds to hairy-rod segments of DP10-PPV, where the stiffness of the polymer chain gives rise to the q^{-1} power law under large spatial resolution ($q > l_{ps}^{-1}$, with l_{ps} being the persistent length).

In the low-q region ($q < 0.02$ Å^{-1}) the scattering intensity of 0.1 wt% solution

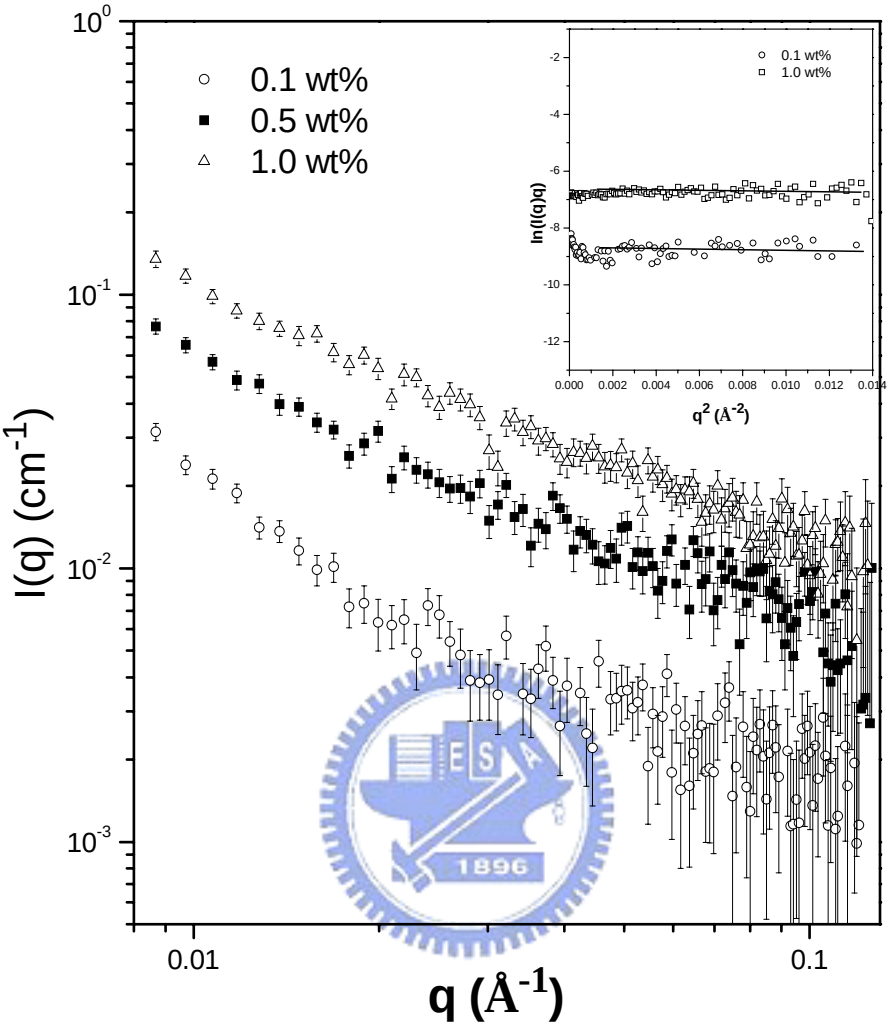

Figure 3-1. The SANS profiles in log-log plots of DP10-PPV/chloroform solutions with different concentrations at room temperature. The inset shows the Kratky-Porod plot over the q region where the intensities closely follow q^{-1} dependence. The radius of the rodlike segments can be obtained from the slope of the plot.

exhibits the power law of $q^{-1.67}$. Such an upturn may be due to the aggregation of the chain segments or simply associated with the form factor of the individual polymer chains prescribed by their global conformation. It is known that the form factor scattering of an expanded coil (i.e., a polymer chain in good solvent) displays an asymptotic power law of $q^{-1.67}$, whereas that of an ideal Gaussian coil shows q^{-2} power law. The contribution of inter-chain aggregation to the intensity upturn in Figure 3-1 is indeed unlikely considering that the intensity is quite weak (with the order of magnitude of 10^{-2} cm^{-1}). Moreover, when the intensities are normalized by the overall polymer concentration (Figure 3-2), the normalized intensities of the 0.5 wt% and 1.0 wt% solutions are indeed lower than that of the 0.1 wt% solution in the low-q region. If the inter-chain aggregation dominated the low-q intensity upturn, the opposite trend should have been observed due to stronger aggregation power at higher polymer concentration. Therefore, we consider the whole scattering curves in Figure 3-1 to be contributed predominantly by the form factor of the DP10-PPV chains. In other words, DP10-PPV chains are well dispersed in chloroform with their conformation being describable by the "expanded wormlike chain".

The wormlike chain model has been widely adopted to describe the conformation of semi-rigid polymers with relatively large persistent length. In the low-q region ($q < l_{ps}^{-1}$) the scattering intensity of a wormlike chain displays the power law prescribed by its global conformation, i.e. $q^{-1.67}$ for expanded linear coil and q^{-2} for ideal Gaussian chain. In the high-q region ($q > l_{ps}^{-1}$) where the scattering behavior is governed by the local chain structure, the intensity closely follows q^{-1} dependence corresponding to the rigid rod behavior of the segments constituting the chain.[23, 24] The cross-over from the rod to the expanded coil regime (q_c) yields an estimate for l_{ps} *via* $l_{ps} \approx 3.5/q_c = 3.5/0.02$ Å^{-1} = 175 Å for DP10-PPV dissolved in

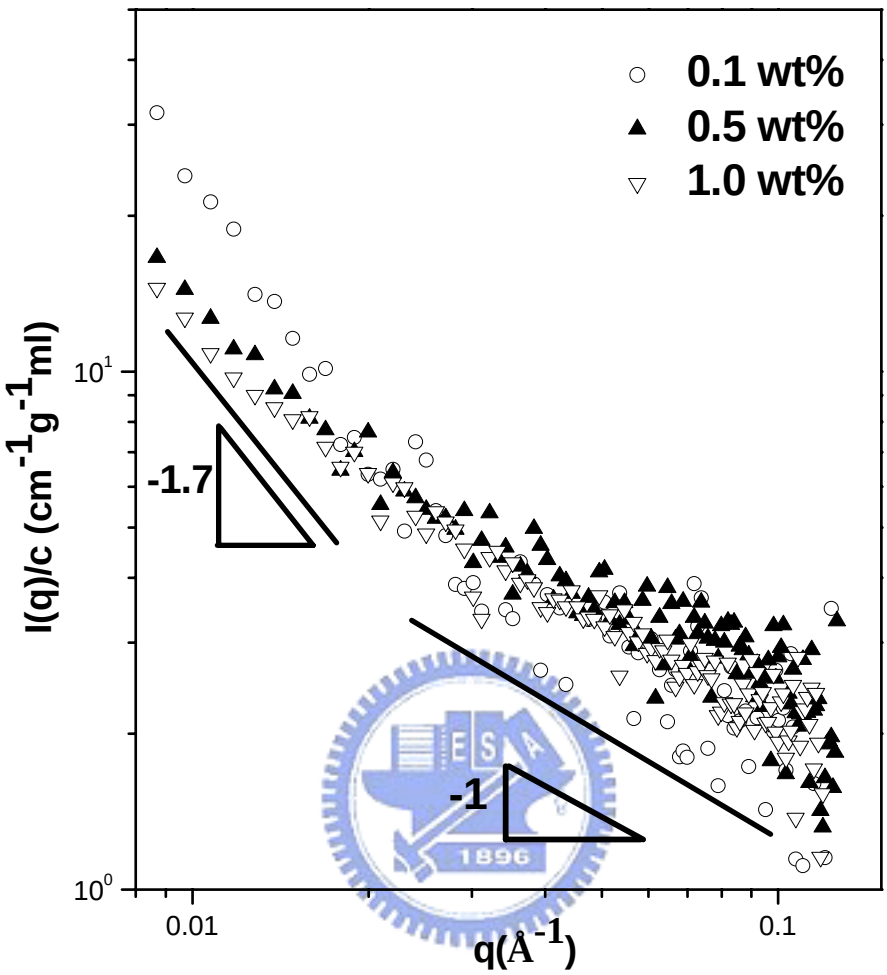

Figure 3-2 The concentration-normalized SANS profiles of DP10-PPV in chloroform solutions.

chloroform with the concentration of 0.1 wt%.[27-29]

It is interesting that at the higher overall polymer concentration (i.e.0.5 and 1.0 wt%), the q^{-1} power law extends towards lower q as compared to that of the 0.1 wt% solution. The whole scattering curve is nearly covered by this power law at the concentration of 1.0 wt%. This means that the persistent length of DP10-PPV chain increases with increasing concentration, namely, from 17 nm at 0.1 wt% to 25 nm at 0.5 wt% and 28 nm at 1.0 wt%. This behavior is in clear distinction from the flexible polymers, where the conformation of the latter is nearly independent of concentration.[6] The concentration dependence of the chain rigidity of DP10-PPV may be attributed to the excluded volume interaction between the rigid segments constituting the polymer chains (analogous to the excluded volume interaction between rodlike molecules that leads to the formation of nematic phase in the solution state). At higher concentration the excluded volume interaction between the rodlike segments becomes more significant; in this case, the polymer chains have to stretch more to reduce this interaction so as to increase the persistent length.

The persistent length of a wormlike chain is half the Kuhn length and can be related to the radius of gyration, R_g, through the following relation[30]

$$R_g = \left(\frac{l_{ps}L}{3}\right)^{1/2} = \left(\frac{l_{ps}L_m M}{3M_u}\right)^{1/2} \quad (4)$$

where L and M are the contour length and molecular weight of the polymer chain, respectively. Given that the molecular weight of DP10-PPV is 524,800 g/mol and the monomer molecular weight and length are 394g/mol and 5.7Å, respectively, the contour length of DP10-PPV is about 593 nm. The radius of gyration of DP10-PPV in chloroform is calculated from Eq. (4) is hence 58.0, 70.3 and 74.4 nm for 0.1, 0.5 and 1.0 wt%, respectively.

The structure of DP10-PPV in chloroform is further studied by dynamic light scattering (DLS). DLS is a powerful instrument for probing the relaxation modes of polymer chains in solution state. The hydrodynamic radius, R_H, corresponding to a certain relaxation motion of polymer chains is the "correlation length" which can be determined by the autocorrelation function. In the dilute regime where the interaction between the polymer chains is insignificant as the chains are well separated from each other, DLS probes the translational motion of the individual chains, such that the correlation length corresponds to the average hydrodynamic radius of the polymer chains. In the semidilute regime, the properties of polymer chains are drastically different from those in the dilute solutions, as the mobility of chain segments is constrained by each other, which then slows down the relaxation rate.[31, 32] An even slower relaxation mode associated with the cluster motion can be identified when the polymer chains undergo aggregation in the solution.

Figure 3-3 shows the hydrodynamic radius distributions at various concentrations of DP10-PPV in chloroform solutions obtained from the DLS measurements at 25℃. Three distinct relaxation modes can be identified. The ultrafast mode with the average R_H of about 0.1 nm represents the motion of the flexible side chains. The fast mode with the average R_H of ca. 30 nm at 0.1 wt % is attributed to the motion of the rodlike segments. The ratio $\rho = R_g/R_H$ serves as a index for the stiffness of the polymer; ρ is 1.5 for flexible coils and a larger value indicates a more extended conformation[33] For DP10-PPV, the value of ρ is about 1.93 for the concentration of 0.1 wt%, indicating that DP10-PPV exhibits a highly extended chain conformation in chloroform. With the increase of concentration, the interaction between the chain segments becomes stronger and hence limits the mobility of the

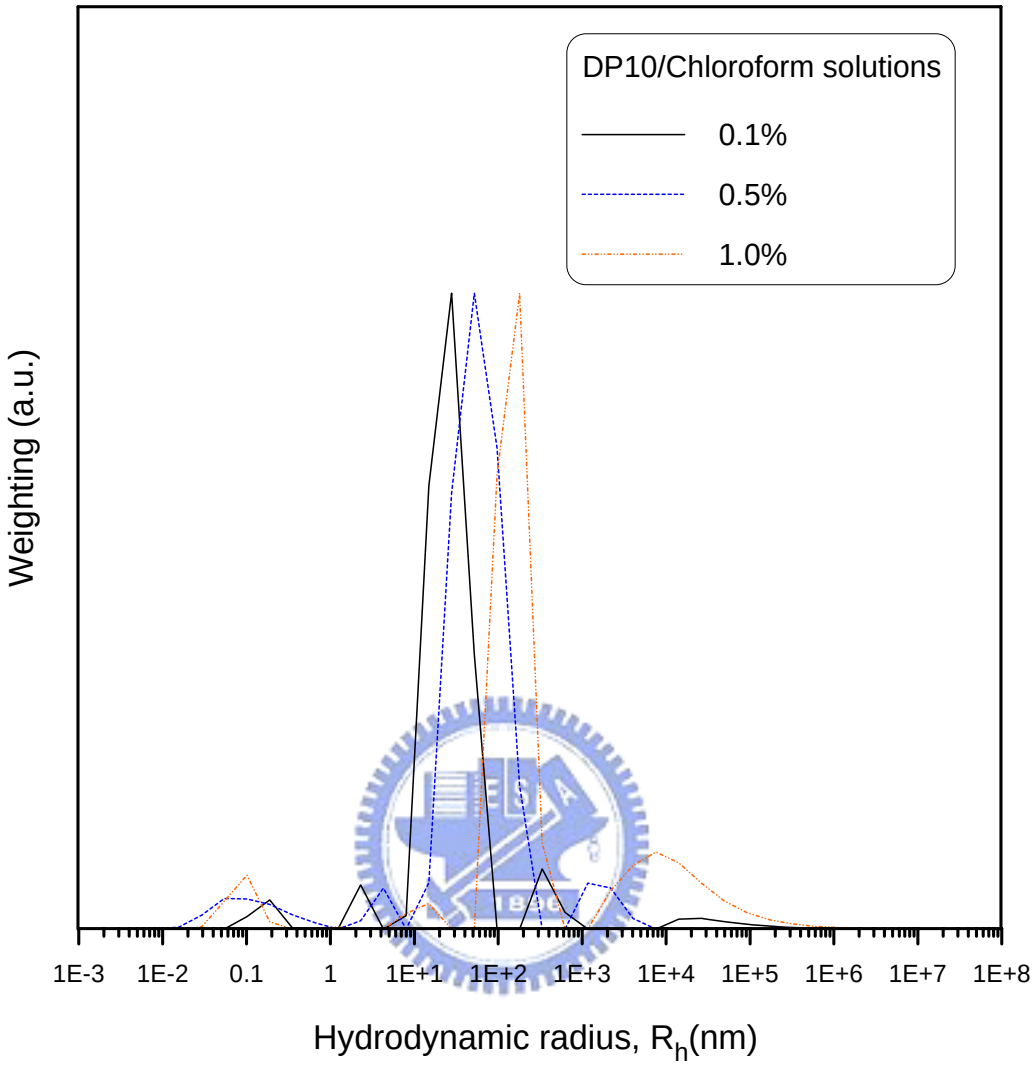

Figure 3-3 The hydrodynamic radius distributions of DP10-PPV/chloroform solutions with different concentrations at room temperature.

chain segments, thereby leading to an increase of R_H associated with this mode. This is consistent with the SANS results showing the increase of l_{ps} with increasing concentration due to increased strength of excluded volume interaction.

An additional "slow mode" with the average R_H of 200 nm ~ 10 μm is also observable in Figure 3-3. This relaxation mode is attributed to the aggregation of DP10-PPV chains. Nevertheless, the extent of aggregation must be very minor as the peak height of this mode is small. In this case, a predominant fraction of DP10-PPV chains still remain well dissolved in chloroform, such that our assertion that the corresponding SANS profiles are dominated by the form factor of the polymer chains is justified.

We have also attempted to reveal the wormlike chain conformation of DP10-PPV dissolved in chloroform by the real-space observation of the polymer chains using atomic force microscopy (AFM). The AFM samples were prepared by drop-casting 0.1 mg/ml or 0.008 mg/ml DP10-PPV/chloroform solutions on highly ordered pyrolytic graphite (HOPG). To arrest the structure of the polymer chains in the solution, the solvent was evaporated extremely rapidly by blowing a nitrogen gas stream over the solution droplet during the casting. This procedure allowed the solvent to be removed within two seconds. The structure of the polymer on the HOPG substrate was subsequently observed by a Seiko SPA-300HV atomic force microscopy operated under tapping mode.

Figure 3-4 displays the topographic image of DP10-PPV on HOPG cast from 0.1 mg/ml solution. A uniform dense network structure is observed over a large area. The network appears to be formed by the interpenetration of numerous threads which

may be the DP10-PPV chains. The average height of the network is ca. 2.0 nm. In a recent work on the visualization of the single chain of a monodendron-jacketed polymer, 14-ABG-PS, Sheiko et al. has found that the height of a monolayer of the polymer was about 1.2 ± 0.2 nm.[34] Because each repeating unit of 14-ABG-PS carries a bulky side group attached with three tetradecyl chains which are longer than the decyl chain in DP10-PPV, the height of a monolayer of DP10-PPV chains is expected to be significantly lower than 1.2 nm. Consequently, the network observed in Figure 3-4 is formed by the interpenetration of more than one layers of DP10-PPV chains due to the relatively high solution concentration used for the casting.

In order to obtain the image of a true monolayer of DP10-PPV chains, a solution with the concentration of 0.008mg/ml was used to prepare the sample. Figure 3-5 shows the resultant topographic image of the polymer. In contrast to the dense network shown in Figure 3-4, a number of clusters formed by the aggregation of the polymer chains are observed. These aggregates are formed during solvent evaporation. The average height of clusters is ca. 0.8 nm; therefore, the threads tying with each other to form the clusters do correspond to a monolayer of polymer chains.

Although identification of isolated single DP10-PPV chains is not accessible due to aggregation of polymer chains during solvent evaporation, the topological feature of the chains forming the aggregates can shed some light on the conformational structure of this conjugated polymer. It can be seen from Figure 3-5 that the polymer chains are indeed quite flexible in contrast to the common intuition suggesting that the conjugated polymer backbone behaves like a stiff rod. Consequently, the “wormlike chain model” used for interpreting the SANS results is indeed a more plausible model.

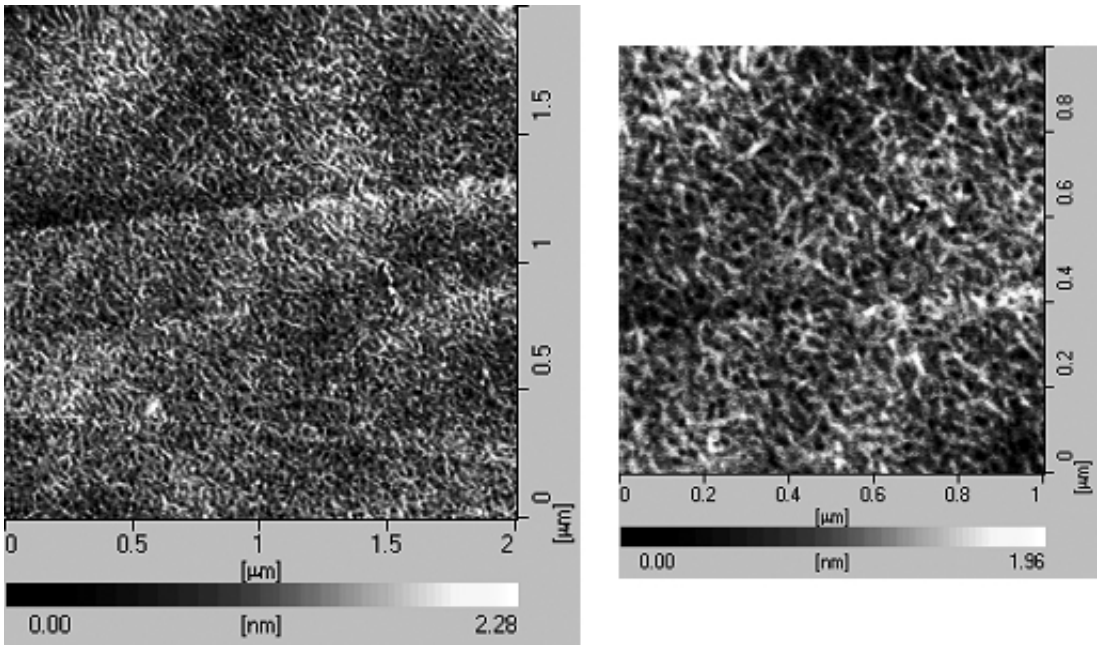

Figure 3-4 AFM topographic images of DP10-PPV cast from 0.1 mg/ml chloroform solution on HPOG.

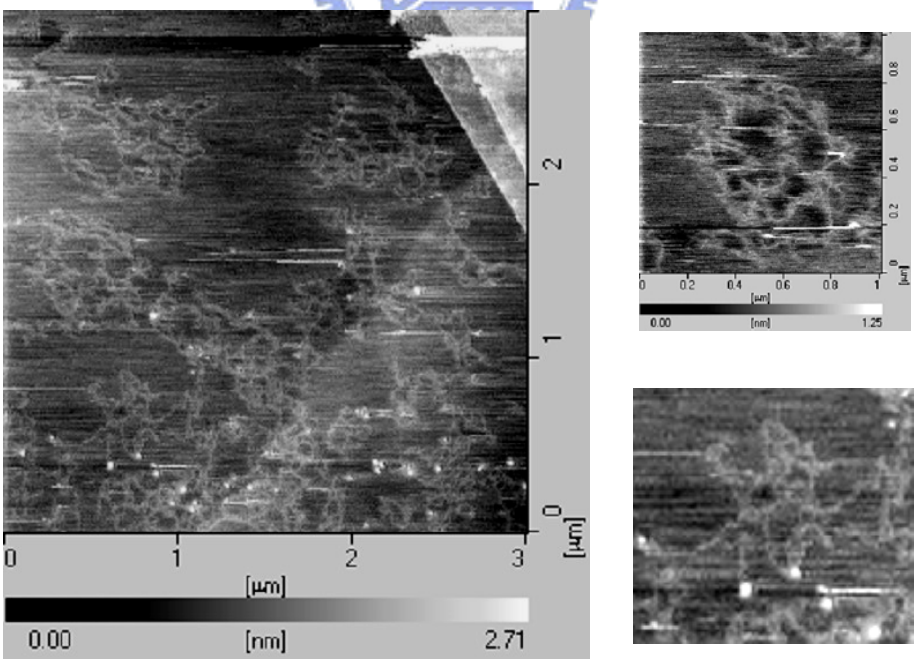

Figure 3-5 AFM topographic images of DP10-PPV cast from 0.008 mg/ml chloroform solution on HPOG. The two images on the right provide a better view on the topological feature of the aggregates formed by the polymer chains.

The chain flexibility may stem from the inevitable presence of the chemical tetrahedron defects which introduce a minor population of skew bond conformation or from the spontaneous fluctuation of the chain contour from a straight line. The image we obtained thus far is not clear enough for us to estimate the persistent length of the chains. More efforts are hence required to obtain images with better resolution to allow quantitative study of conformational feature and aggregate structure of the conjugated polymer.

In chapter 2, the aggregation behavior of poly(2,3-diphenyl-5-hexyl-1,4-phenylenevinylene) (DP6-PPV) bearing hexyl side chains in solution state has been examined.[16] This polymer was shown to exhibit a strong inter-chain aggregation in chloroform and the network aggregates (with the fractal dimension of 2.6) thus generated dominated the SANS intensity. However, here we found that the predominant fraction of DP10-PPV chains were well dispersed in chloroform, indicating that increasing the length of the side chains attached to the PPV backbone tend to suppress the inter-chain aggregation. The different dissolution behavior of these two polymers is further demonstrated by comparing their SANS intensities normalized by the corresponding neutron scattering length density (SLD) contrasts, $I(q)/\Delta\rho^2$, as shown in Figure 3-6 for the 1.0 wt% solution. It can be seen that DP6-PPV clearly shows a much stronger intensity in the low-q region, which is consistent with a much more severe inter-chain aggregation in the system. For DP6-PPV, we have proposed that the aggregation observed for the chloroform solution stemmed primarily from incomplete dissolution of the hairy-rod segments in the polymer powders used for solution preparation. In this case, a fraction of the segments formed highly stable π-π complex in the DP6-PPV powder used for solution preparation. This kind of complex was formed by the in-plane stacking of the

phenylene or phenyl moiety in DP6-PPV and the characteristic distance of ca. 3.0 Å between the aromatic groups forming the complex would lead to a peak at $2\theta \approx 29^{o}$ in the wide-angle X-ray scattering (WAXS) profile.[35] This species could neither be solvated by chloroform nor be disrupted by heating; as a result, the chains tied firmly by the π-π complex formed network aggregates in the solution.

Because most chains of DP10-PPV remain well dispersed in chloroform, we may speculate that the highly stable π-π complex found in DP6-PPV may be absent in the DP10-PPV powder used for the solution preparation. This assertion is consolidated by Figure 3-7 which compares the WAXS profile of DP6-PPV with that of DP10-PPV powders. It can be seen that DP6-PPV shows a scattering peak at $2\theta = 29^{o}$ (corresponding to a Bragg spacing of 3.0 Å) associated with the highly stable π-π complex. This π-π complex is however absent in DP10-PPV powder as the WAXS peak at 29° is missing. In this case, the stronger steric hindrance imposed by the longer decyl side chains in DP10-PPV may impede the complex formation in the powder. Hence, a uniform dispersion of polymer chains in chloroform becomes accessible for DP10-PPV

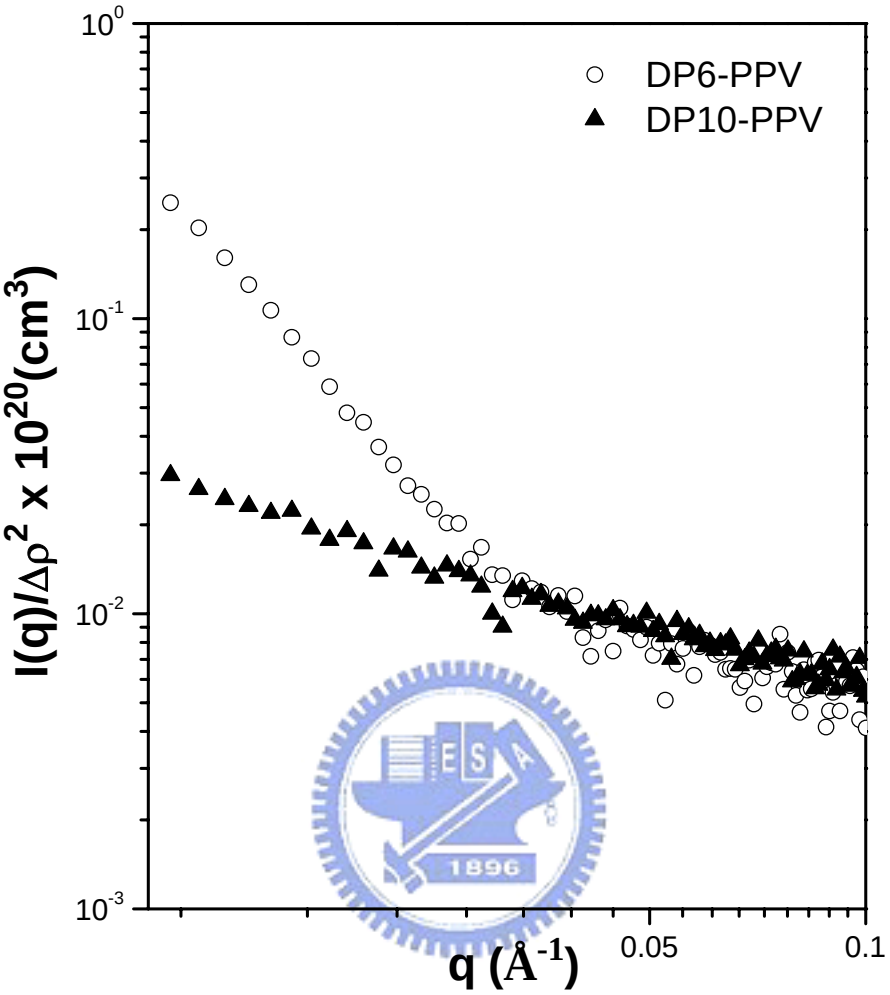

Figure 3-6 A comparison between the contrast-normalized SANS intensities of 1 wt% DP6-PPV and DP10-PPV solutions. DP6-PPV solution is found to exhibit a much stronger low-q intensity, signaling significant degree of inter-chain aggregation.

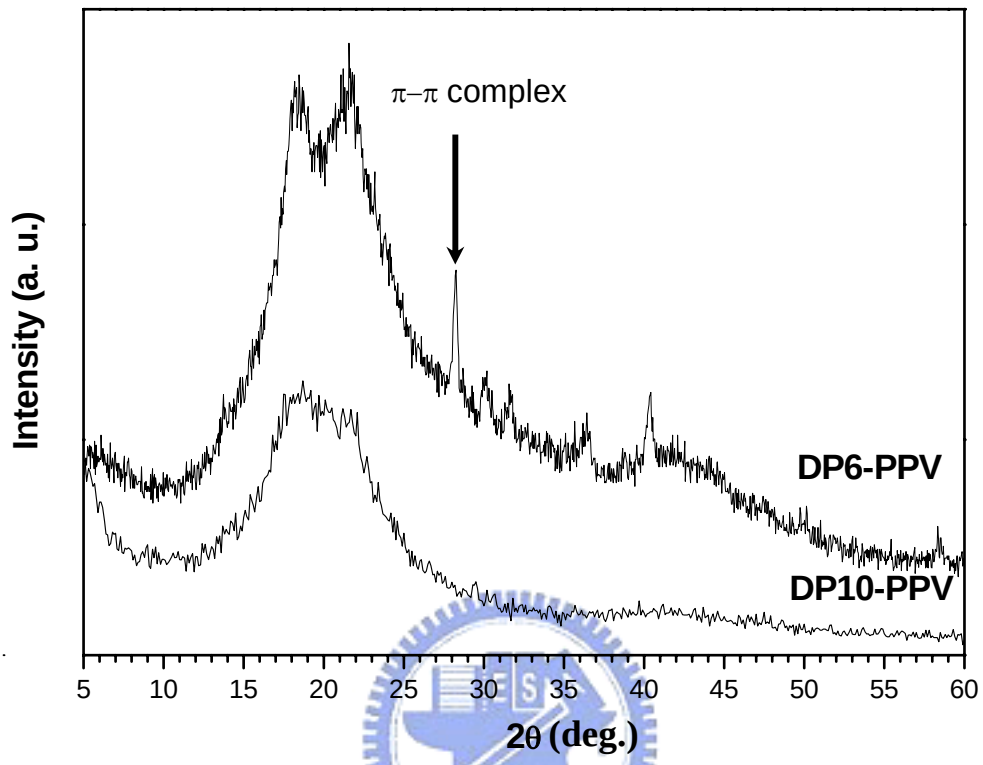

Figure 3-7 The wide-angle X-ray scattering (WAXS) scans of DP6-PPV and DP10-PPV powders used for the solution preparations. DP6-PPV powder is seen to exhibit strong diffraction peaks signaling the presence of a significant degree of crystallinity. The crystal diffraction becomes nil for DP10-PPV showing that the polymer is essentially uncrystalline in the powder. A scattering peak at $2\theta = 29^{o}$ (corresponding to a Bragg spacing of 3.0 Å) associated with the π-π complex is also identified for DP6-PPV powder.

3.3.2 Aggregation Behavior of DP10-PPV in Toluene

The foregoing study reveals that DP10-PPV chains are well dispersed in chloroform with only a minor extent of aggregation. Now we turn to the dissolution behavior of this polymer in a poorer solvent, toluene. Figure 3-8 shows the hydrodynamic radius distribution obtained from DLS experiment for DP10-PPV/toluene solutions with the concentrations of 0.1, 0.5 and 1.0 wt%. Three distinct relaxation modes associated with the side chain motion (R_H < 1.0 nm), segmental motion (R_H ~ 30 nm) and inter-chain aggregation (R_H = 0.3 ~ 10 μm) are again observed. In contrast to the chloroform solution, the slow mode becomes the dominant relaxation mode for the toluene solutions irrespective of the overall polymer concentration. This attests that most DP10-PPV chains in toluene aggregate to form clusters of μm in size due to the poorer solvent quality of toluene. It is noted that the R_H of the slow mode of 0.5 wt % solutions is approximately the same as that of 1.0 wt% solution. This suggests that the aggregates in these solutions are largely confined to each other and hence limits their mobilities.

Figure 3-9 shows the SANS profiles in log-log plot of DP10-PPV/toluene solutions with the three concentrations. In contrast to the scattering profiles of the chloroform solutions showing q^{-1} power law in the high-q region, the scattering intensity of the 0.1 wt% solution displays a power law of $q^{-1.3}$ over nearly the entire q range studied. The q-dependence of the intensity transforms to another power law of q^{-2} at the higher concentrations of 0.5 and 1.0 wt%. In the light of the DLS result showing that a predominant fraction of the polymer chains form aggregates, the SANS intensities in Figure 3-9 are considered to be overwhelmed by the aggregates formed in toluene. In this case, the SANS profiles are governed by the internal structure of the aggregates with μm in size. This postulate is consolidated by

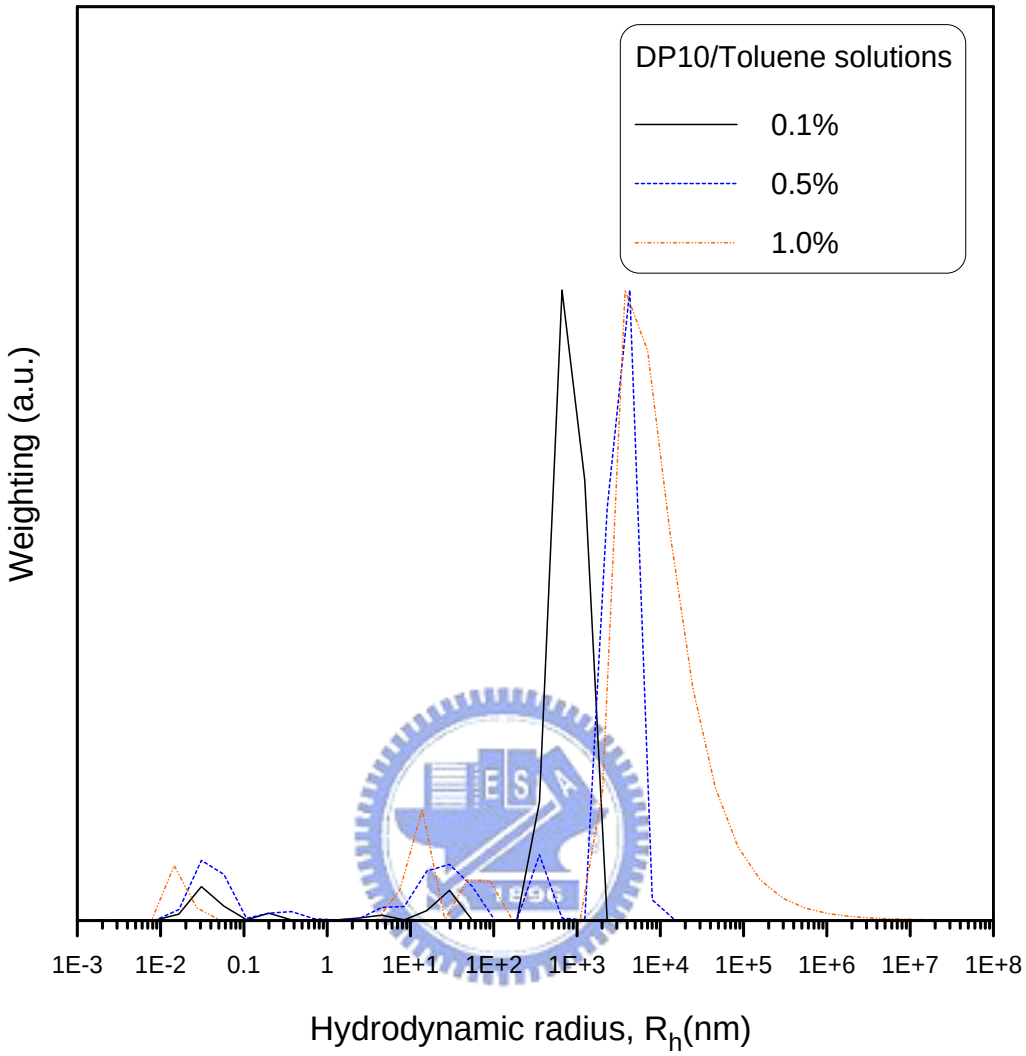

Figure 3-8 The DLS result of DP10-PPV in toluene solutions with different concentration.

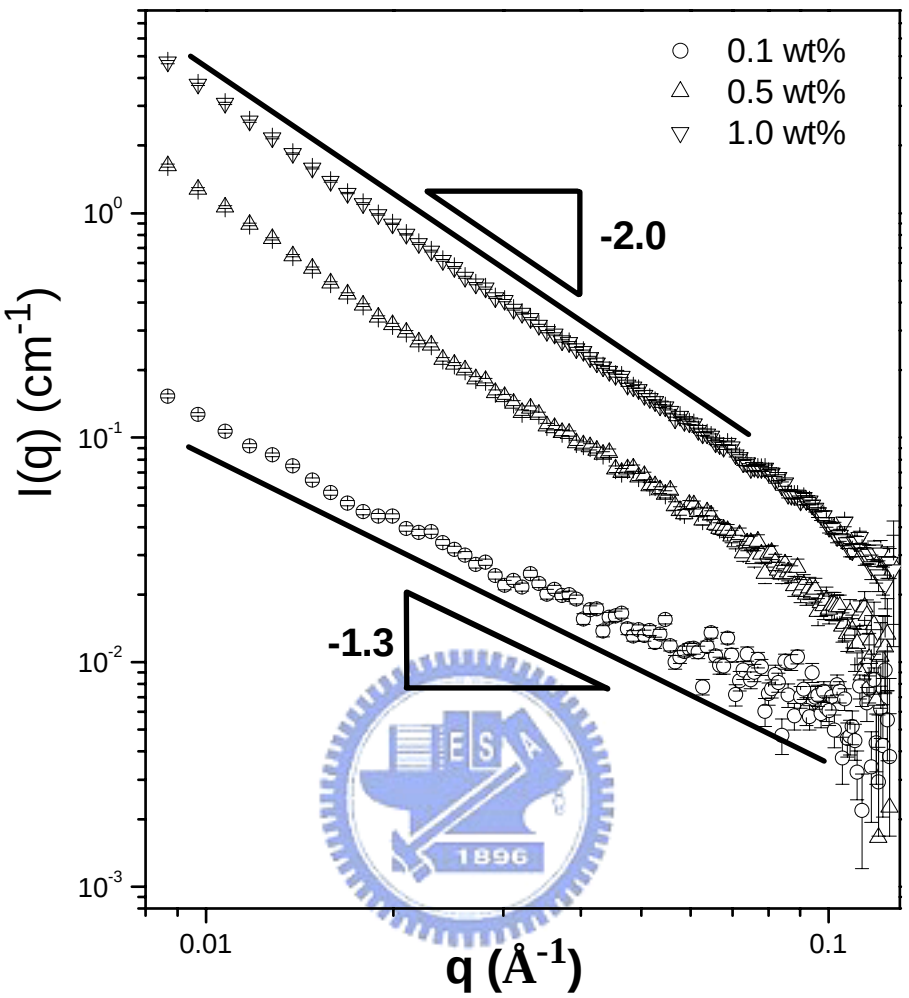

Figure 3-9 The log-log plot SANS profiles of DP10-PPV dissolved in toluene solutions with different polymer concentration at room temperature.

comparing the intensity profiles normalized by the SLD contrast of the toluene solutions with those of the chloroform solutions, as shown in Figure 3-10. It can be seen that the toluene solutions consistently exhibit a stronger intensity in the low-q region at a given concentration, which signals that DP10-PPV chains in toluene do display significant degree of inter-chain aggregation.

We assert that the observed SANS profiles are overwhelmed by form factor of the aggregates. In this case, the power law of I(q) ~$q^{-1.3}$ observed for the 0.1 wt% solution indicates that over the length scale covered by the q region the internal structure of the aggregates is characterized by a mass fractal dimension of 1.3, which may correspond to a highly defective network generated by the segmental association of the polymer chains, as schematically illustrated in Figure 3-11. The sites of the segmental association act as the (physical) junction points for the chains.

When the concentration is increased to 0.5 wt% and 1.0 wt%, the scattering intensities display q^{-2} power law. This suggests that the aggregates become more compact (due to prevalent segmental association) at higher polymer concentration and may indeed contain disklike domains which give rise to the q^{-2} power-law dependence of the scattering intensities. For a thin plate the scattering intensity in the asymptotic region is given by[30]:

$$I(q) = A\frac{2\pi}{q^2}(\Delta\rho^2)T^2\exp(-\frac{T^2}{12}q^2) \qquad (5)$$

where T is thickness of the plate. Eq. (5) prescribes that the thickness of the plate can be determined from the slope of ln[I(q)q^2] vs q^2 plot, as shown in Figure 3-12. The thickness of the disklike domain thus determined using the intensities of 0.5 and

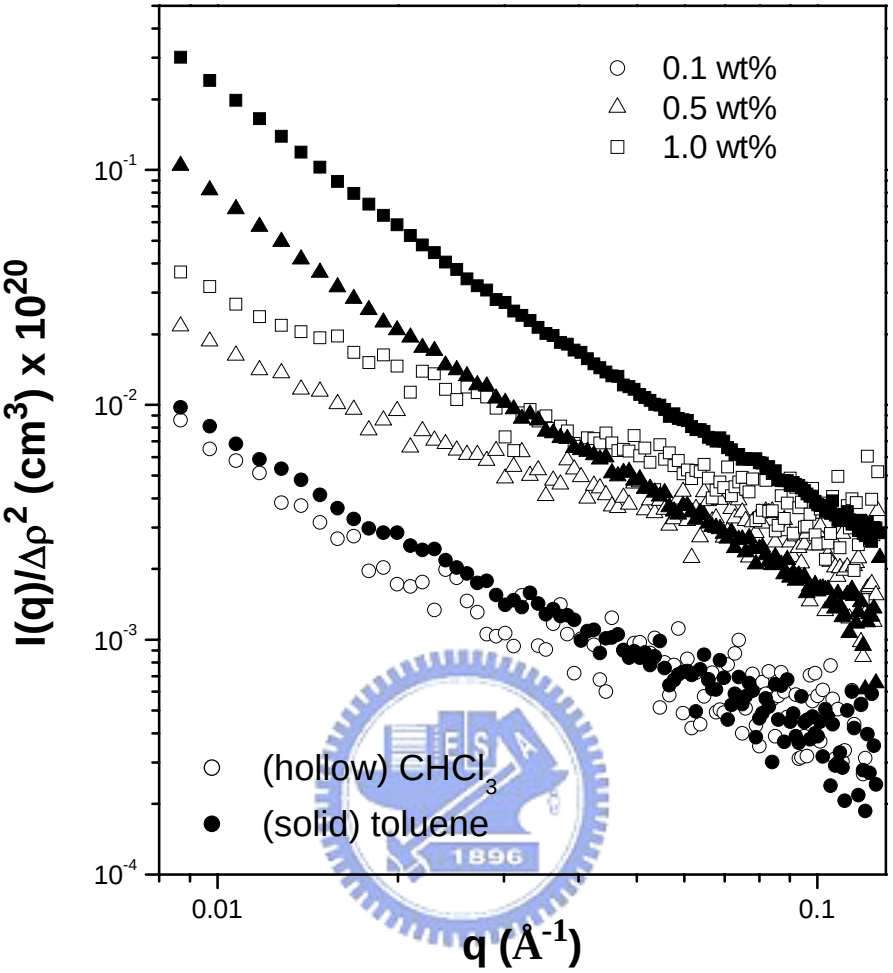

Figure 3-10. The contrast-normalized SANS profiles of DP10-PPV dissolved in different solvent. The scattering intensity of toluene solution is much higher than chloroform especially in high concentration. Asserting the aggregation behavior is prevalent and toluene is relative poor solvent for DP10-PPV molecules.

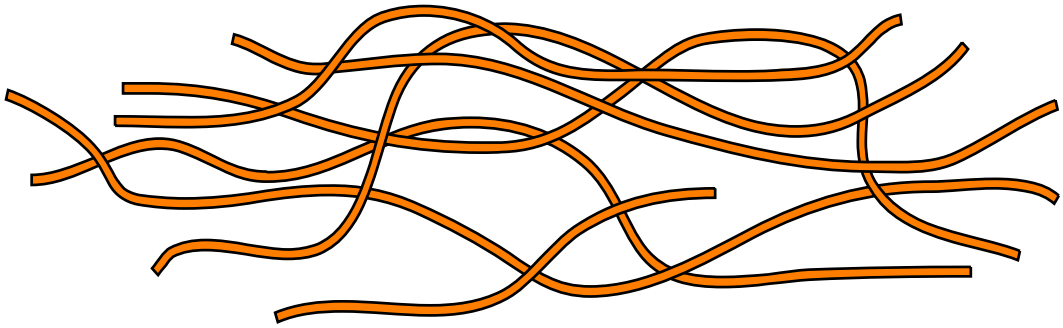

Figure 3-11 Schematic illustration of the fractal aggregate formed in DP10-PPV/toluene 0.1 wt% solution.

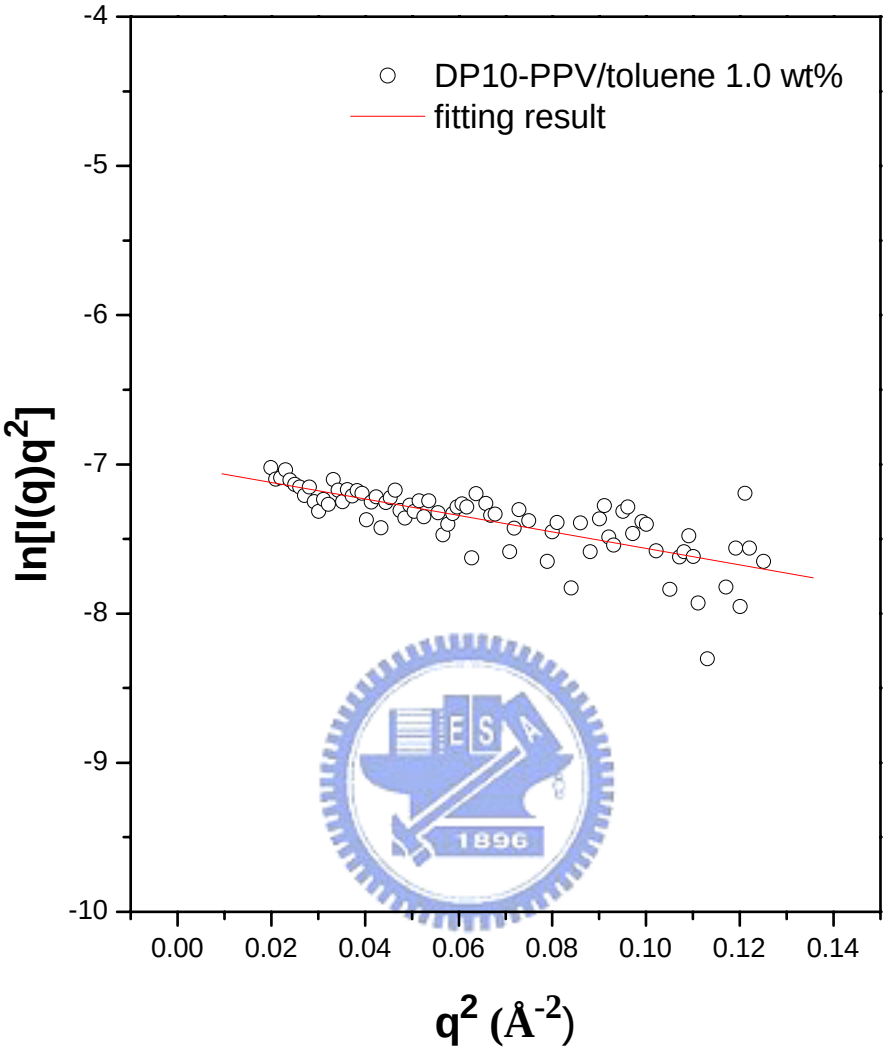

Figure 3-12 Determination of the thickness of disklike domains formed in DP10-PPV/toluene 1.0 wt% solution from the slope of $\ln[I(q)q^2]$ vs. q^2 plot.

1.0 wt% solutions is 20 Å. The diameter of a single DP10-PPV chain obtained from the SANS profiles of chloroform solutions is 10 Å; therefore, the disklike domains in the aggregates compose of two layers of DP10-PPV chains lying flatly on the disk surface, as schematically shown in Figure 3-13. It should be noted that similar disklike domains formed by the segmental aggregation have also been observed for other conjugated polymers such as poly(2-methoxy-5-(2'-ethyl-hexyloxy)-1,4-phenylene vinylene) (MEH-PPV)[36] and poly(6,6-dioctyl fluorene) (PFO)[37] dissolved in relatively poor solvents. In the case of DP6-PPV, the smaller fractal dimensions (~ 2.2) coupled with highly compact internal structure revealed by SANS indicated that the aggregates in toluene tended to collapse into disklike objects due to severe segmental association.[37] These results may imply a tendency of the hairy-rod polymers to aggregate to form disklike domains in the solvents with relatively poor quality. This may be related to the general tendency of the polymers to self-organize into a lamellar structure consisting of alternating backbone and side chain layers in the bulk state. As the formation of the lamellar structure in the bulk state is driven by repulsion between the conjugated backbone and the side chains, the aggregation of DP10-PPV chains to form a bilayer structure in toluene may likewise be driven by the amphiphicility of the segments, since toluene was a relatively poor and good solvent for the aliphatic side chains and the aromatic backbone, respectively. In this case, a “micelle-like” segmental association with the backbone facing towards the solvent to shield the side chains may take place, leading to the formation of the disklike domains.

According to our previous study of DP6-PPV, the micelle-like segmental association is relatively unstable as it can be disrupted by moderate heating. Figure 3-14 shows a series of scattering profiles of 1.0 wt% DP10-PPV/toluene solution

collected *in-situ* at various temperatures in a heating process. The scattering intensity in the low-q region drops suddenly when the temperature is increased to 55 ℃, showing the occurrence of de-aggregation upon the heating, similar to DP6-PPV system. In this case, the q^{-1} power law emerges in the high-q region because the population of the molecularly dissolved chains increases. Heating to 70 ^{o}C is found to completely wipe out the segmental aggregation as the scattering profile at this temperature nearly matches that collected at an even higher temperature 85 ^{o}C. As a matter of fact, the contrast-normalized scattering profiles at these temperatures nearly match with that of the 1.0 wt% chloroform solution at room temperature (inset of Figure 3-14), where the scattering profile is dominated by the form factor of DP10-PPV chains.

After the data acquisition at 85 ^{o}C the toluene solution was cooled right back to 25 ^{o}C to examine the re-aggregation behavior of DP10-PPV. The SANS profile of the cooled solution collected within 1 hr after reaching 25 ^{o}C is shown in Figure 3-15. Although the low-q intensity increases slightly upon the cooling, the scattering profile do not recover to that of the as-prepared solution (which has been stored at 25 ^{o}C for more than 24 hrs prior to SANS experiment), indicating that the re-aggregation is spontaneous but is very slow.

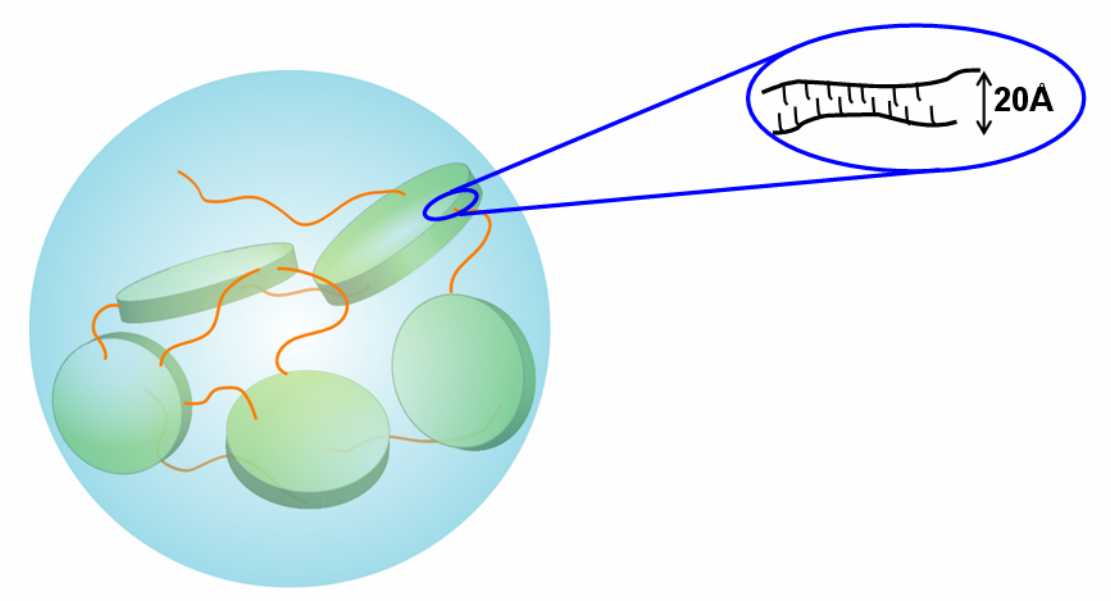

Figure 3-13. Schematic illustration of the disk domains formed in DP10-PPV/toluene solutions with higher polymer concentration (i.e. 0.5 and 1.0 wt%). The disklike domains compose of two layers of polymer chains.

.

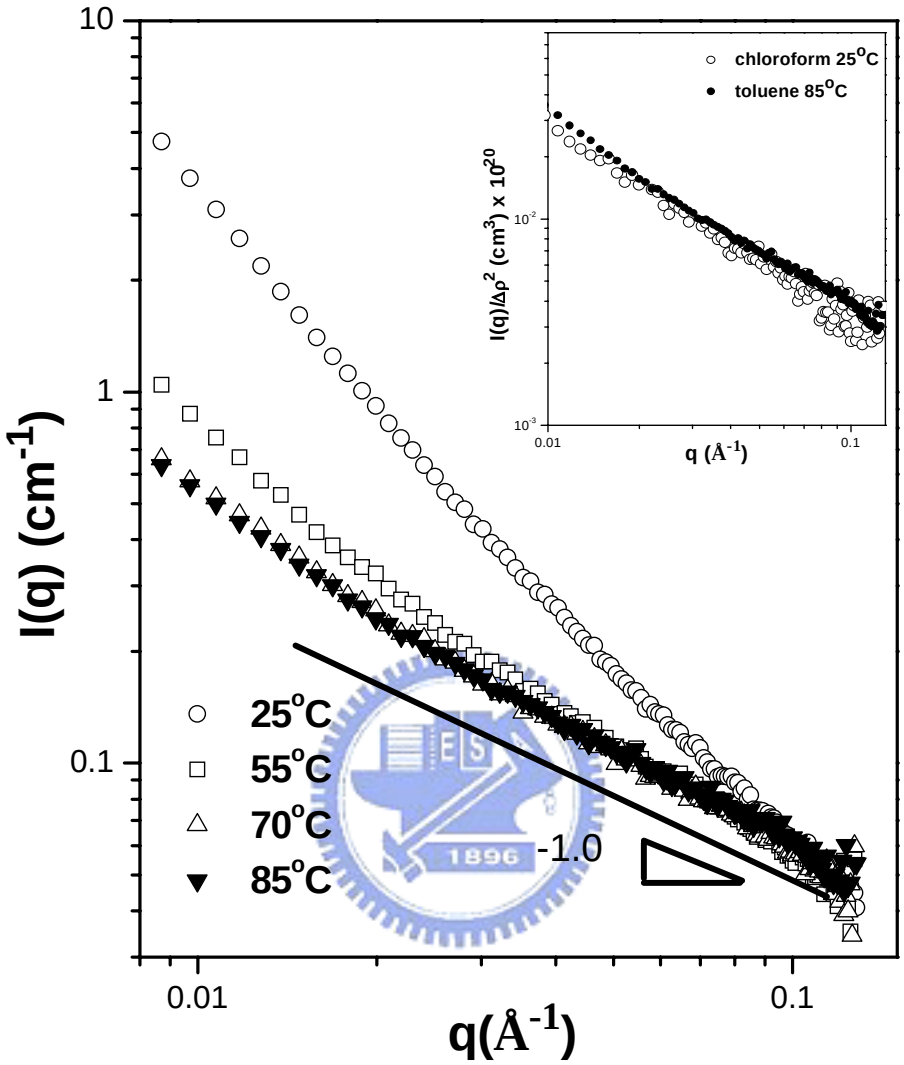

Figure 3-14. A series of SANS profiles of DP10-PPV 1.0 wt% toluene solution in a heating cycle.

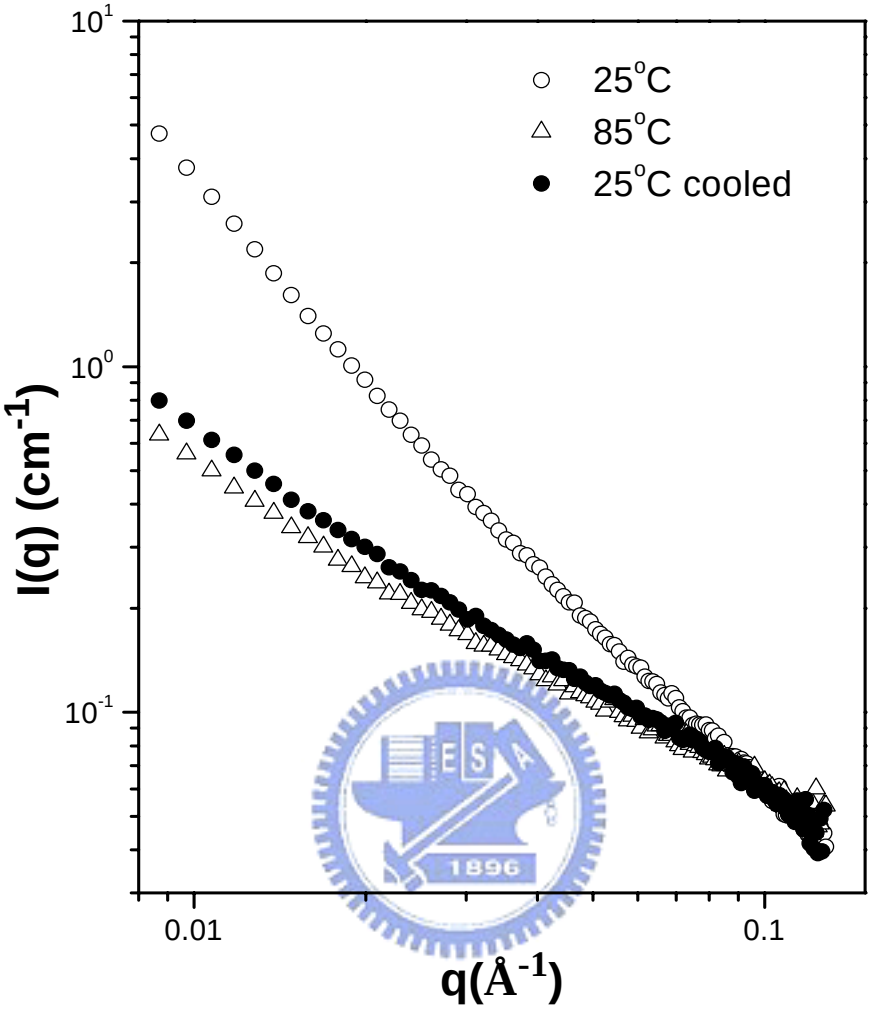

Figure 3-15. The scattering profile of DP10-PPV/toluene 1.0 wt% solution obtained by cooling from 85 °C to 25 °C

Reference

1. Tracy, M. A.; Garcia, J. L.; Pecora, R. *Macromolecules* **1993**, 26, 1862.

2. Sato, T.; Ohshima, A.; Teramoto, A. *Macromolecules* **1994**, 27, 1477.

3. Takada, Y.; Sato, T.; Teramoto A. *Macromolecules* **1991**, 24, 6215.

4. Petekidis, G.; Vlassopoulos, D.; Fytas, G.; Rulkens, R.; Wegner, G. *Macromolecules* **1998**, 31, 6129.

5. Petekidis, G.; Vlassopoulos, D.; Fytas, G.; Rulkens, R.; Wegner, G.; Fleischer, G. *Macromolecules* **1998**, 31, 6139.

6. Rubinstein, M.; Colby, R. H. *Polymer Physics*. Oxford: New York, **2003**.

7. de Gennes, P. G. *Scaling Concepts in Polymer Physics*. Cornell University Press: New York, **1979**.

8. Liu, A. J.; Nagel, S. R. *Nature* **1998**, 396, 21.

9. Flory P. J. *Principals of Polymer Chemistry*. Cornell University Press: New York, **1953.**

10. Lopez, D.; Guenet, J.-M. *J. Phys. Chem. B.* **2002**, 106, 2160.

11. Burroughes, J. H. B., D. D. C.; Brown, A. R.; Marks, R. N.; Mackay, K.; Friend, R. H.; Burns, P. L.; Holmes, A. B. *Nature* **1990,** 347, (539).

12. Friend, R. H. G., R. W.; Holmes, A. B.; Burroughes, J. H.; Marks, R. N.; Taliani, C.; Bradley, D. D. C.; dos Santos, D. A.; Bredas, J. L.; Loglund, M.; Salaneck, W. R. . *Nature* **1999,** 121, 379.

13. Shi Y.; Liu, J.; Yang, Y. *J. Appl. Phys.* **2000**, 81, 4254.

14. Nguyen, T. Q. D.; V.; Schwartz, B. J. *J. Chem. Phys.* **1999**, 110, 4068.

15. Chen, S. H.; Su, A. C.; Chang, C. S.; Chen, H. L.; Ho, D. L.; Tsao, C. S.; Peng, K. Y.; Chen, S. A. *Langmuir* **2004**, 20, 8909.

16. Li, Y. C.; Chen, K. B.; Chen, H. L.; Hsu, C. S.; Tsao, C. S.; Chen, J. H.; Chen, S. A. *Langmuir* **2006,** 22, 11009.

17. Hsieh, B. R.; Antoniadis, H. *Adv Mater* **1995,** 7, 36.

18. Hsieh, B. R.; Yu, Y.; Forsythe, E. W.; Schaff, G. M.; Feld, W. A. *J. Am. Chem. Soc.* **1998,** 120, 231.

19. Wan, W. C.; Antoniadis, H.; Choong, V. E.; Razafitrimo, H.; Gao, Y.; Feld, W. A.; Hsieh. B. R. *Macromolecules* **1997**, 30, 6567.

20. Hsieh, B. R.; Yu, Y. U.S. Patent 5,945,502 **1999**.

21. Glinka, C. J.; Barker, J. G.; Hammouda, B.; Krueger, S.; Moyer, J. J.; Orts, W. J. *J. App. Cryst.* **1998**, *31*, 430.

22. Cold Neutron Research Facility at the National Institute of Standard and Technology, *NG3 and NG7 30-Meter SANS Instruments Date Acquisition Manual* **1999**.

23. Higgins, J. S.; Benoit, H. C. *Polymers and Neutron Scattering*, Oxford: New York **1994**.

24. Roe, R. J., *Methods of X-ray and Neutron Scattering in Polymer Science*. Oxford: New York, **2000**.

25. Schmitz, K. S. *An Introduction to Dynamic Light Scattering by Macromolecules*. Academic Press: Boston San Diego New York, **1990**.

26. Brown. W., *Dynamic Light Scattering,* Clarendon Press, Oxford **1993**.

27. Des Cloizeaux, J. *Macromolecules*, **1973**, 6, 403.

28. Yoshizaki, T.; Yamakawa, H. *Macromolecules*, **1980**, 13, 1518.

29. Aime, J. P.; Bargain. F.; Schott, M.; Eckhardt, H.; Miller, G. G.; Elsenbaumer, R. L. *Phys. Rev. Lett.* **1989**, *62*, 55.

30. Glatter, O.; Kratky O. *Small Angle X-ray Scattering*. Academic press inc: London, **1982**.

31. Amis, E. J.; Janmey, P. A.; Ferry, J. D.; Yu, H. *Macromolecules* **1983,** 16, 441.

32. Teraoka, I. *Polymer solutions: An introduction to physical properties*. John Wiley

& Sons: New York, **2002**.

33. Kromer, H.; Kuhn, R.; Pielartzik, H.; Siebke, W.; Eckhardt, V.; Schmidt, M. *Macromolecules* **1991,** 24, 1950.

34. Sheiko, S. S.; Moller, M. *Chem. Rev.* **2001,** 101, 4099.

35. Huang, Y. F.; Yang, S. H.; Hsu, C. S.; Chen, S. A.; Su, A. C. *ICMAT International Conference on Materials for Advanced Technologies,* Singapore **2001**.

36. Ou-Yang, W. C.; Chang, C. S.; Chen, H. L.; Tsao, C. S.; Peng, K. Y.; Chen. S. A.; Han, C. C. *Phys. Rev. E*, **2005**, 72, 031802.

37. Knaapila, M.; Garamus, V. M.; Dias, F. B.; Almasy, L.; Galbrecht, F.; Charas, A.; Morgado, J.; Burrows, H. D.; Scherf, U.; Monkman, A. P. *Macromolecules* **2006,** 39, 6505.

CHAPTER 4

Conclusions and Suggestions for Future Works

4.1 Conclusions

This thesis provided a systematic study on the conformational structure and aggregation behavior of DP-PPVs. The effects of intrinsic solvent quality, solution concentration, temperature and side chain length of the conjugated polymers have been revealed by means by SANS and DLS experiments. For DP6-PPV bearing the shorter hexyl side chains, the polymer chains were found to exhibit inter-chain aggregation in the solutions with both chloroform and toluene. The aggregation generated relatively large network aggregates with their internal structures characterized by the mass fractal dimensions of 2.2 ~ 2.7. In chloroform the segmental association was attributed to the π-π complex already present in the DP6-PPV powder used for the solution preparation. This highly stable complex remained unsolvated in chloroform and hence tied the polymer chains to form network aggregates. The SANS profiles associated with these networks displayed two power-law regimes characterizing the mass fractal dimension of the networks and the rodlike sub-chains between the junction points in the networks. Further segmental association took place in toluene due to the poor affinity of the aliphatic side chains of DP6-PPV to the solvent. The resultant aggregates were highly compact and the small ξ_s caused the shift of the q^{-1} power-law regime to the region beyond the measurable q range of the SANS experiment. The aggregates of DP6-PPV in toluene thus consisted of two types of segmental associations, namely, the π-π complex which persisted even after heating to 85 ^{o}C and the micelle-like segmental association which could be disrupted by moderate heating.

For DP10-PPV composing of the longer decyl side chains, its conformational structure and the aggregation behavior have been investigated and compared with those of DP6-PPV to reveal the effect of side chain length on the dissolution behavior of DP-PPVs. DP10-PPV molecules were found to disperse fairly well in chloroform, such that the form factor of the polymer chains dominated the SANS profile. In this case, DP10-PPV chains were found to exhibit the expanded wormlike chain conformation with the persistent length increasing with overall polymer concentration due to the increase of excluded volume interaction. Therefore, DP10-PPV was dissolved at molecular level in chloroform, in contrast to DP6-PPV which was dissolved at the colloidal level due to the incomplete dissolution of the hairy-rod segments forming $\pi-\pi$ complex. Like DP6-PPV, DP10-PPV chains aggregated significantly in toluene to form aggregates of several μm in size. The aggregates were loose at the overall polymer concentration of 0.1 wt%. However, the aggregates were found to compose of compact disklike domains as the concentration was increased to 0.5 wt% and 1.0 wt%. The disk domains were formed by stacking two DP10-PPV chains normal to the domain interface with the backbone facing towards the solvent to shield the side chains. These “micelle-like” domains may likewise be disrupted easily by moderate heating.

4.2 Suggestions for Future Works

The present study has revealed the solution structures of two representative conjugated semiconducting polymers. This class of polymers was found to exhibit highly different dissolution behavior from the conventional flexible polymers in the sense that the chains undergo inter-chain aggregation due to the π–π interactions and disparity in the affinity of the backbone and side chain to the solvents. More studies are indeed necessary to establish a definitive universal picture describing the dissolution behavior of hairy-rod conjugated polymers and to make a close connection of the solution structure to the practical applications of the polymers in opto-electronics.

In the preset study, two DP-PPVs with different side chain lengths have been investigated. Comprehensive studies on this polymer derivative with systematic variations of the chemical structures of backbone (e.g. incorporation of conjugated comonomer unit) and side chain (e.g. a wider variation of chain length, introduction of chain branching, etc.) will be of interest to affirmatively establish the roles of π–π interactions, amphiphicility and other significant factors governing the aggregation of hairy-rod polymers in solution state. Moreover, the results will also be important for identifying the molecular design strategy for tailoring the solution structure of conjugated semiconducting polymers.

In the present study, we have examined the solution structures of the polymers in two solvents with relatively distinct qualities and different dissolution behavior was observed. It will be of interest to resolve the dissolution behavior over an even wider range of variation of intrinsic solvent quality by investigating the solutions with other solvents (commonly used for the device fabrication) such as tetrahydrofuran (THF), chlorobenzene and DMF. Moreover, the solvent quality may also be

systematically varied by the addition of different amount of a non-solvent such as methanol.

The effect of temperature on the solution structure has also been investigated in this thesis with the lowest accessed temperature of ca. 25 ^{o}C. It will be of interest to reveal the structure at the subambient temperature. It has been shown that hairy-rod conjugated polymers may undergo gelation upon prolonged aging at subambient temperatures, indicating further structural reorganization during the aging. The structure changes associated with the gelation should be able to be resolved by the scattering methods such as small angle X-ray scattering (SAXS), SANS and light scatterings. Moreover, it will also be important to explore the relationship between the structure and the photophysical properties of the aged gels.

For the practical applications, the conjugated polymer solutions are used to cast into thin films for device fabrication. It has been proposed that the dispersion state of the polymer in the solution may influence the morphology and hence the photophysical properties of the light-emitting films formed after solvent removal. This indicates a solution-phase controlled morphology and photo-physics as the structure of the as-cast film is metastable presumably due to the fast solvent removal and the sluggish mobility of the stiff conjugated chains that prevent the polymer from attaining its equilibrium morphology during solvent casting. However, a reasonable correlation among the solution structure, processing condition, film morphology and photpphysical properties has not been established. Establishment of such a relationship is a complex problem and will require a combination of a wide variety of experimental tools, including spectroscopies (UV-Vis, PL, EL, time-of–flight,etc.), scatterings (for solution structure study: LS, SANS and SAXS; for film morphology study: GI-SAXS, X-ray or neutron reflectivity) and microscopies (AFM, SEM and TEM). The results will be of paramount importance for effectively tailoring the

efficiency and performance of the devices made of conjugated semiconducting polymers.

List of Publication

Journal Article

Lagmuir (2006, vol 22, p. 7521)
Thermally-Induced Order-Order Transition of DNA-Cationic Surfactant Complexes
Wei-Long Hsu, Yen-Cheng Li, Hsin-Lung Chen, Willisa Liou, U-Ser Jeng,, Hsien-Kuang Lin,Wen-Liang Liu,and Chain-Shu Hsu

Lagmuir (2006, vol 22, p. 11009)
Fractal Aggregates of Conjugated Polymer in Solution State
Yen-Cheng Li, Kuei-Bai Chen, Hsin-Lung Chen, Chain-Shu Hsu, Cheng-Si Tsao and Show-An Chen

Lagmuir (2007, vol 23, p. 975)
Two-Dimensional Densely Packed DNA Nanostructure Derived from DNA Complexation with a Low-Generation Poly(amidoamine) Dendrimer
Chun-Jen Su, Yi-Chun Liu, Hsin-Lung Chen, Yen-Cheng Li, Hsien-Kuang Lin, Wen-Liang Liu, and Chain-Shu Hsu

Conference Paper

Polymer Symposium
2004 P.189
Aggregation Behavior in Semi-dilute Solution of Poly(2,3-diphenylphenylene vinylene) (DP-PPV) Resolved by Small Angle Neutron Scattering
Yen-Cheng, Li, Chain-Shu Hsu, Hsin-Lung Chen, Show-An Chen, Cheng-Si Tsao and Derek L. Ho

2005 P.122
Aggregation Behavior of Conjugated DP-PPV in Solution State Studied by Small Angle Neutron Scattering
Yen-Cheng, Li, Chain-Shu Hsu, Hsin-Lung Chen, Show-An Chen, Cheng-Si Tsao and Derek L. Ho

2006 P.73
Fractal Aggregates of Conjugated Polymer in the Solution State
Yen-Cheng, Li, Hsin-Lung Chen, Chain-Shu Hsu, Show-An Chen, Cheng-Si Tsao

National Synchrotron Radiation Research Center, Users' Meeting & Workshops
2004 P. s8
Molecular Aggregation of Hairy-rod Conjugated Polymer in Solution State Study by SANS
Yen-Cheng Li, Kuei-Bai Chen, Chain-Shu Hsu, Hsin-Lung Chen, Cheng-Si Tsao and Show-An Chen

SAS 2006 Kyoto XIII International Conference on Small-angle Scattering
Fractal Aggregates of Conjugated polymer in Solution State
Yen-Cheng Li, Kuei-Bai Chen, Hsin-Lung Chen, Chain-Shu Hsu, U-Ser Jen Show-An Chen and Cheng-Si Tsao

2007 Taiwan-US Soft Materials Symposium
Conformational Structure and Inter-chain Aggregation of Semi-rigid Hairy-rod Polymer in Solution State
Yen-Cheng Li, Hsin-Lung Chen, Chain-Shu Hsu, Cheng-Si Tsao and Show-An Chen